UNIVERSITY OF SOUTHAMPTON

FACULTY OF NATURAL AND ENVIRONMENTAL SCIENCES

Chemistry

Synthesis of Small Molecule Endohedral Fullerenes

by

Andrea Krachmalnicoff

Thesis for the degree of Doctor of Philosophy

February 2015

UNIVERSITY OF SOUTHAMPTON

ABSTRACT

FACULTY OF NATURAL AND ENVIRONMENTAL SCIENCES

Chemistry

Thesis for the degree of Doctor of Philosophy

SYNTHESIS OF SMALL MOLECULE ENDOHEDRAL FULLERENES

Andrea Krachmalnicoff

Endofullerenes, namely fullerenes enclosing atoms, small molecules or atom clusters, are very convenient systems for the investigation of spectral properties and physical processes at the atomic / molecular level.

Endofullerenes encapsulating small molecules can be synthesised by "molecular surgery" - a sequence of organic reactions that open an orifice in the fullerene, encapsulate a molecule inside the cage, and suture the opening.

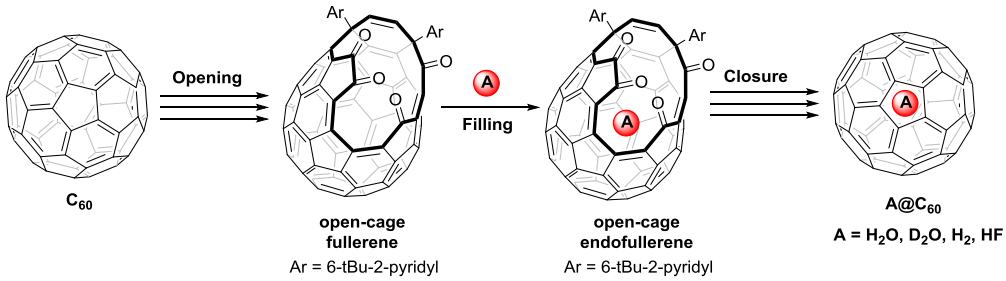

A known route to $H_2O@C_{60}$ was substantially improved, the mechanisms of key steps established, and extended to the formation of $H_2@C_{60}$. Among the improvements, a method for high levels of incorporation of H_2O and D_2O at low pressure was developed, and a new closing procedure based on a Diels-Alder/retro-Diels-Alder sequence was introduced.

A novel protocol for the encapsulation of hydrogen fluoride and a new partial closure reaction were discovered, and applied to the first synthesis of $HF@C_{60}$.

Table of Contents

ABSTRACT i

Table of Contents i

List of tables iii

List of figures v

List of schemes vii

DECLARATION OF AUTHORSHIP xi

Acknowledgements xiii

Definitions and Abbreviations xv

Chapter 1: Introduction 1

1.1 The Buckminsterfullerene molecule 1
1.2 Endohedral fullerenes 7
1.3 The molecular surgery approach 9

Chapter 2: Discussion 27

2.1 Opening an orifice in C_{60} 27
2.2 Filling a hydrophobic cavity with water 33
2.3 The case of deuterium oxide 37
2.4 Suturing the orifice of **H_2O@29** 41
2.5 Ortho-para conversion study of water inside C_{60} 61
2.6 A new synthesis of **H_2@C_{60}** 66
2.7 Filling the fullerene cavity with hydrogen fluoride 69
2.8 Trapping hydrogen fluoride inside C_{60} 72

Chapter 3: Conclusion 85

Chapter 4: Experimental 87

4.1 General 87
4.2 Materials 88
4.3 Experimental procedures and characterisation data 88
4.3.1 Preparation of precursors 88
4.3.2 Preparation of water open-cage endofullerenes 93
4.3.3 Synthesis of **29a** 94

4.3.4 Partial closure of water endofullerenes 96
4.3.5 Synthesis of **50** 102
4.3.6 Synthesis of **H_2O@50-d_{60}** 103
4.3.7 Preparation and partial closure of hydrogen endofullerenes 104
4.3.8 Preparation and partial closure of hydrogen fluoride endofullerenes 107
4.3.9 Synthesis and purification of C_{60} endofullerenes 113
4.4 Computational 116
4.4.1 General 116
List of References **123**

List of tables

Table 1: DFT B3LYP/6-31G(d) calculated free energies (Hartree). 117
Table 2: DFT B3LYP/6-31G(d) calculated free energies (KJ/mol). 118
Table 3: Free energy profile (KJ/mol) for the reduction of **28** to **27** via oxepin **47** and ylide **36b**. 119
Table 4: Free energy profile (KJ/mol) for the reduction of **28** to **27** via oxepin **47** and ylide **36a**..... 120
Table 5: Free energy profile (KJ/mol) for the reduction of **28** to **27** via epoxide **48**. 121

List of figures

Figure 1: Schematic representation of the 1985 Kroto *et al.* experiment. 1
Figure 2: Structural moieties in C_{60}. 3
Figure 3: Schematic representation of an arc reactor. 3
Figure 4: Apparatus used for the oxidation of OCF **26**. 29
Figure 5: HPLC chromatograms (Buckyprep, toluene) of the reaction of C_{60} with variable amounts of pyridazine **25** after completion. Equimolar amounts (*a*); Excess (1.5 eq) of pyridazine (*b*). 31
Figure 6: HPLC chromatogram of the oxidation of **26** with $^1O_2$ after completion (*a*). Chromatogram of the C_{60} recovered from the reaction mixture after chromatography (*b*). 32
Figure 7: ^{1}HNMR ($CDCl_3$, 400 MHz) spectrum of 78% filled **H_2O@29**. 35
Figure 8: ^{2}H NMR (61 MHz, toluene) spectrum of a 40:10:1 sample of $D_2O/HOD/H_2O@C_{60}$. 38
Figure 9: ^{13}C NMR (75 MHz, $CDCl_3$) spectrum of compound **28**. The peaks of the characteristic CO groups are indicated by red arrows. 39
Figure 10: ^{2}H NMR (61 MHz, toluene) spectrum of 78% filled $D_2O@C_{60}$. 41
Figure 11: DFT-GIAO calculated ^{13}C spectra of **35a** (*a*) and **35b** (*b*). The peaks of the characteristic C-H and C-OH orifice carbons are respectively indicated by red and blue arrows . Experimental ^{13}C (75 MHz, $CDCl_3$) spectrum (*c*) and ^{1}H (300 MHz, $CDCl_3$) spectrum (*d*) of compound **35**. 43
Figure 12: ^{13}C NMR (125 MHz, $CDCl_3$) spectrum of ylide **36**. The ylide carbon signal is indicated by a blue arrow. The signal of the CO group showing correlation to the phosphorus is indicated by a red arrow. 46
Figure 13: DFT-GIAO simulated ^{13}C spectra of ylides **36a** (*a*) and **36b** (*b*). Experimental ^{13}C (125 MHz, $CDCl_3$) spectrum of ylide **36** (*c*). The peaks of the characteristic CO and C-P orifice carbons are respectively indicated by red and blue arrows. 47
Figure 14: Structural motifs on OCF **28**. 49
Figure 15: HPLC chromatogram of the vacuum pyrolysis of OCF **26** after 0 (*a*) and 1 hour (*b*) at 360 °C. 58
Figure 16: HPLC chromatograms of 78% filled chromatographed (*a*) and sublimed **$H_2O@C_{60}$** (*b*). 61

Figure 17: Energy levels of the spin isomers of water. 62
Figure 18: structure of **H_2O@50-d_{60}**. 63
Figure 19: Different [6,6] double bonds of a C_{60}-monomalonate. 64
Figure 20: ^{13}C NMR (100 MHz, $CDCl_3$) chemical shift values of **H_2O@50-d_{60}**. 65
Figure 21: structures of OCFs **23**, **28** and **29**. 66
Figure 22: ^{1}H NMR (400 MHz, $CDCl_3$) spectrum of **HF@29**. 70
Figure 23: ^{19}F NMR (376 MHz, $CDCl_3$) spectrum of **HF@29**. 71
Figure 24: HPLC chromatogram showing formation of **36b** from **29** and triphenylphosphine in the presence of molecular sieves. 73
Figure 25: DFT-GIAO calculated ^{13}C spectra of **51** (*a*) and **51a** (*b*). The peaks of the characteristic CO and CH_2 orifice carbons are respectively indicated by red and blue arrows. Experimental ^{13}C (125 MHz, $CDCl_3$) spectrum (*c*) and ^{1}H (400 MHz, $CDCl_3$) spectrum (*d*). 76
Figure 26: HPLC chromatogram of the reaction between **29** and tri(2-furyl)phosphine after 89 hours at room temperature. 77
Figure 27: HPLC chromatogram of the reaction between **29** and di(2-furyl)phenylphosphine after 48 hours at room temperature. 82
Figure 28: ^{13}C NMR (odcb-d_4, 100 MHz) spectrum of 30% filled HF@C_{60}. 83
Figure 29: HPLC chromatogram (Buckyprep, toluene) of 30% filled HF@C_{60}. 84
Figure 30: Apparatus for the sublimation of C_{60} endofullerenes 113
Figure 31: Recycling HPLC, black arrows indicate the direction of the flow. 115

List of schemes

Scheme 1: The “pentagon road” mechanism. 4
Scheme 2: Rational synthesis of C_{60}. 6
Scheme 3: Hypothetic mechanism for the release of helium from $He@C_{60}$ at high temperature.[38] 9
Scheme 4: The molecular surgery approach 10
Scheme 5: Synthesis of OCF **3**. 11
Scheme 6: Rubin’s “triple scission” sequence. 12
Scheme 7: Synthesis of OCF **7**. 13
Scheme 8: Synthesis of OCF **12**. 15
Scheme 9: Synthesis of OCF **13**. 15
Scheme 10: Hypothetic mechanism for the formation of **13**. 16
Scheme 11: Synthesis of **15**. 16
Scheme 12: Structures of OCF **16** as determined by Iwamatsu *et al.* (**16a**) or Orfanopoulos et al (**16b**). 17
Scheme 13: Synthesis of OCF **17**. 18
Scheme 14: Gan’s synthesis of OCF **18**. 19
Scheme 15: Synthesis of OCF 23. 20
Scheme 16: Rubin’s synthesis of fulleroid **4**. 21
Scheme 17: Synthesis of $\mathbf{H_2@C_{60}}$ from $\mathbf{H_2@23}$. 21
Scheme 18: Proposed mechanism for the formation of $\mathbf{H_2@C_{60}}$ from $\mathbf{H_2@20}$. .. 22
Scheme 19: Synthesis of OCF **29**.[72] 23
Scheme 20: Equlibria of formation of $\mathbf{H_2O@29}$. 24
Scheme 21: Synthesis of $\mathbf{H_2O@C_{60}}$ from $\mathbf{H_2O@29}$. 24
Scheme 22: Generation of OCFs **30**, **31** and thio-fulleroid **32**.[73] 25
Scheme 23: Synthesis of pyridazine **25** via Kumada coupling. 27
Scheme 24: Synthesis of **25** via Neghishi coupling. 28
Scheme 25: Reactivity of **25** towards C_{60} and OCF **26**. 30
Scheme 26: Equilibria of formation of $\mathbf{H_2O@29}$ in the presence of liquid water. 36
Scheme 27: Hypothetical mechanism for the addition of ethanol to OCF **28**. .. 40
Scheme 28: Reduction of $\mathbf{H_2O@29}$ with triisopropyl phosphite. 42
Scheme 29: Reactivity of **29** and **28** towards triisopropyl phosphite. 44
Scheme 30: Reactivity of OCF **18** towards triethyl phosphite. 44
Scheme 31: Reactivity of $\mathbf{H_2O@29}$ towards triphenylphosphine. 45
Scheme 32: Formation of ylide **36b**. 45

Scheme 33: Reactivity of fluorenone towards phosphorus (III) reagents.[98]..... 48
Scheme 34: Free energy profile for the attack of triphenylphosphine on **28**. Energies are reported in KJ/mol. Only the reacting portion of the OCF structures has been represented. 50
Scheme 35: Free energy profile for the direct elimination of triphenylphosphine oxide from **44a** and **44b**. Energies are reported in KJ/mol. Structures are drawn following the convention used in Scheme 34. 51
Scheme 36: Free energy profile for the elimination of triphenylphosphine oxide from intermediate and **44b**. Energies are reported in KJ/mol. Structures are drawn following the convention used in Scheme 34. 52
Scheme 37: Free energy profile for the interconversion of **47** and **48**. Energies are reported in KJ/mol. Structures are drawn following the convention used in Scheme 34. 53
Scheme 38: Reduction of epoxide **48** to OCF **27**. Free energies are reported in KJ/mol. Structures are drawn following the convention used in Scheme 34. 54
Scheme 39: Free energy profile for the formation of **36a** and **36b**. Energies are reported in KJ/mol. Structures are drawn following the convention used in Scheme 34. 55
Scheme 40: Free energy profile for the formation of **27**. Energies are reported in KJ/mol. Structures are drawn following the convention used in Scheme 34. 56
Scheme 41: Hypothetic mechanism for the oxidation of OCF **27** with NMO. Structures are drawn following the convention used in Scheme 34. 57
Scheme 42: Novel reduction of $\mathbf{H_2O@29}$. 57
Scheme 43: Rubin's studies on the defunctionalisation of **4**.[69] 59
Scheme 44: Proposed mechanism for the alternative defunctionalisation of **26**.60
Scheme 45: mechanism of the Bingel cyclopropanation via nucleophilic attack (route *a*) or addition of carbene (route *b*). 64
Scheme 46: Synthesis of $\mathbf{H_2@C_{60}}$ from **29**. 68
Scheme 47: synthesis of **HF@29**. 70
Scheme 48: Reduction of **HF@29** with triphenylphosphine in refluxing toluene.73

Scheme 49: Reactivity of **29** towards triphenylphosphine and triisopropyl phosphite at room temperature in the presence of molecular sieves. 74
Scheme 50: Reactivity of **HF@29** towards triphenylphosphine at room temperature in the presence of molecular sieves..... 74
Scheme 51: Formation of OCF **51**. 75
Scheme 52: Free energy profile for the reaction of **28** with tri(2-furyl)phosphine. Energies are reported in KJ/mol. Structures are drawn following the convention used in Scheme 34. 79
Scheme 53: Free energy profile for the reaction of **28** with di(2-furyl)phenylphosphine. Energies are reported in KJ/mol. Structures are drawn following the convention used in Scheme 34..... 81
Scheme 54: synthesis of **HF@C_{60}** from **HF@27**..... 82

DECLARATION OF AUTHORSHIP

I, Andrea Krachmalnicoff,

declare that this thesis and the work presented in it are my own and has been generated by me as the result of my own original research.

Synthesis of Small Molecule Endohedral Fullerenes

I confirm that:

1. This work was done wholly or mainly while in candidature for a research degree at this University;
2. Where any part of this thesis has previously been submitted for a degree or any other qualification at this University or any other institution, this has been clearly stated;
3. Where I have consulted the published work of others, this is always clearly attributed;
4. Where I have quoted from the work of others, the source is always given. With the exception of such quotations, this thesis is entirely my own work;
5. I have acknowledged all main sources of help;
6. Where the thesis is based on work done by myself jointly with others, I have made clear exactly what was done by others and what I have contributed myself;
7. Parts of this work have been published as:
    - "Synthesis and characterisation of an open-cage fullerene encapsulating hydrogen fluoride" *Chem. Commun.* **2015**, *51*, 4993-4996.
    - "An optimised scalable synthesis of $H_2O@C_{60}$ and a new synthesis of $H_2@C_{60}$" *Chem. Commun.* **2014**, *50*, 13037-13040.
    - "Nuclear spin conversion of water inside fullerene cages detected by low-temperature nuclear magnetic resonance" *J. Chem. Phys.* **2014**, *140*, 194306.

Signed:.....

Date:.....

Acknowledgements

I would like to express my special gratitude to my supervisor, Prof. Dr. Richard J. Whitby: thank you for helping me grow as an experimental scientist and for encouraging me to undertake my first computational experiments. During these three years your guidance, calculations on feasible endofullerene candidates, and help with writing publications have been priceless. I would also like to thank Prof. Dr. Malcolm H. Levitt for organising the endofullerene project, making this research possible in the first place, and for very helpful comments on publications. My appreciation goes also to all the scientists working in the endofullerene field, and in particular to Dr. Salvatore Mamone, Dr. Benno Meier, Dr Marina Carravetta and Richard Bounds; your studies have made my work more interesting, enjoyable and gratifying. I would like to thank Prof. Dr. Yasujiro Murata for his extensive work on endofullerenes, and particularly for his elegant synthesis of $H_2O@C_{60}$ that is the basis for my work.

I am grateful to the EPSRC (EP/I029451/1) and to the ERDF (Interreg-IVB,MEET project) for funding, and acknowledge the use of the IRIDIS High Performance Computing Facility and associated support services at the University of Southampton. I would like to thank the University of Southampton and its staff respectively for providing and maintaining state of the art research facilities.

A very special thanks goes to my wife, Lorely, who always supported me, and encouraged me in the bad times. Without you, I would never have been able to accomplish all of this.

Definitions and Abbreviations

NMR: nuclear magnetic resonance

IUPAC: International Union of Pure and Applied Chemistry

EMF: endohedral metallo-fullerene

HPLC: high performance liquid chromatography

OCF: open-cage fullerene

MEM: 2-methoxyethoxymethyl

odcb: o-dichlorobenzene

DDQ: 2,3-dichloro-5,6-dicyano-1,4-benzoquinone

HOMO: highest occupied molecular orbital

LUMO: lowest unoccupied molecular orbital

TDAE: tetrakis(dimethylamino)ethylene

m-CPBA: m-chloroperoxybenzoic acid

THF: tetrahydrofuran

1-Cl-nap: 1-chloronaphthalene

NMO: 4-methylmorpholine N-oxide

dppp: 1,3-bis(diphenylphosphino)propane

b.p.: boiling point

DFT: density functional theory

GIAO: gauge invariant atomic orbitals

TLC: thin layer chromatography

ESI: electrospray ionisation

MS: mass spectrometry

RT: retention time

DMA: 9,10-dimethylanthracene

HF-Py : 70% hydrogen fluoride in pyridine

ms: molecular sieves

PHIP: para hydrogen induced polarisation

MRI: magnetic resonance imaging

PTFE: polytetrafluoroethylene

PE: polyethylene

R_f: retention factor

Chapter 1: Introduction

1.1 The Buckminsterfullerene molecule

According to History, the Greek scientist and mathematician Archimedes of Syracuse was the first to describe a truncated icosahedron in an opera now lost. This highly symmetric solid was re-discovered by several artists during the Renaissance era in their studies of shapes and perspective. During the first half of the twentieth century, Tisza published the first theoretical study on the vibrational spectrum of an hypothetic icosahedral molecule,[1] and later theoretical studies suggested the existence of C_{60} and other higher fullerenes.[2,3]

The first practical identification of C_{60} in the gas phase was accomplished in 1985 by Kroto *et al.*, while working on an experiment aimed at studying carbon clusters that could be present in interstellar and circumstellar space.[4] This very first and serendipitous synthesis used a laser pulse to vaporise carbon from a graphite target into a stream of helium gas, where the vaporised fragments would collide and form clusters. After cooling, the gas stream carrying the carbon clusters was sent to a mass spectrometer to analyse its composition (Figure1).

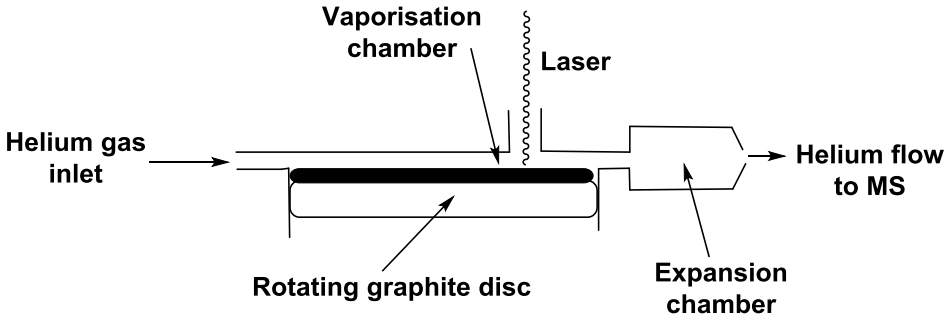

Figure 1: Schematic representation of the 1985 Kroto *et al.* experiment.

The resulting mass spectrum showed the presence of several carbon clusters grouped around a peak counting 60 atoms. It was then shown that, by using conditions that favoured collision and growth of the clusters, the C_{60} peak could be greatly enhanced with respect to all the others.

Five years later, in a remarkable development that greatly boosted fullerene research, Krätschmer *et al.* isolated C_{60} through a simpler and scalable method:

graphite rods were heated resistively under partial pressure of helium to produce carbon soot rich in C_{60}.[5,6] Shortly after Haufler *et al.* described the first apparatus and purification procedure for the production of C_{60} in gram quantities.[7] The isolation of C_{60} in considerable amounts allowed the structural characterisation of this new molecule. Indeed, the ^{13}C NMR spectrum showed a single resonance frequency and was evidence for its icosahedral structure. Since the first identification of C_{60}, it was clear that only a spheroidal shape provided the possibility of organise 60 sp^2 carbon atoms without leaving any free valences. Among all the possible options the icosahedral geometry was the only possibility to arrange all 60 carbon atoms in equivalent positions. Theoretical calculations for C_{60} predicted two different bond lengths;[8] these estimations were confirmed experimentally through various techniques.[9,10] In particular, the bond located at the junction between two six-membered rings ([6,6] bond) has a length of 1.38 Å and is formally represented as a double bond, while the bond located at the junction between a six- and a five-membered ring ([6,5] bond) has a length of 1.45 Å and is formally represented as a single bond. Since these bonds are of unequal lengths, C_{60} is not a perfectly regular truncated icosahedron; however, the deformation is negligible. This polyenic structure is at the origin of the reactivity of C_{60}. Instead of behaving like a stable “super-aromatic” sphere, C_{60} reacts similarly to an electron deficient olefin. Indeed, the [6,6] double bonds participate in reactions with a vast array of nucleophiles, or as components in cycloadditions.[11] Strain energy, released through a sp^2 to sp^3 change in the hybridisation of the carbon atoms that form the [6,6] double bond, provides the driving force for all of these reactions. The origin of this strain is due to the fact that, in order to adopt a spherical structure, the [6,6] double bonds have to deviate considerably from planarity. A closer look at the C_{60} structure shows that each pentagon is completely surrounded by hexagons to form a corannulene-like moiety, sometimes referred to as “buckybowl”. A second repeating pattern can be identified around the [6,6] bond and can be related to a bent pyraclene molecule (Figure 2).

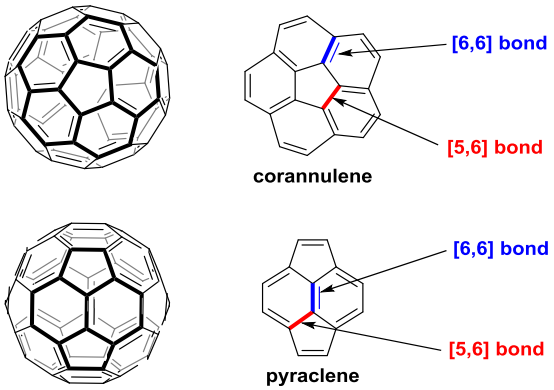

Figure 2: Structural moieties in C_{60}.

These two structural units interlock so that two pentagons never share a common edge: two fused pentagons would, in fact, introduce antiaromaticity in the system and generate an excessive bend that would completely destabilise the structure. This condition is usually referred to as the "isolated pentagon" rule. C_{60} and C_{70} are respectively the first and the second fullerenes of the series that can satisfy this particular condition and are thus the ones isolated in larger amount.

Nowadays, C_{60} is produced industrially on a kilogram scale. Large amounts of carbon soot containing 6-20% by weight of soluble fullerenes are prepared using arc (Figure 3) or radiofrequency plasma reactors; less commonly pyrolysis of hydrocarbons such as toluene or tetralin is used to produce carbon vapour suitable for fullerenes synthesis.[12]

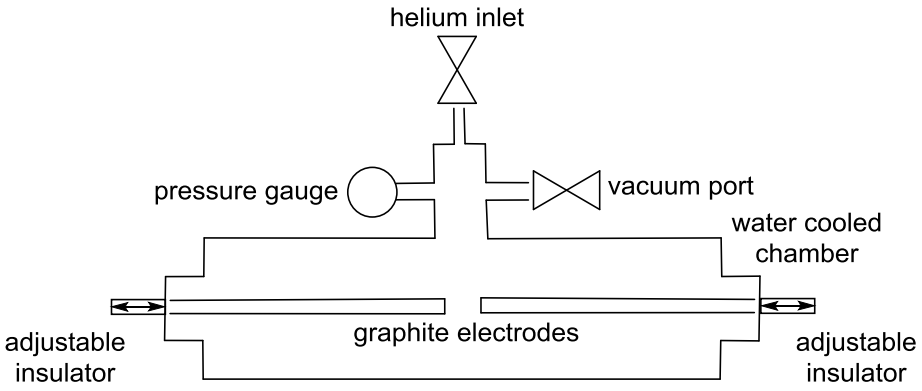

Figure 3: Schematic representation of an arc reactor.

The soot produced by any of these methods is collected and washed with diethyl ether to remove most of the hydrocarbon contaminants, then extracted with toluene in a Soxhlet apparatus; the soluble fraction is isolated and finally

subjected to column chromatography to afford 99.5% pure C_{60}. Samples of higher purity (99.9%) are prepared by sublimation.

Several mechanisms have been proposed to rationalise the formation of fullerenes in plasma, many of which differ only slightly from one another.[13] In his first attempt to explain the process, known as "party line" mechanism, Smalley[14] proposed that oligoacetylene chains were initially formed by addition of C_2 units that make up graphite vapour. These chains would eventually grow long enough to form macrocycles. These would still continue to grow via addition of C_2 units until a C_{25}-C_{35} size was reached. At this point, the macrocycles would rearrange into an aromatic polycycle. These clusters would continue to grow indefinitely, via addition of C_2 units. The formation of C_{60} and C_{70} was explained by assuming that graphite-like clusters containing only hexagons could rearrange into buckybowls in order to minimise the number of free valences. These would gradually grow to C_{60} or C_{70} and then the process would stop, given the inertness of fullerenes to further add C_2 units. In a later modification, known as the "pentagon road" mechanism,[14] the particular efficiency of formation of fullerenes was explained by postulating that the buffer gas favoured the synthesis of clusters following the isolated pentagon rule (Scheme 1).

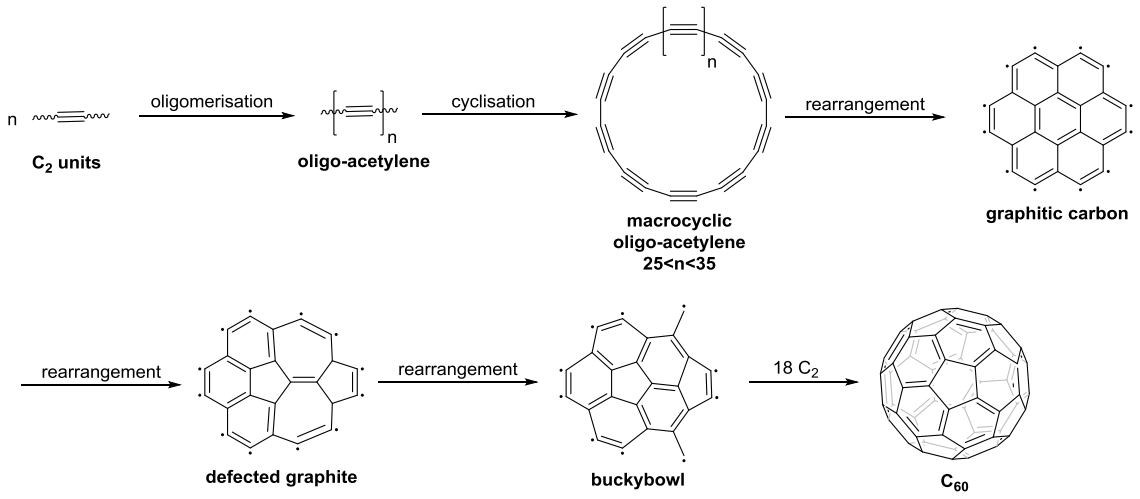

Scheme 1: The "pentagon road" mechanism.

It was assumed that these clusters were thermodynamically more stable than the ones containing only hexagons. In a similar mechanism known as "fullerene road", Heath proposed that C_{60} and C_{70} were the products of the addition of C_2 units to smaller pre-formed fullerenes; although this approach

could not explain how these were formed in the first place. By contrast, Hunter *et al.* proposed that fullerenes could arise by "zipping-up" of an acetylene macrocyclic precursor folded into a spiral spheroidal conformation, through a series of radical cyclisations.[15] A different hypothesis provided by Irle *et al.*, known as "the shrinking hot giant road", proposes that giant fullerenes are the predominant species formed in carbon vapour, and that C_{60} arises from a series of irreversible fragmentations of these much larger precursors.[16] More recently the mechanism of formation of fullerene from graphene was investigated,[16a] demonstrating that loss of carbon atoms on the edge of the graphene sheet results in the formation of pentagonal rings. These generate a bend on the graphene plane that activates the formation of fullerenes. Many more hypothetic mechanisms are reported in the literature, and until today, a definitive answer on the mechanism of formation of fullerenes is yet to be found.

Although methods for the production of fullerenes in large scale have been available since the 1990s, many research groups still pursued the fascinating objective of synthesising C_{60} from precursors made through classical methods. The first example of a rational synthesis of C_{60} from simple precursors prepared by classical organic chemistry reactions was published in 2001;[17] however, research in this field still continues today.[18–20] In this work, the authors built the aromatic precursor $C_{60}H_{30}$. The synthesis starts from the Wittig reaction of (1-bromoethyl)benzene with 2-naphthaldehyde that yields the corresponding alkene; this undergoes a Mallory–Katz cyclisation to produce the polycyclic aromatic compound $C_{19}H_{14}$. A nitrile group is introduced on the methyl side chain through radical bromination, followed by displacement with KCN. The nitrile is hydrolysed to the acid, which in turn is transformed into the acid chloride. Friedel–Crafts acylation gives the ketone $C_{20}H_{12}O$ that is transformed into the final precursor $C_{60}H_{30}$ via cyclotrimerisation promoted by $TiCl_4$ (Scheme 2).

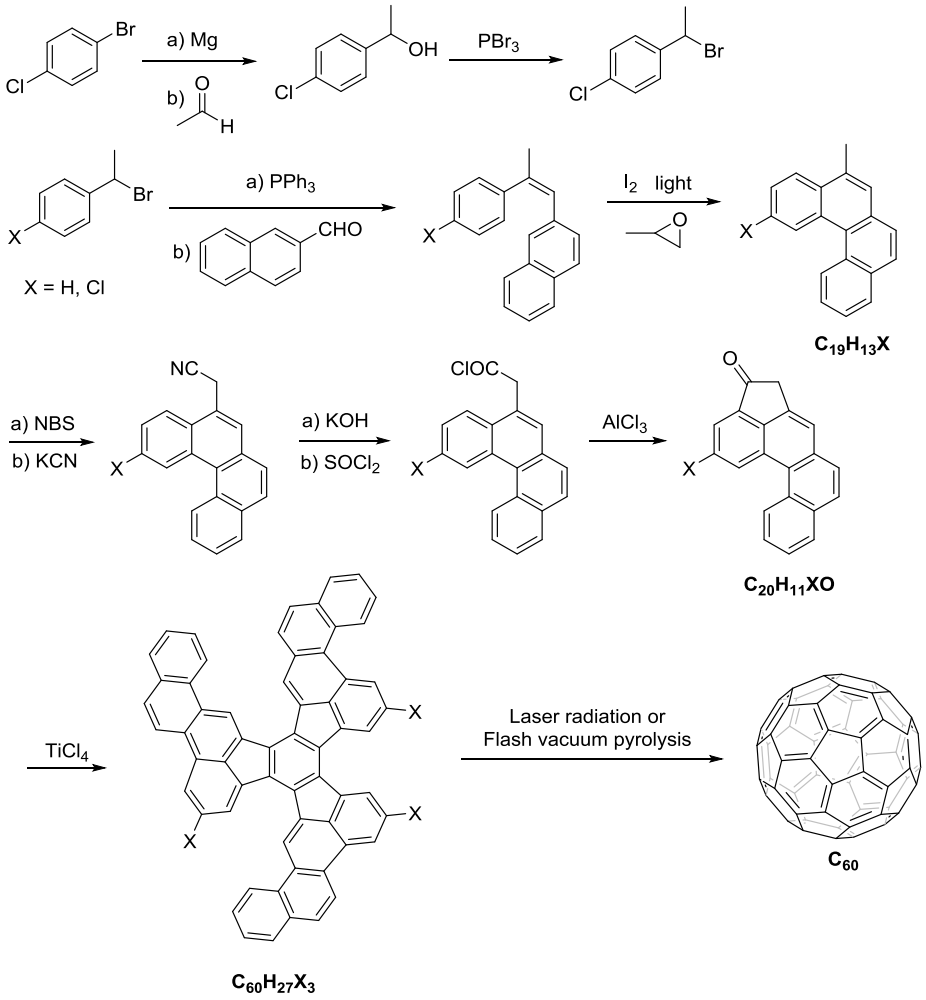

Scheme 2: Rational synthesis of C_{60}.

The $C_{60}H_{30}$ molecule is extremely stable and is marginally converted into C_{60} when it is introduced inside the photo-ionisation chamber of a mass spectrometer. The following year, the same group synthesised the precursor $C_{60}H_{27}Cl_3$ in a comparable way. This substrate was cyclised to C_{60} by flash vacuum pyrolysis at 1100 °C in very low yield (≤1%), thanks to the C-Cl bonds favouring homolytic cleavage.[21] In the following years, several groups reported other experiments that achieved formation of small quantities of C_{60}, most of the time in the gas phase.[22–24] Clearly, all of these routes are not suitable for the production of bulk amounts of material, but definitely demonstrate that the rational synthesis of fullerenes through "zipping-up" of a carbon shell, even if extremely difficult, is practically feasible.

1.2 Endohedral fullerenes

Taking in consideration its electronic density, the C_{60} molecule has an outer diameter of 10.3 Å, and encloses a cavity spanning 3.5 Å.[25] Indeed, since the very first identification of C_{60}, the possibility of trapping atoms and molecules inside this empty space was envisioned. As early as 1985, Kroto *et al.* collected evidence of formation of stable "C_nLa complexes" by repeating their experiment using a graphite disk impregnated with lanthanum.[4,26] In the years that followed, while experimentalists were collecting the first structural data on C_{60}, a number of theoretical studies were published on the stability and properties of fullerenes encapsulating atoms and small molecules. In one of these studies Cioslowski coined the term "endohedral fullerenes" (often shortened to "endofullerenes") to describe such supra-molecular compounds. This name was coined by combining the two Greek words *endon*, meaning "within" and *edra*, meaning "faces".[27] Today, endofullerene is the name commonly used to refer to these molecules. The notation, first introduced by Smalley,[28] "A@C_n", where "A" indicates the incarcerated specie and "C_n" specifies the carbon cage, is used as molecular formula. The recommended IUPAC nomenclature "incar-fullerene", and the related notation "*i*AC_n", are rarely encountered instead. The first endohedral fullerenes were produced using graphite electrodes impregnated with metal oxides in a regular arc reactor (Figure 3). Although the initial yield of endohedral metallo fullerenes (EMFs) was very low (≤2%), the process was relatively simple and cost-effective. The different solubility behaviour and vapour pressures of the EMFs and their corresponding empty fullerenes, allowed an easy enrichment of the endohedral fraction by solvent extraction or sublimation. In 1999, it was discovered that when a partial pressure of nitrogen gas was present inside the reactor, nitride cluster endofullerenes were formed in relatively high yield (3-5%).[29] This study led to the isolation of a completely new class of endofullerenes which, thanks to later improvements in the synthesis technique,[30] comprises today many readily accessible compounds. On the wake of this discovery, it was shown that sulphide cluster endofullerenes[31] and methano cluster endofullerenes[32] could be synthesised respectively in the presence of partial pressures of SO_2 and CH_4.

The first non-metal endofullerenes ever isolated were N@C_{60} and P@C_{60}. Both compounds were synthesised by the group of Weidinger respectively in 1996

and 1998.[33,34] The syntheses were realised by bombarding preformed C_{60} with N or P ions generated by a plasma discharge. The fraction of cages filled with N or P (filling factor) achieved using this technique is extremely low (~0.0001%). The pure endofullerenes $N@C_{60}$ and $N@C_{70}$ were isolated through extensive use of HPLC.[35] Small amounts of $N_2@C_{60}$ which contaminated the $N@C_{60}$ sample were isolated as well.[36] The endofullerene containing the smallest atom, $He@C_{60}$, was identified in the gas phase just some years before.[37] In this experiment, accelerated C_{60}^+ cations were collided with stationary gases such as helium, hydrogen, deuterium, argon and SF_6; the products of collision were then analysed by mass spectrometry. In all cases a pattern of ions at *m/z* $[C_{60-2n}]^+$ (n = 1-6) was observed, showing that the high energy collision was stripping C_2 units off the carbon cages. Only when helium was used as stationary gas, a secondary pattern was evident at *m/z* 4 units higher of each signal corresponding to the loss of a C_2 unit. An isotopic shift was observed in the pattern when ^{3}He was used instead of ^{4}He: in this case, the new ions were only 3 units apart from the $[C_{60-2n}]^+$ peaks. It was concluded that, following the removal of a single or of multiple C_2 units, a single atom of helium was encapsulated and a pattern of $[C_{60-2n} + He]^+$ ions generated. Under the same conditions, C_{70}^+ cations produced an analogous trace of $[C_{70-2n} + He]^+$ ions. Among those was the $[C_{60} + He]^+$ cation produced from splitting of 5 C_2 units off the C_{70} cage and helium encapsulation. Assuming that the open-cage ion rearranged itself into a closed structure, this was indeed the first observation of the non-metal endofullerene $He@C_{60}$.

In a successive work by Saunders *et al.* C_{60} samples, synthesised under helium partial pressure using a conventional arc reactor, were reported to release helium gas at high temperature (660 °C). The ^{3}He/^{4}He isotopic ratio of the gas evolved was typical of the commercial, rather than the natural occurring gas. Therefore, the researchers concluded that the helium was encapsulated inside the cage during the synthesis. The amount of $He@C_{60}$ relative to the empty C_{60} cages (filling factor) was estimated to be of the order of 1 ppm.[38] Moreover, the experimentally measured energy barrier for the escape of the helium atom was much lower than the theoretically calculated barrier for the ejection through one of the hexagonal faces. The authors explained this finding by postulating that the encapsulated atom was lost through a larger orifice, formed by reversible cleavage of one or more C-C bonds (Scheme 3).

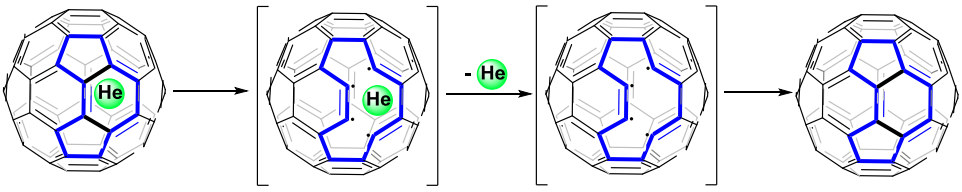

Scheme 3: Hypothetic mechanism for the release of helium from He@C_{60} at high temperature.[38]

This assumption was demonstrated shortly thereafter by the same authors: He, Ne, Ar, Kr and Xe were encapsulated inside C_{60} or C_{70} by heating the preformed fullerenes at high temperatures (~600 °C) and under high pressure of noble gas (1200 - 2700 atm). The filling factor of each sample was estimated by mass spectroscopy and ranged between 0.04 and 0.3% depending on the identity of the gas and the pressure used.[39] The use of high pressure was critical to achieve filling factor detectable by mass spectrometry.

Even if the synthesis of endofullerenes containing noble gases was achieved through this technique, the very low filling factors and the scarce reproducibility[39] of the method, precluded the isolation of endofullerenes in large amount.

1.3 The molecular surgery approach

The studies of Saunders *et al.* prompted the search for an alternative strategy for the synthesis of non-metal endofullerenes. Additional inspiration was provided by the abundance of reports on the reactivity of C_{60}, which showed that the carbon cages displayed a very diverse chemistry. Consequently, researchers began to consider the idea of using a set of reactions to open an orifice on the fullerene; then using the open-cage fullerene (OCF) to incorporate an atom or small molecule, and finally close the orifice to regenerate the C_{60} pristine structure. This approach is nowadays called "molecular surgery" (Scheme 4).[40]

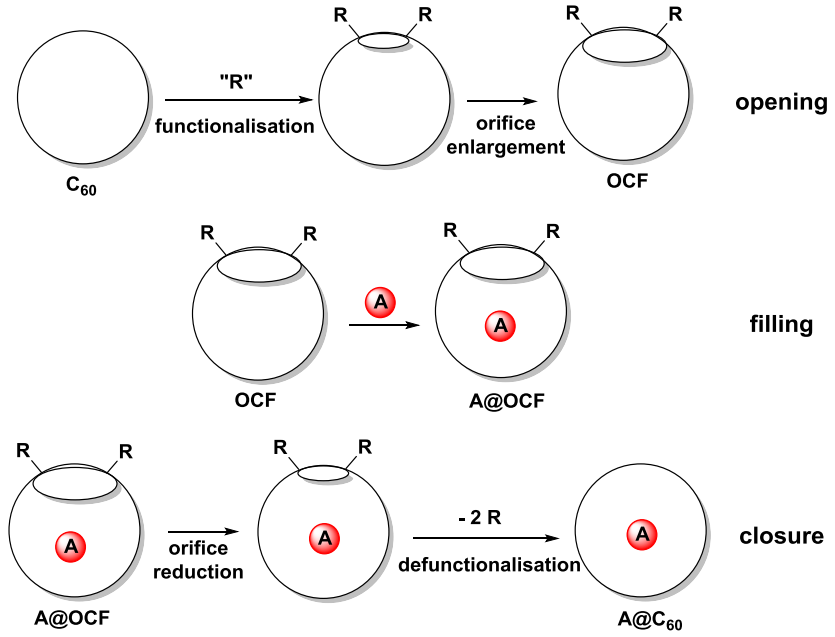

Scheme 4: The molecular surgery approach.

Considering that C_{60} has 30 double bonds, it is extremely difficult to open an orifice directly on its unmodified surface in a controlled fashion. Indeed the C_{60} cage can be severed by reaction with $^1O_2$; [41] however, the second and subsequent additions are non-selective and therefore of scarce importance in the molecular surgery setting. Nevertheless, if C_{60} is first functionalised, the added groups induce a change in its structure and reactivity allowing the controlled scission of other bonds. This necessity introduces the additional challenge of removing these groups from the fullerene core to regenerate its pristine structure and complete the surgery. The group of F. Wudl reported the first efficient procedure for the cleavage of two adjacent bonds of C_{60}.[42] Applying their knowledge on the reactivity of C_{60} towards diazomethane and azides to the molecular surgery approach, they were able to open an 11-membered orifice by oxidation of fulleroid **2**. In the reaction sequence, first a [5,6]bond is severed by addition of MEM azide; this cleavage occurs via a thermally induced rearrangement of triazine **1**, which in turn, forms via a 1,3-dipolar cycloaddition between the azide and the reactive [6,6] double bond.[43] The rearrangement of fulleroid **1** takes place in multiple steps and is triggered by the loss of molecular nitrogen.[44] After the [2+2] cycloaddition of **2** with $^1O_2$, ketolactam **3** is isolated in 70% yield (Scheme 5).

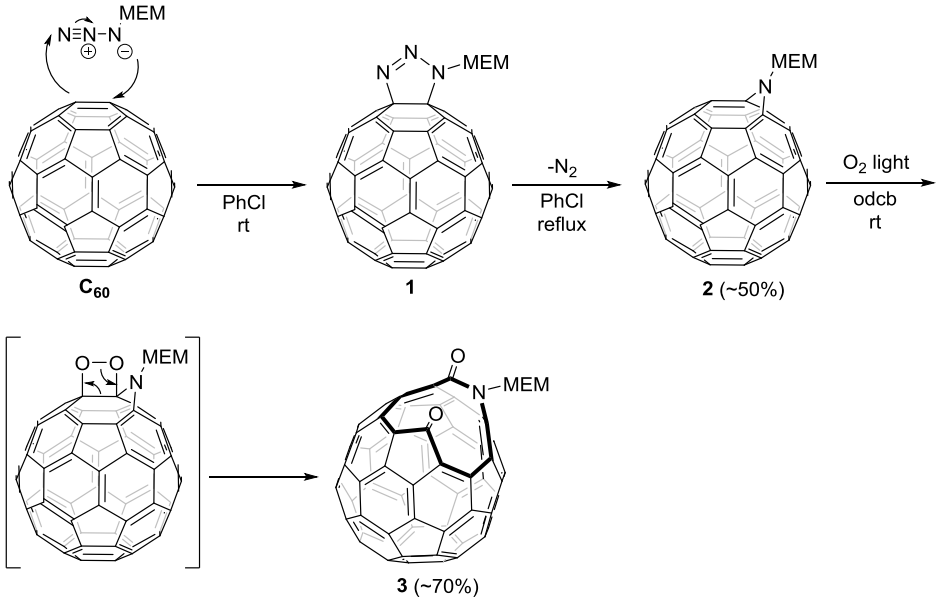

Scheme 5: Synthesis of OCF **3**.

The regioselectivity of the last transformation is due to the strain experienced by the two equivalent anti-Bredt double bonds, adjacent to the nitrogen atom. Moreover, the nitrogen atom increases the electronic density on the double bond by mesomeric effect, raising the energy of its HOMO and thus augmenting its reactivity towards electrophiles. It is interesting to note that all oxidations involving $^1O_2$ and C_{60} or, by analogy, a fulleroid having an intact 60 π-electron structure, do not require a photo-sensitiser in order to proceed. In fact, C_{60} is known to be a great photo-sensitiser itself.[45] The reactivity of **3** is drastically changed by the introduction of the carbonyl and lactam functional groups. At this stage, all the double bonds on the orifice are conjugated to the electron-withdrawing CO groups, thus their reactivity towards the electrophilic $^1O_2$ is decreased. Even the double bond next to the nitrogen is not activated anymore since the heteroatom is now part of the amide group. Because some of the spherical tension has been released by opening the orifice, the double bonds on the rim are as well less strained. Consequently, oxidation of **3** does not take place. The size of the orifice in **3** was still too small to afford the incorporation of helium, the smallest atom. Practically the filling of OCF **3** was never attempted, but all efforts to eject helium from **He@3** (synthesised from He@C_{60}) failed.

Shortly after, the group of Y. Rubin reported a procedure for the scission of three bonds of the C_{60} cage. In this case, the initial attack was done through a [4+4] followed by a retro [2+2+2] cycloaddition on fulleroid **4**. The

transformations effectively severed two [5,6] bonds and led to the formation of **5**. In an attempt to crystallise **5** by complexing the cyclooctatriene moiety to a metal centre, a third [5,6] bond was cleaved and the cobalt bridged fulleroid **6** was isolated (Scheme 6).[46]

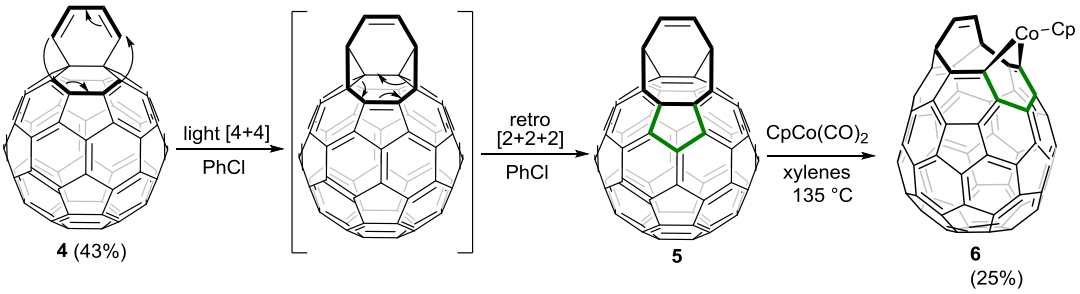

Scheme 6: Rubin's "triple scission" sequence.

Although the scission of three C-C bonds was a remarkable achievement, the introduction of a methano or cobalt bridge across each fragmentation still limited greatly the size of the orifice. The use of a "scalpel" carrying several reactive functional groups connected by spacers, was envisioned by Rubin as a possible way to create larger openings.[47] When C_{60} was reacted with one of such compounds, the diazido butadiene **7**, compound **8** was formed as the product of a complex cascade reaction. The process was triggered by a [3+2] azide-double bond cycloaddition, which was followed by a further analogous [3+2], and finally by a [4+2] cycloaddition of the butadiene moiety. The ditriazine fullerene derivative then underwent a double rearrangement to diazafulleroid **8** cleaving two [5,6] bonds in the process (Scheme 7).

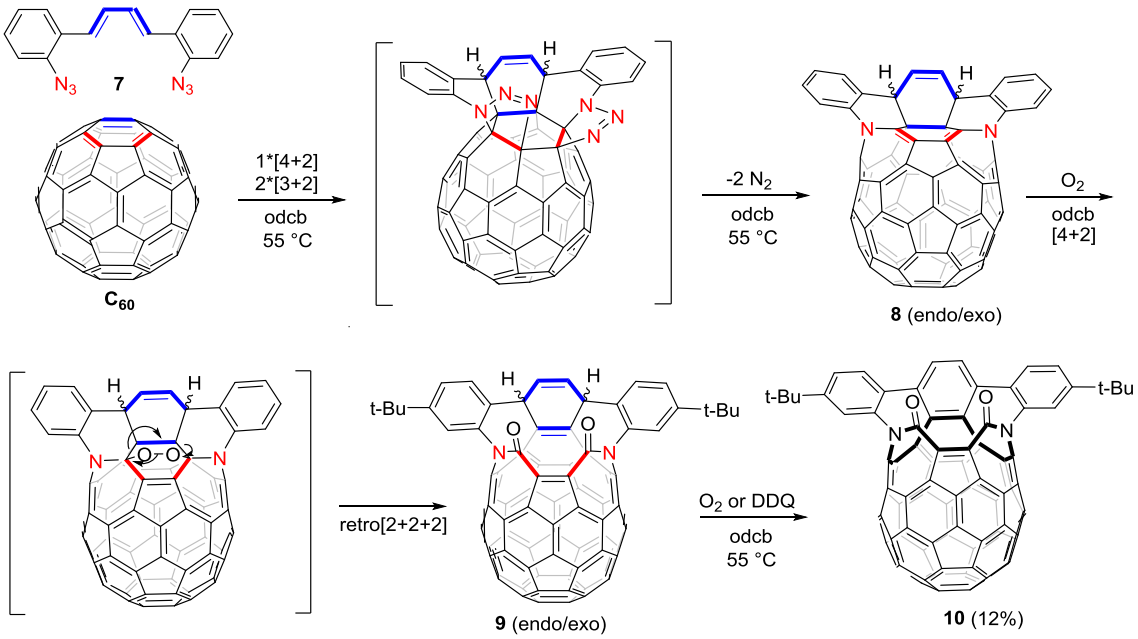

Scheme 7: Synthesis of OCF **7**.

The 1,4-diamino butadiene function on **8** was reacted with $^1O_2$, forming dilactam **9** through a domino [4+2] / retro [2+2+2] reaction, the latter cleaving two more former [5,6] bonds. In this instance the conjugation of the two enamine functions results in the selection of the [4+2] endoperoxide pathway, rather than the [2+2] dioxoethane course taken by fulleroid **2** (Scheme 5). Exposure to air, or treatment with the oxidant DDQ, afforded the aromatisation of the cyclohexa-1,4-diene ring converting the diastereomeric mixture into the C_{2d} symmetric compound **10**.[48]

This work demonstrated that a 14-membered orifice could be opened in a one-pot process. More importantly, compound **10** was the first OCF able to incorporate helium and hydrogen. Due to its small size, ^{3}He (atomic volume 11.0 Å^3), was incorporated at low pressure (4 atm) and relatively low temperature (100 ˚C), in a simple experiment carried out inside an NMR tube. In these conditions a filling factor of 0.05% was reached after 24h. When the experiment was repeated, using the same apparatus employed by Saunders for his incorporation experiments on C_{60} (cf. 1.2), a filling factor of 1.5% was afforded after 7.5 hours at 305 ˚C and 475 atm. The more voluminous hydrogen (molecular volume 19.0 Å^3), required a temperature of 400 ˚C to overcome its higher barrier to insertion (173 KJ/mol compared to 102 KJ/mol for the entry of helium). A filling factor as high as 5% was reached using

relatively low pressure (100 atm). The filling factor was estimated by ^{3}He or ^{1}H NMR spectroscopy. In the first case $^{3}He@C_{60}$ was used as reference, and in the second the integrated endohedral hydrogen signal was compared with the signals of the exohedral protons.[49]

Certainly, the soundness of the molecular surgery approach was proved by this breakthrough study, which as well highlighted some central aspects of the molecular surgery approach. Calculations showed that the incorporation process was overall slightly exothermic as the guest species can undergo favourable Van der Waals interaction with the carbon atoms of the cage. The activation barrier for the insertion, or the escape, was found to originate from the loss of degree of freedom and from the steric repulsion that the guest species experienced when constricted by the orifice. The extent of these barriers was dependent on the size of the guest. Larger species, having more area exposed to the rim of the cage, were more difficult to encapsulate but more difficult to remove. Undoubtedly the size of the opening is a crucial aspect of the molecular surgery approach. A large orifice allows for the incorporation of voluminous guests, and makes the incorporation process easier so that moderate pressure and temperature can be used. The same large opening also provides an easy way out of the cage for the endohedral specie. On the contrary, a small orifice will make the incorporation step more difficult; nevertheless, once the cage is filled, it will trap the endohedral specie much more effectively. Irrespective of the size of the opening, the incorporation process is overall entropically demanding as the guest molecule loses translational freedom. Therefore the use of high pressure was necessary to shift the equilibrium to the side of the endofullerene and achieve a higher filling factor.

Additionally, this work also emphasised that a 14-membered orifice was still quite small, and that a larger opening was needed to achieve higher filling factor at lower pressure and temperature. The most active research on the expansion of OCF orifices by controlled step-wise severing of bonds was undertaken by Iwamatsu *et al.*. The starting point of their research was fulleroid **11**, synthesised using a similar approach to Rubin's strategy.[50] Reaction of **11** with $^{1}O_{2}$ afforded **12** in high yield; the regioselectivity of this transformation was accounted to the localisation of the HOMO on the rim of the opening (Scheme 8).[51]

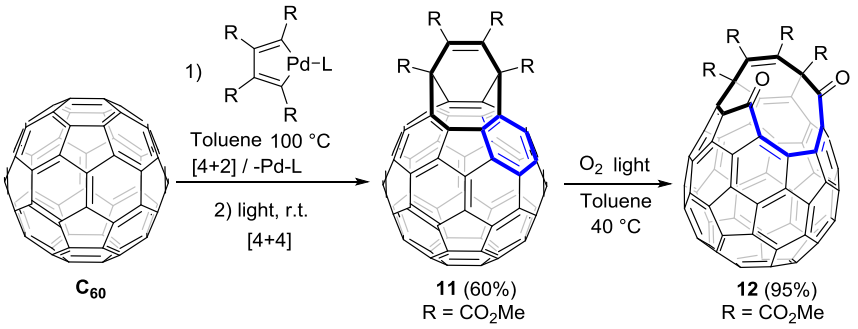

Scheme 8: Synthesis of OCF **12**.

Knowing that the orifice of **12** was still too small to afford the incorporation of any species, the authors began investigating new reactions to expand the opening. Calculations done on **12** revealed that while the HOMO had moved away from the rim after the oxidation, the LUMO was instead localised on the [5,6] bond on the orifice, reflecting the double α,β-unsaturated carbonyl structure. Indeed, several nitrogen nucleophiles were found out to be reactive towards **12**. Compound **13** was isolated as the only reaction product when a solution of **12** was treated with aromatic hydrazines or hydrazones, bearing an un-substituted -NH_2 group (Scheme 9).[52,53]

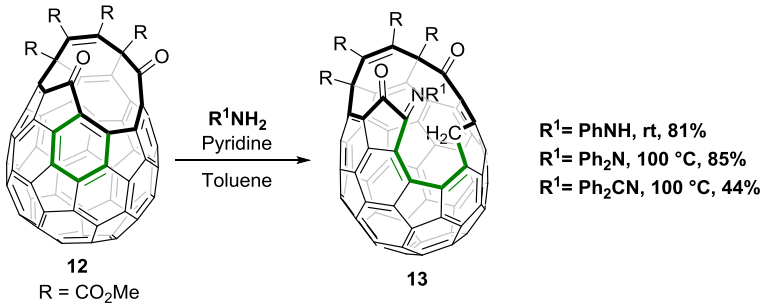

Scheme 9: Synthesis of OCF **13**.

This kind of reactivity has no precedents in the literature. The reaction mechanism has not been studied in detail but it is plausible that the delocalisation of a negative charge on the carbonyl group might drive the nucleophilic attack. The regioselectivity can be explained considering that just one carbonyl can overlap well with the double bonds due to the distortion originated by the cage scission (Scheme 10, path *a*). Alternatively, it is plausible that the nucleophilic attack could be driven by delocalisation of the negative charge on the cyclopentaphenanthrene-like motif (Scheme 10, path *b*). The negative charge is then neutralised by the protic environment and the methylene group formed.

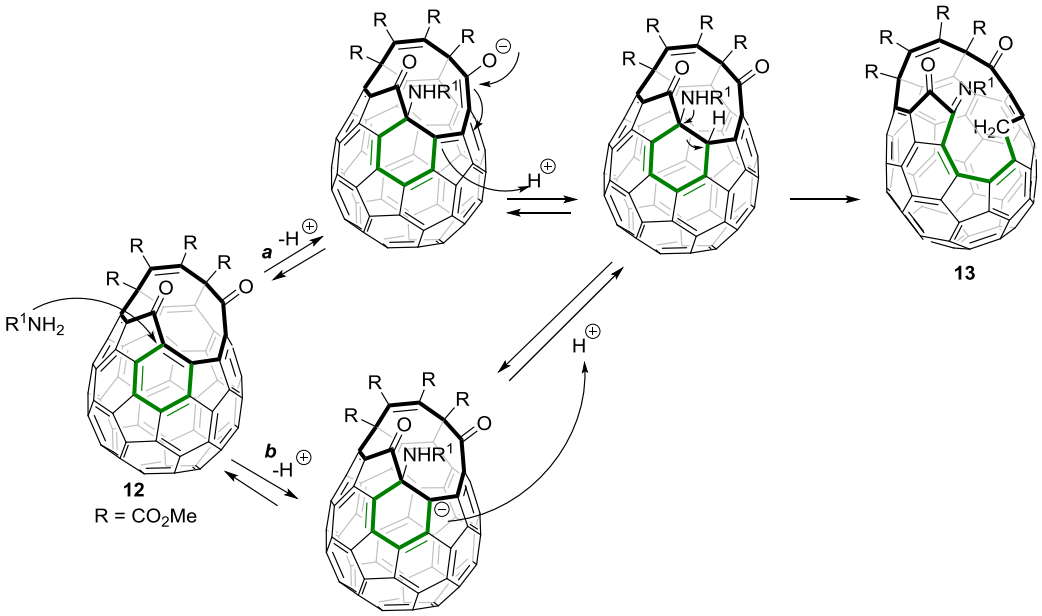

Scheme 10: Hypothetic mechanism for the formation of **13**.

The 16-membered ring of OCF **13** was wide enough to allow the incorporation of hydrogen under relatively mild conditions. 62% filled **H_2@13** was afforded after 4 hours at 100 °C and 135 atm.[54] 42% filled **Ne@13** was produced at 180 °C and 825 atm.[55]

The same authors later demonstrated that electron rich 1,2-diaminobenzenes can be used to cut a larger orifice. These nitrogen dinucleophiles showed reactivity similar to aromatic hydrazines and hydrazones towards OCFs having α,β-unsaturated carbonyl function on their rim. However the presence of a vicinal amine function led to the formation of a spiro-fused hydro-benzimidazole ring rather than a CN double bond. Thus reaction of **12** with o-phenylenediamine at room temperature afforded **14** as the only reaction product. Treatment of **14** with excess pyridine resulted in the formation of OCF **15** possessing a 20-membered orifice (Scheme 11).[56]

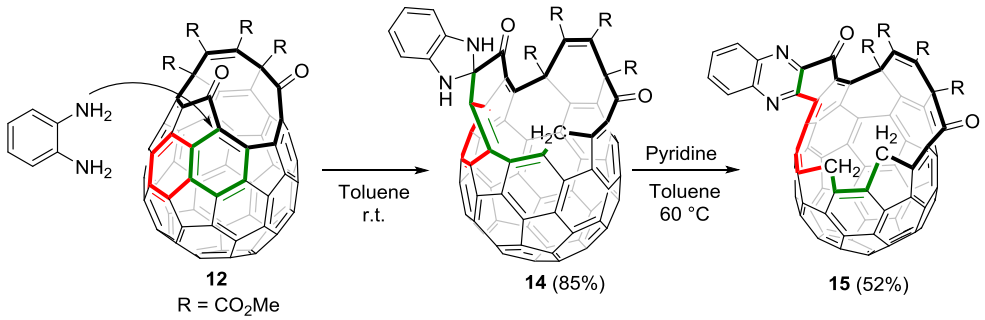

Scheme 11: Synthesis of **15**.

Compound **15** is the OCF with the largest opening reported in the literature. It was the first OCF that could incorporate water, affording 75% filling factor at ambient temperature and pressure. Ammonia was also incorporated at room temperature and 1-7 atm, with filling factors ranging from 5 to 50%.[57] Higher pressures (80-180 atm) were used to encapsulate gases such as nitrogen, noble atoms, and carbon monoxide.[55,58] Methane, which with its diameter of 3.8 Å is considered the largest guest that can be encapsulated inside C_{60}, was incarcerated (39% filling factor) at 200 ˚C and 19 atm.[59] On the other hand, all attempts to fill **15** with hydrogen failed,[60] probably because the opening is too wide to stop the small molecule from escaping.

The same reactivity with hydrazines was successfully extended to Wudl's OCF **3** producing 15-membered **16**. Two groups studied this reactivity roughly at the same time. There is a discrepancy between the structure proposed by Iwamatsu *et al.* (**16a**) and that proposed by Orfanopoulos *et al.* (**16b**); however no definitive proof was provided (Scheme 12).[61,62]

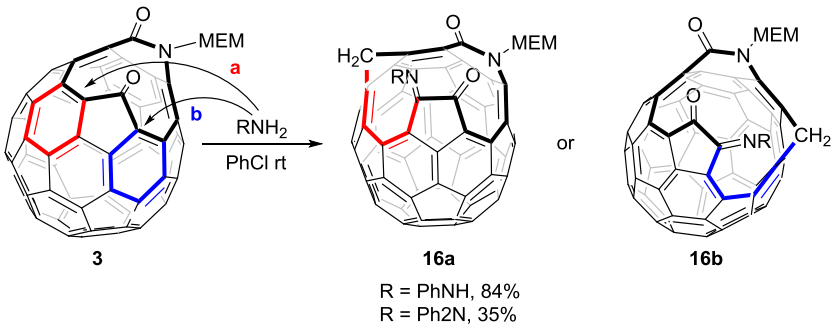

Scheme 12: Structures of OCF **16** as determined by Iwamatsu *et al.* (**16a**) or Orfanopoulos et al (**16b**).

The size of the orifice of **16** is still quite small; incorporation of hydrogen inside **16** was indeed attempted by Iwamatsu *et al.* without success.[60]

Similarly, reaction of **3** with o-phenylenediamine was used to synthesise 19-membered derivative **17** (Scheme 13).[63]

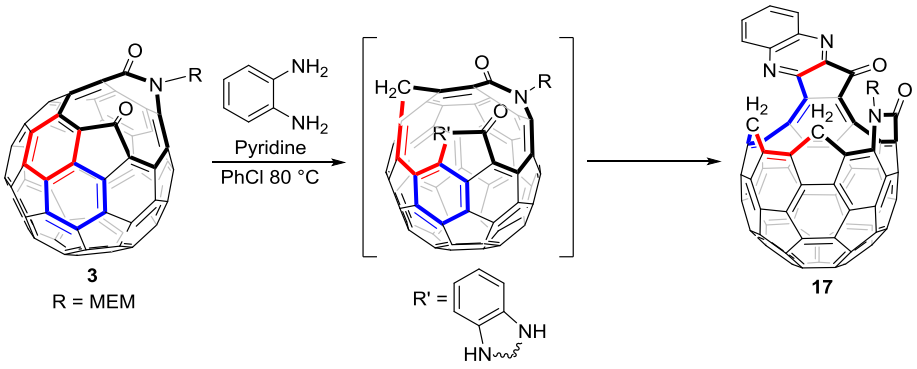

Scheme 13: Synthesis of OCF **17**.

Quite expectedly, the barrier for the encapsulation of water in **17** is significantly higher than the one of its relative OCF **15**, possessing a wider orifice. While **H_2O@15** was formed spontaneously at room temperature, **H_2O@17** was formed efficiently (85% filling factor) only in refluxing toluene (110 °C). The release of water from **H_2O@17** was also impeded by the smaller orifice, with the guest molecule still not being completely ejected after 27 hours at 120 °C.

Years later the group of Gan synthesised the novel 18-membered OCF **18**. This derivative was prepared from a peroxide fulleroid through a series of transformations which included epoxide ring-opening, oxidative cleavage of a vicinal diol, and final de-acetalisation (Scheme 14).[64–66]

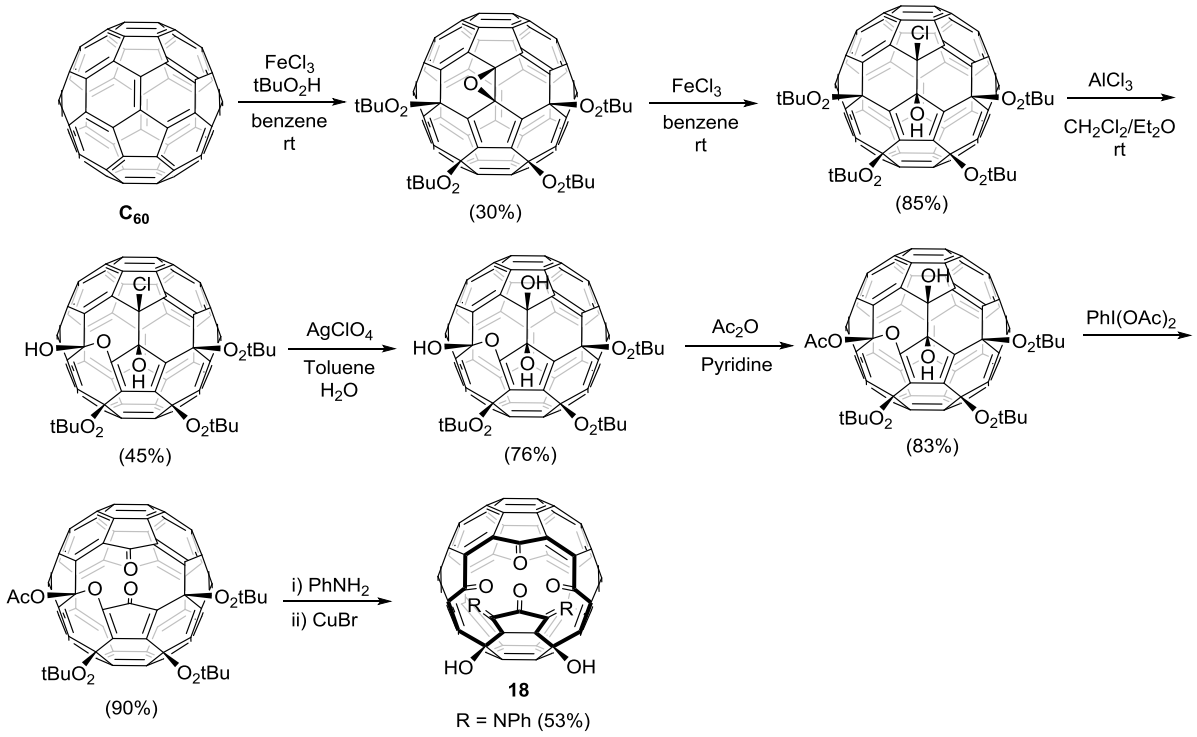

Scheme 14: Gan's synthesis of OCF **18**.

Compound **18** was shown to incorporate water similarly to compound **17**; 87% filled H_2O@**18** was achieved after a solution of **18** in toluene was heated at 70 °C for 24 hours.[66]

Certainly the works of Wudl, Rubin and Iwamatsu succeeded in developing efficient methods for the controlled severing of the C_{60} cage, underscoring the crucial aspect of the size of the orifice in the molecular surgery approach. However none of these groups undertook the challenge of suturing the orifice back to the pristine C_{60} structure, in conditions that would trap the guest atom or molecule inside the cage. In Wudl's ketolactam **3**, and Rubin's dilactam **10**, this challenge was complicated by the presence of the unreactive amide group which made the cage scission hardly reversible. In Iwamatsu's OCFs the suturing process was made very difficult by the high functionalization of the cage and by the mere size of the orifice. In fact, any reaction which reforms bonds is an intramolecular process and will not occur if the two atoms that have to bind are kept far apart by a large gap. Moreover, a large opening provides an easy way out for the guest molecule under ordinary reaction conditions. Indeed, Iwamatsu's research focused uniquely on the controlled scission of the C_{60} cage and on the incorporation of atoms and molecules.

Shortly after Rubin published **H_2@10**, Komatsu *et al.* accomplished the quantitative incorporation of hydrogen inside an open-cage fullerene.[67] The OCF used, 13-membered compound **23**, was once again prepared starting from the [4+2] cycloaddition of C_{60} with 3-(2-pyridyl)-5,6-diphenyl-1,2,4-triazine, followed by a cascade retro[4+2]/[4+4]/retro[2+2+2] reaction to form fulleroid **21**. Reaction with $^1O_2$ and finally an electrophilic addition of elemental sulphur on compound **22** afforded OCF **23** in 23% overall yield (Scheme 15).[68]

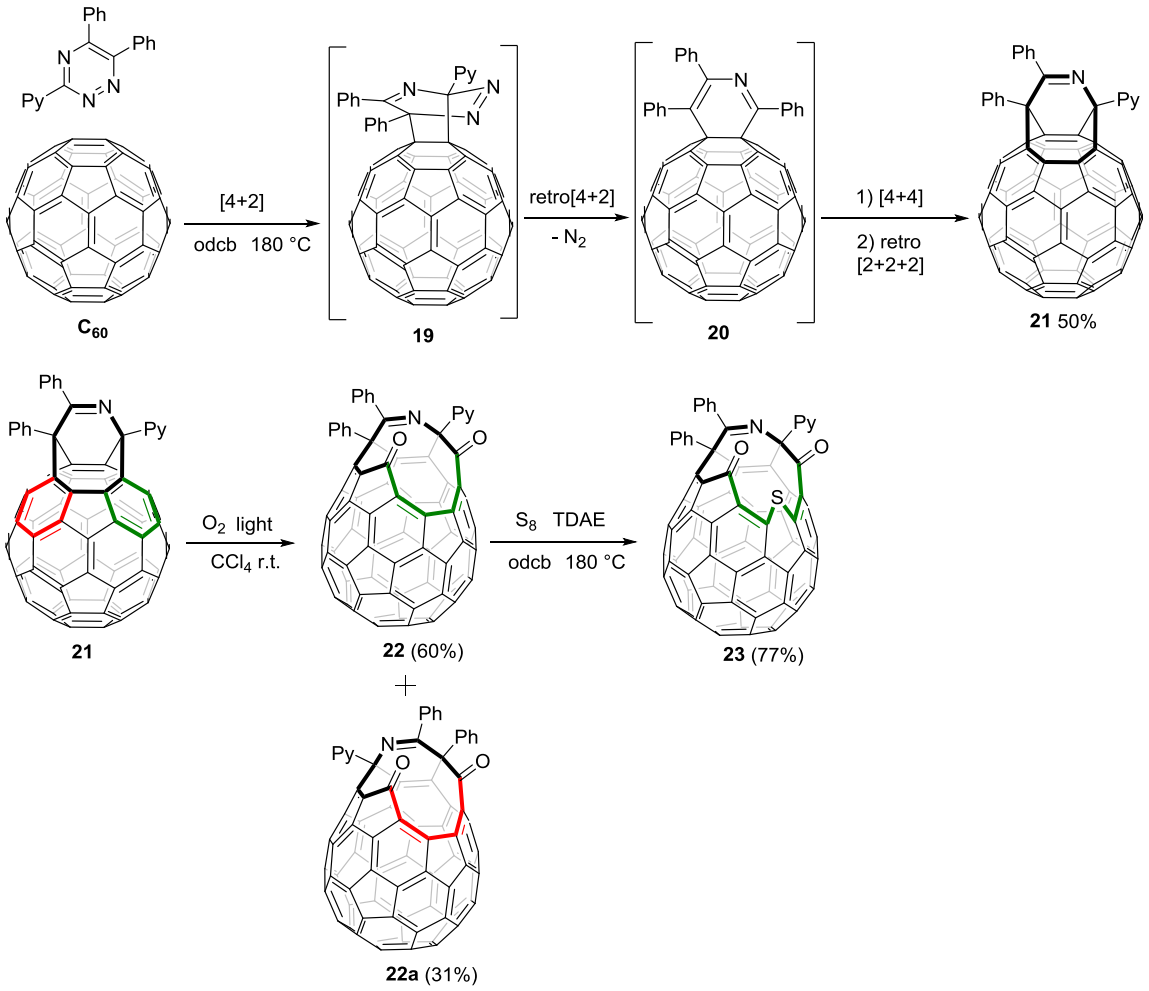

Scheme 15: Synthesis of OCF 23.

The first four transformations are very similar to Rubin's synthesis of fulleroid **5** (Scheme 6), the only difference being that the possibility of extruding molecular nitrogen results in the *in situ* formation of the intermediate **20**, avoiding the need of its pre-synthesis. By contrast, Rubin had to pre-form **4** via 4 steps (Scheme 16).[69]

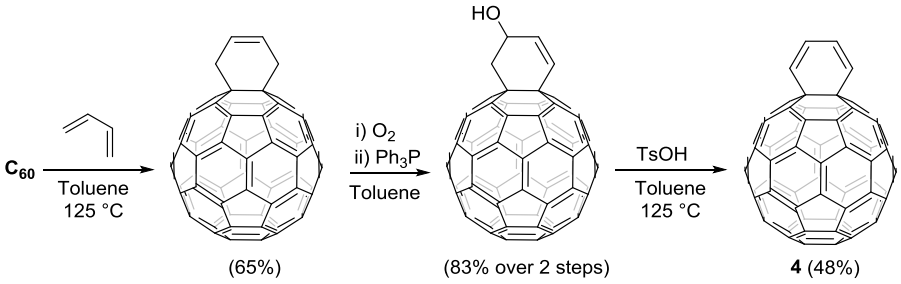

Scheme 16: Rubin's synthesis of fulleroid **4**.

In Komatsu's synthesis the [4+4] step takes place without irradiation, probably through a thermally induced radical mechanism. Oxidation of asymmetric **21** leads to formation of the two regioisomers **22** and **22a**, the former being reacted with elemental sulphur in the presence of the strong reducing agent tetrakis(dimethylamino)ethylene (TDAE) to afford **23**. Exposure of solid **23** to 800 atm of hydrogen at 200 ˚C for 8 hours resulted in the quantitative filling without decomposition of the substrate. The filling factor was dependent on the pressure and dropped to 90 and 51% when the pressure was lowered respectively to 560 and 180 atm. Due to the small size of the orifice, hydrogen was released from **H_2@23** only by heating above 160 ˚C. The following two years saw the development of a strategy for the suturing of **H_2@23**; in 2005 the synthesis of **H_2@C_{60}** by molecular surgery was finally accomplished (Scheme 17).[70]

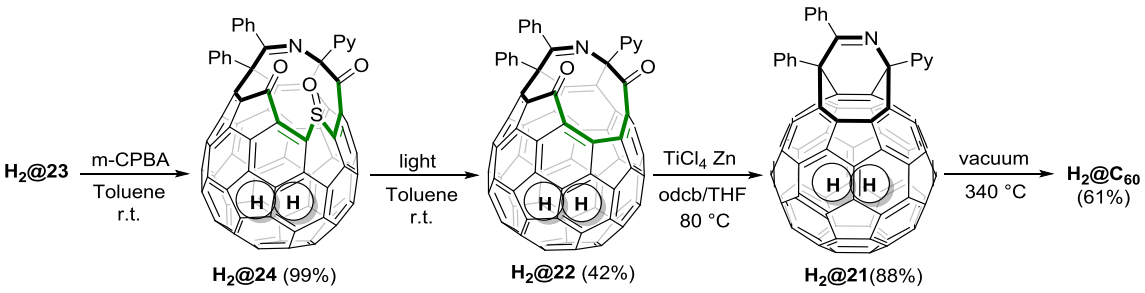

Scheme 17: Synthesis of **H_2@C_{60}** from **H_2@23**.

The step-wise reduction of the orifice started with the oxidation of **H_2@23** to the sulphoxide **H_2@24**, which was reduced to **H_2@22** by extrusion of sulphur monoxide under irradiation. Coupling of the two carbonyl groups on **H_2@22** through a McMurry reaction resulted into the isolation of **H_2@21**. All of these steps were carried out at temperatures well below 160 ˚C so that the loss of hydrogen was completely avoided. Finally **H_2@C_{60}** was obtained by vacuum

thermolysis of H_2@**21** at 340 °C. These conditions allowed the re-forming of the C_{60} cage by a cascade [2+2+2]/retro-[4+4]/retro-[2+2+2]; but some endohedral hydrogen (~9%) was lost in the process (Scheme 18).

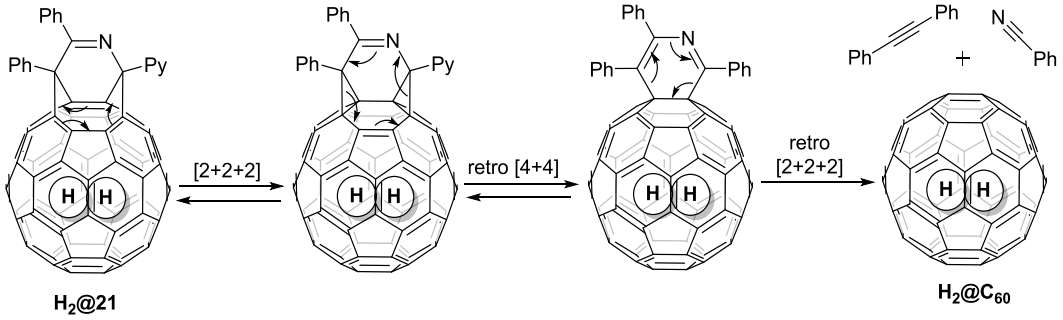

Scheme 18: Proposed mechanism for the formation of H_2@C_{60} from H_2@**20**.

Overall 90% filled H_2@C_{60}, was afforded in 8 steps and 5% yield from C_{60}. In 2010 the same group extended this molecular surgery to the synthesis of He@C_{60}; in this case the encapsulation inside **23** was complicated by the low binding energy of the guest atom with the cage (-8.8 KJ/mol for **He@24** compared to -22.3 KJ/mol for H_2@**23**).[71] This shifted the filling equilibrium to the side of the empty OCF. Moreover the tiny helium atom trapped inside **He@23** was easily lost at room temperature. For this reason the incorporation was carried out on **24** so that, once the equilibrium was reached, the orifice size could be reduced directly avoiding the isolation of **He@23** or **He@24**. The filling was carried out at 115 °C under 1230 atm of helium; the use of high pressure was necessary to counter-balance the low binding energy of the guest with the cage. Finally 30% filled He@C_{60} was isolated after closing the orifice of **He@22** as for H_2@C_{60}. While quantitatively filled H_2@C_{60} was isolated by HPLC, 30% filled He@C_{60} could only be enriched to 60% after 70 consecutive HPLC cycles.[70,71]

The small orifice of OCF **23** limited the utility of the first complete molecular surgery to the incorporation of helium and hydrogen, and clearly precluded the encapsulation of any larger molecule. This limit was outdone in 2011 by the group of Y. Murata with the first synthesis of H_2O@C_{60}.[72] This novel complete molecular surgery used a new OCF, compound **28**, fitted with a 16-membered orifice. Its precursor, OCF **27**, was still synthesised using an approach similar to that used to prepare compound **22** (Scheme 19).

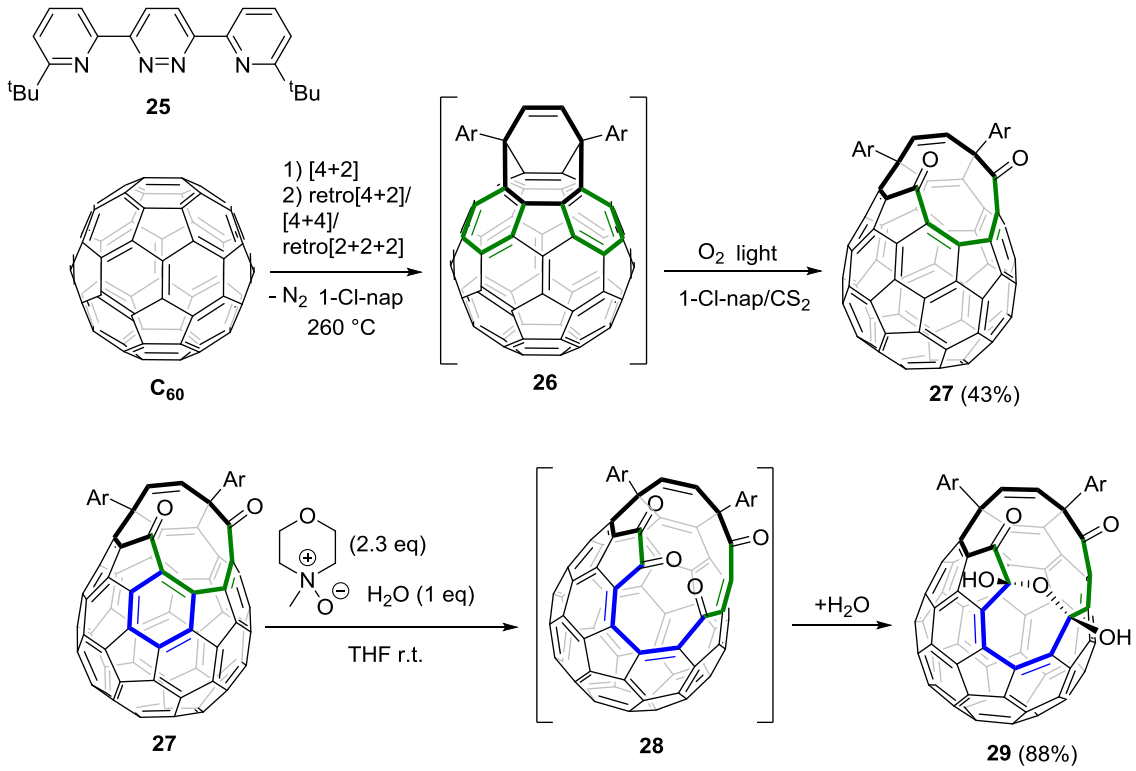

Scheme 19: Synthesis of OCF **29**.[72]

In this particular case C_{2d} symmetric **26**, obtained by [4+2] cycloaddition of C_{60} with pyridazine **25**, followed by a thermal cascade reaction analogous to the one employed for the synthesis of **21** (Scheme 15), was reacted with $^1O_2$ to afford **27** as the only product. Reaction with the oxygen nucleophile NMO on the electron-poor butadiene moiety located on the rim, led to the formation of **28**; this OCF was isolated as its hydrate **29** after work up and chromatography. OCF **28** was never isolated in the original work and its existence was not definitely demonstrated. Refluxing a solution of **29** in toluene in the presence of water resulted in the isolation of 8% filled **H_2O@29**. When the process was repeated under pressure, 40% and quantitatively filled **H_2O@29** were isolated respectively applying 5000 and 9000 atm.[72] Water is too large to pass through the 13-membered orifice of OCF **29**. The formation of **H_2O@29** was therefore explained assuming that, initially, equilibrium between compounds **28** and **29** was established in the filling conditions. The water molecule could then pass through the 16-membered orifice of OCF **28** and relocate into its cavity. Finally, hydration of **H_2O@28** resulted into **H_2O@29**, with the reduction of the orifice effectively locking the water molecule inside the fullerene (Scheme 20). The latter is the crucial aspect of this molecular surgery, since water is not only

used to fill the empty cage, but as well to act as a removable stopper to close the orifice.

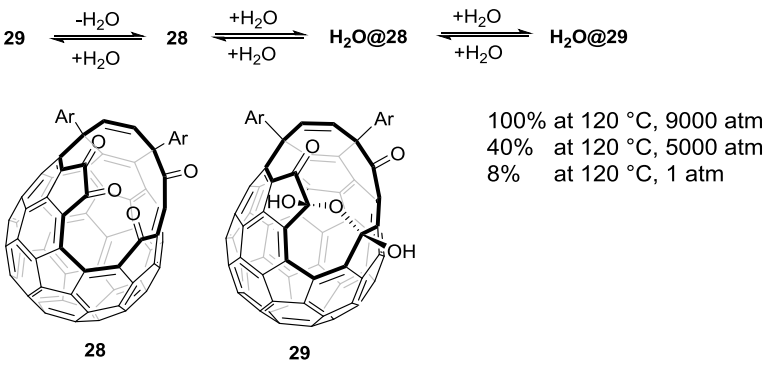

Scheme 20: Equlibria of formation of **H_2O@29**.

The reduction of the orifice of **H_2O@29** was carried out in only two steps (Scheme 21).

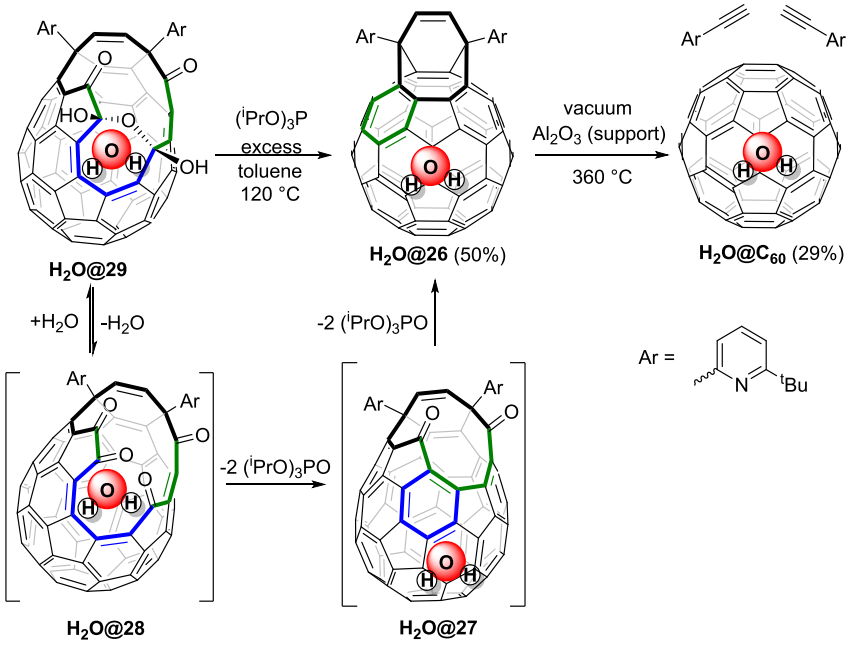

Scheme 21: Synthesis of **H_2O@C_{60}** from **H_2O@29**.

The first reaction consisted in a sequential carbonyl coupling with a phosphite alkyl ester. In order to explain this reactivity, it was once again postulated the formation of the intermediate **H_2O@28** in the reaction environment. The second reaction was a thermolysis under vacuum, similar to that employed for the closure of **H_2@21** and **He@21**. No endohedral water was lost during the closure and quantitatively filled **H_2O@C_{60}** was overall synthesised in 5 steps and 5% yield from pristine C_{60}. Komatsu's and Murata's syntheses are the only

complete molecular surgeries that have been reported so far. The challenge for the enclosure of other guests is still ongoing. Recently, Murata *et al.* extended the reaction of insertion of electrophilic sulphur in the presence of TDAE to OCF **28**. The 16-membered orifice was enlarged and OCFs **30** and **31** having respectively 17- and 18-membered openings were isolated. Lower amounts of TDAE were found to favour the formation of the intermediate **30** over the double insertion product **31**. The thio-fulleroid **32** was the only product formed when an excess of TDAE was used for prolonged reaction time (Scheme 22).[73]

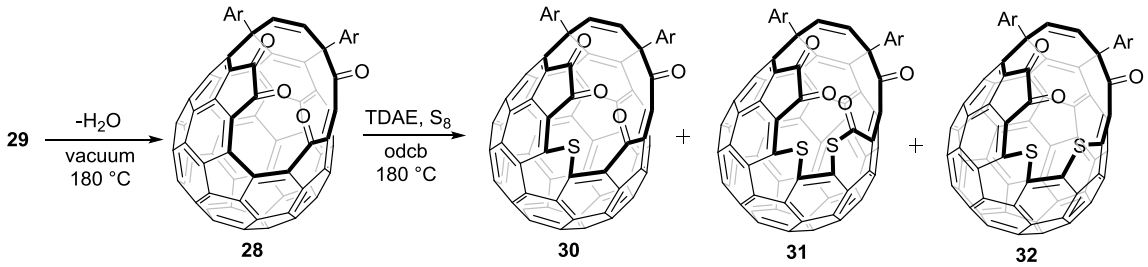

Scheme 22: Generation of OCFs **30**, **31** and thio-fulleroid **32**.[73]

OCFs **30** and **32** were found to readily encapsulate water at room temperature producing filling factors of 40 and 70% respectively. This marked difference originates from the reduced size of the orifice of **32** since a carbon atom on the rim has been replaced by the more voluminous sulphur. Consequently, the smaller opening makes OCF **32** much more efficient at trapping water. The larger opening of OCF **31** made the encapsulation of water (30% filling factor) already possible at -25 °C, while at room temperature the endohedral molecule was irreversibly lost. When a solution of **32** was equilibrated in the presence of water and under nitrogen atmosphere, water and nitrogen competed for the empty cage. **H_2O@32** and **N_2@32** were formed respectively in 52 and 48% yield. A procedure for the suturing of these new large orifices is still under development.

Chapter 2: Discussion

2.1 Opening an orifice in C_{60}

The molecular surgery technique allows the encapsulation of a virtually isolated small molecule inside an inert three-dimensional environment. Due to their stability and ease of handling, endofullerenes are very convenient systems for the study of isolated molecules over a wide range of conditions. For instance, $\mathbf{H_2@C_{60}}$ and $\mathbf{H_2O@C_{60}}$ have been used to study the hydrogen and water molecules as quantum rotors, and their energy level structure has been mapped by IR spectroscopy,[74–76] neutron scattering,[77–79] and NMR.[77,80]

At the beginning of this work, the very limited supply of small molecule endofullerenes available for physical studies prompted the research for improvements in their preparation. The recently discovered $\mathbf{H_2O@C_{60}}$ was, by far, the most demanded endofullerene and consequently, its molecular surgery was the obvious starting point of this investigation. A convenient route to pyridazine **25** is the crux to produce a steady supply of the key OCF **29**. The reported route[72] to **25** featured a Kumada coupling of Grignard **34** with 3,6-dichloropyridazine. Pyridine **33** was in turn synthesised by addition of t-butylcyanocuprate to 2,6-dibromopyridine (Scheme 23).

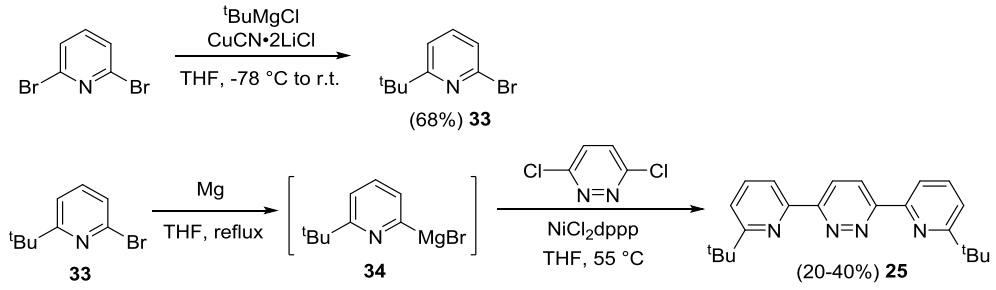

Scheme 23: Synthesis of pyridazine **25** via Kumada coupling.

The cross-coupling reaction was the limiting step of the procedure, giving yields ranging from 20-40% due to low reproducibility in the formation of the Grignard reagent. The best results were achieved when activated Mg, prepared using Rieke's method,[81] was used for the synthesis of the Grignard. In order to avoid the use of stoichiometric amounts of CuCN, a CuI catalysed coupling of tertiary Grignard reagents[82] to nitrogen heterocycles was extended to the synthesis of **33**. To overcome the reproducibility problem associated with the

synthesis of **34**, the coupling reaction was attempted using the Negishi[83] protocol. Pyridine **33** was initially lithiated. Low temperature (-95 °C) and slow addition of n-buthyllithium was crucial to avoid deprotonation of the pyridyl ring and consequential loss of regioselectivity. The lithium pyridine was then transmetalated with $ZnCl_2$, and the resulting organozinc specie finally coupled with 3,6-dichloropyridine in the presence of catalytic palladium-tetrakis(triphenylphosphine). Through this route, pyridazine **25** was isolated in 68% yield after work up and chromatography (Scheme 24).

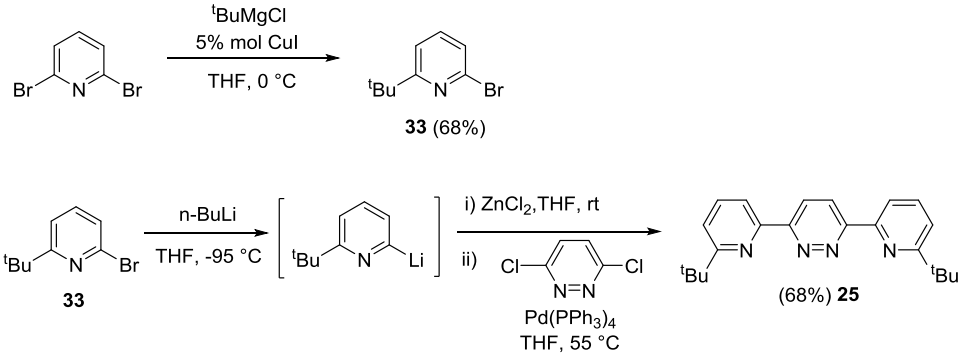

Scheme 24: Synthesis of **25** via Neghishi coupling.

Heating the cross-coupling reaction mixture above 45 °C afforded selectively the di- over the mono-substituted pyridazine. This temperature effect has already been reported in the literature for similar reactions.[84]

Refluxing pyridazine **25** with one equivalent of C_{60} in thoroughly degassed 1-chloronaphtahlene yielded a solution of the intermediate fulleroid **26**. HPLC analysis showed complete conversion of **25** within one day. The crude reaction mixture was then diluted with carbon disulphide and directly used for the next $^1O_2$ oxidation step. A specifically designed jacketed reactor was used to carry out this transformation (Figure 4). This reactor maintained the reaction mixture at room temperature while illuminating with a 400 W halogen lamp placed at close distance.

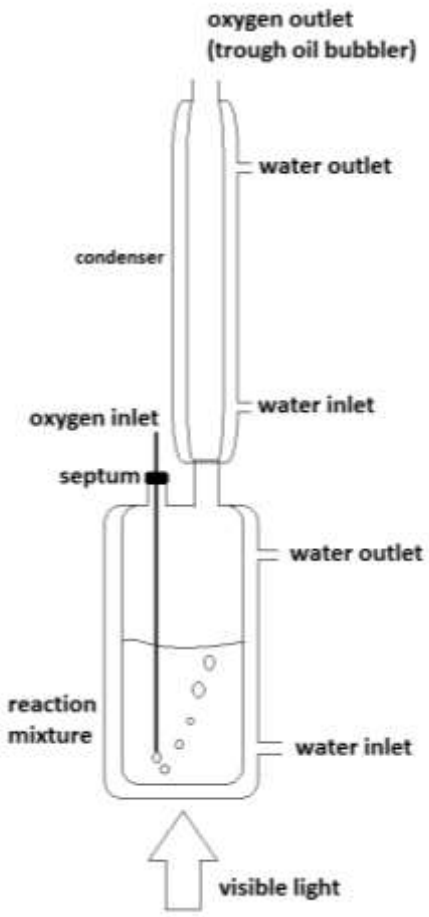

Figure 4: Apparatus used for the oxidation of OCF **26**.

This set-up greatly reduces the risk of explosion associated with having a carbon disulphide/oxygen mixture inside a hot vessel. A 1.3% mixture of the volatile (b.p. = 46 ˚C) carbon disulphide in air is flammable and its auto ignition temperature is as low as 90 ˚C.

HPLC analysis of the oxidation mixture showed complete conversion of **26** within twenty hours; OCF **27** was isolated after chromatography over a short silica gel column affording a comparable yield to the reported reaction. With this apparatus, a diligent worker could safely produce more than two grams of **27** in three working days. The optimisation of this synthesis of OCF **27** was attempted next. As precedent work by Murata *et al.* described,[68] the oxidation reaction proceeded cleanly; therefore the attention was focused on the reaction of C_{60} with pyridazine **25**. In particular HPLC analysis of the crude reaction mixture showed complete conversion of **25** after twenty hours; at the same time a significant amount of C_{60} was still present. Refluxing compound **25** in 1-chloronaphthalene for sixty hours resulted in the re-isolation of the unmodified

pyridazine. This experiment demonstrated the stability of **25** under the reaction conditions; hence, its decomposition in the reaction environment was dismissed. Prolonged reaction time for both the cycloaddition sequence, and the oxidation step (respectively 72 and 36 hours), did not lead to lower isolated yield of **27**. Consequently the decomposition of the intermediate **26** and of the product **27** in the reaction conditions was also ruled out. An experiment carried out using an excess (1.5 equivalents) of **25** resulted in increased conversion of C_{60}, but not in an increment of the isolated yield of **27**. This result suggested that OCF **26** competed with C_{60} ($k_1 \approx k_2$) for the reaction with **25**. Therefore, this irreversible side reaction was responsible for consuming **26** in the reaction environment (Scheme 25).

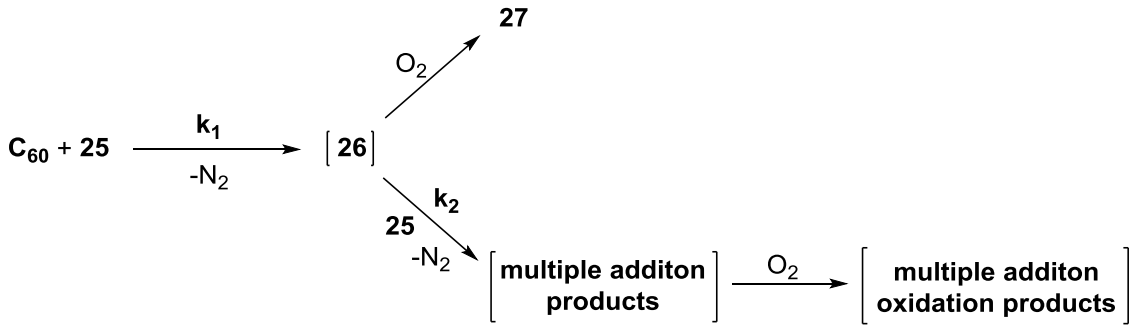

Scheme 25: Reactivity of **25** towards C_{60} and OCF **26**.

The products formed from multiple addition of pyridazine **25** on C_{60} co-elute with the 1-chloronapthalene peak in the HPLC. Indeed the absolute intensity of this peak in the HPLC chromatogram varied over time. Simultaneously its intensity relative to **26** remained virtually unchanged irrespectively to the amount of pyridazine used, further evidence of the similar reactivity of C_{60} and **26** towards **25** (Figure 5).

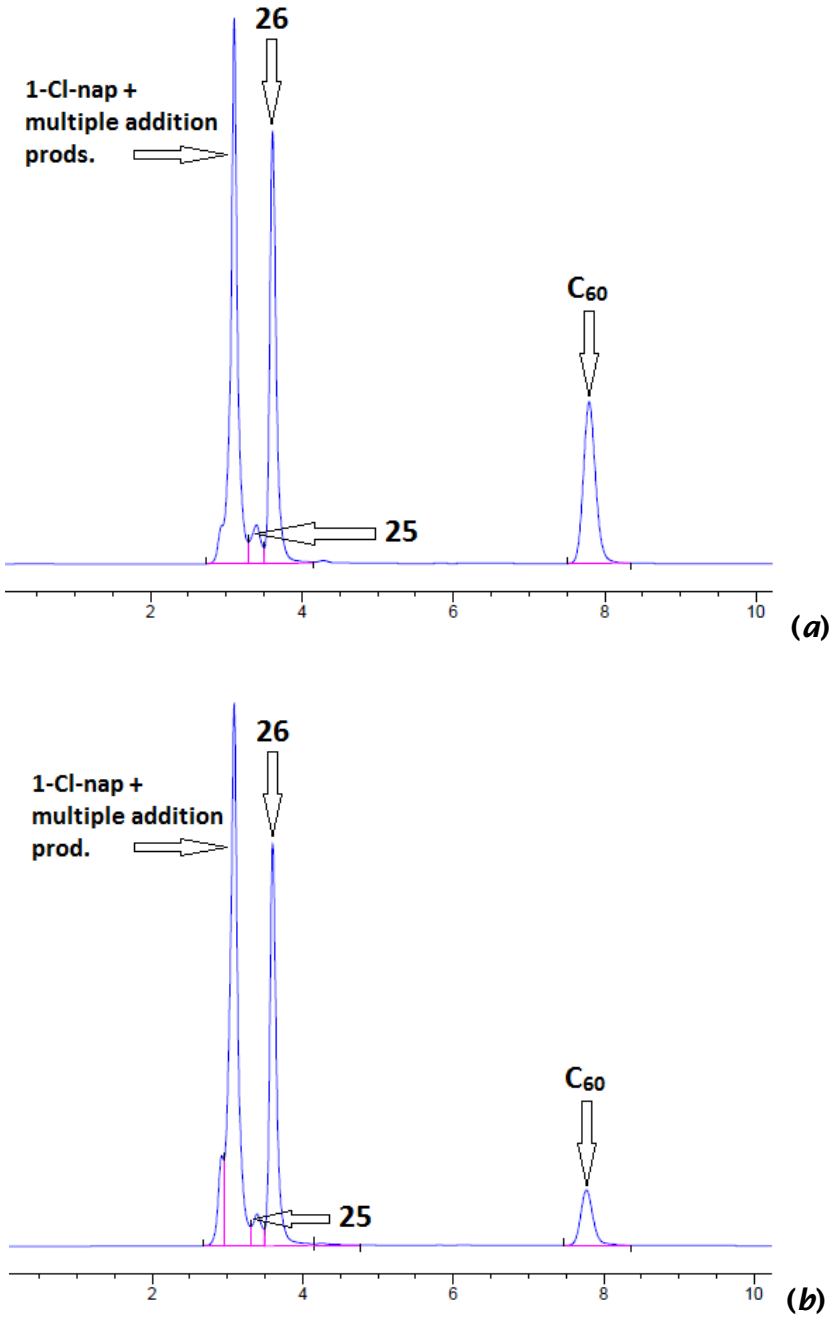

Figure 5: HPLC chromatograms (Buckyprep, toluene) of the reaction of C_{60} with variable amounts of pyridazine **25** after completion. Equimolar amounts (*a*); Excess (1.5 eq) of pyridazine (*b*).

The use of a large excess of C_{60} represented the only way to favour the formation of compound **26** over the multiple addition products. However, this expedient would have resulted in a waste of precious substrate. In fact, the unreacted C_{60} recovered from the reaction mixture had a substantial amount of an impurity, most likely fullerene oxide formed by reaction of $^{3}C_{60}$ with $^{1}O_{2}$.[85]

This contamination precluded the recycling of the substrate used in excess (Figure 6).

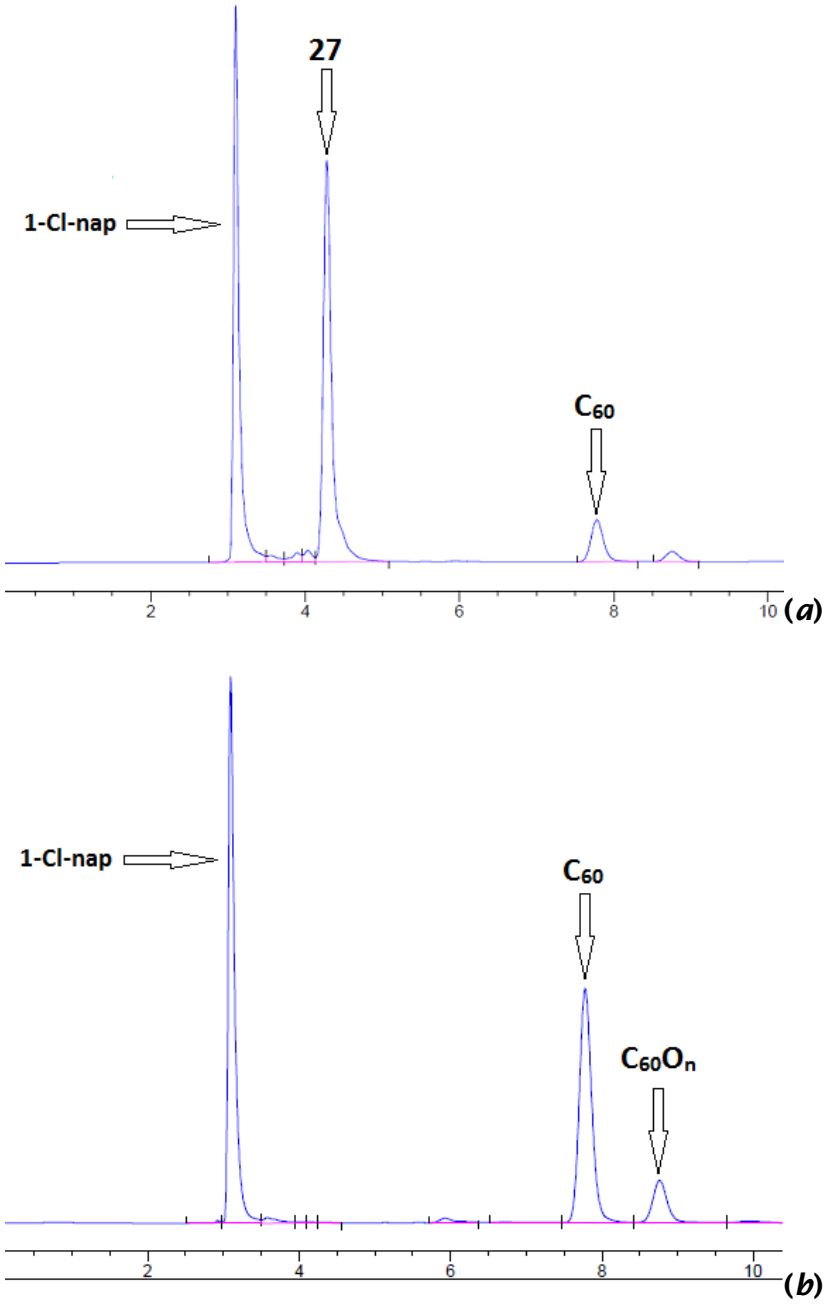

Figure 6: HPLC chromatogram of the oxidation of **26** with $^1O_2$ after completion (*a*). Chromatogram of the C_{60} recovered from the reaction mixture after chromatography (*b*).

Oxidative cleavage of diketone **27** with N-methylmorpholine-N-oxide (NMO), led to the isolation of hemiacetal **29** in yield comparable to the reported value

(88%). Because this final step in the opening sequence worked well, a study on the filling of OCF **29** with water was initiated.

2.2 Filling a hydrophobic cavity with water

Apolar substances show a characteristic tendency to aggregate and form a separate phase in an aqueous environment. Similarly, water is confined into droplets when it comes in contact with a non-wettable surface. The hydrophobic effect is the cause of these common observations and provides the driving force behind many chemical, physical, and biological phenomena. The positive ΔG value of the hydrophobic effect arises from the entropic, rather than the enthalpic contribution. Measured values of ΔH for the dissolution of an apolar solute in water are very close to zero, while negative ΔS values make the process overall endergonic. According to a well-known theory,[86] the decrease in entropy is explained by considering the local change in structure that follows the solubilisation of an apolar solute. The dissolution of the solute leads to the formation of a cavity, where the water molecules rearrange themselves into an ordered ice-like clathrate structure. This increase in order is responsible for the negative ΔS value. The aggregation of the apolar solute arises from the tendency to avoid the formation of clathrates, by minimising the contact surface between the two phases. Alternatively, through a statistical mechanics treatment, the hydrophobic effect has been attributed to the small size of the transient cavities most probably formed in water, which are not suitable to enclose an apolar solute.[87,88]

While the dissolution of apolar compounds in water has been studied in detail, the closely related process of dissolution of water in apolar solvents has not been analysed as much. Experimental evidence points out that water vapour in equilibrium with massive liquid water dissolves in organic solvents.[89] Specifically, liquid water initially vaporises, breaking its clustered structure and becoming a virtually ideal gas (*i.e.* monomeric) for temperatures ≤100 °C, and pressures up to saturation. The isolated water molecules that form the vapour then dissolve in the organic solvent following Henry's law, occupying its transient cavities. Aliphatic, aromatic and chlorinated hydrocarbons dissolve small amounts of water mainly as the monomer. Polar organic solvents, in addition to dissolving much more water, greatly favour its association in solution. The related question, if water can occupy a pre-formed hydrophobic

cavity, is still debated. Some experiments show that, due to the hydrophobic effect, fitting a water molecule inside an apolar cavity is an extremely challenging process. For instance, Wolfenden *et al.*, studying the solubility of water in n-hexane as model (*i.e.* the filling of hydrophobic cavities in n-hexane with water), concluded that a pre-formed hydrophobic cavity can enclose a water molecule; however the probability for such event to occur in the presence of bulk water is extremely low.[90] Vaitheeswaran *et al.* investigated the stability of water clusters inside giant fullerenes and graphitic cavities using Monte Carlo simulations. According to this study, water can fill such cavities; however, a stable situation is achieved only with large cages (≥10 Å in diameter) enclosing hydrogen-bonded water clusters.[91] In contrast, the experimental results of Murata,[72,73] Iwamatsu,[56] and Gan[66] (cf. 1.3) demonstrate that the much smaller hydrophobic cavity of an OCF can incorporate a water molecule with relative easiness.

On these premises, the encapsulation of H_2O inside the cavity of **29** was investigated. Although it was known that a quantitative filling factor could be reached at 120 °C and 9000 atm, the equipment necessary to reach that very high pressure was not available. The experiments carried out by Murata showed that pressure was just used to shift the filling equilibrium towards the endofullerene side, and that heating the solution at 120 °C provided enough energy to overcome the activation barriers behind all of the equilibria involved (cf. 1.3, Scheme 20).[72] The encapsulation of water by an OCF dissolved in an organic solvent can be described as the overall partitioning of water between two environments of different hydrophobicity, one being the solvent and the other the fullerene cavity. Since the chemical potential is a measure of the tendency of particles to diffuse, the distribution of water between the two cavities will be determined by the difference of chemical potential of water inside the OCF cavity and in the organic solvent.[91] The chemical potential of water inside the OCF cavity depends mainly on the attraction between the guest molecule and the walls of the cavity. In this case, pressure is not expected to play a major role since it cannot affect the structurally rigid fullerene cavity. Therefore, this chemical potential cannot really be changed from the outside. In the solvent bulk, the chemical potential will still depend on the attractive force between the transient cavity and the water molecule. Indeed, all the encapsulation experiments reported in the literature are

performed in aromatic or chlorinated hydrocarbons solutions. Water incorporation has not been achieved in polar organic solvents, since those stabilise water so much. In this environment, the chemical potential of water will be affected by pressure as well. In fact, by applying very high pressure, Murata was able to shift quantitatively the water filling equilibrium towards **H_2O@29**. A study by Frunzi *et al.* on the encapsulation of water inside OCF **15** showed that solvents can differ greatly in stabilising a water molecule, producing different filling factors of the same cage in comparable conditions.[92] Therefore, the solvent was envisioned as a possible tuneable parameter to maximise the incorporation of water.

Heating a solution of **29** in wet toluene-d_8 inside an NMR tube, demonstrated that incorporation over 8% could be achieved under atmospheric pressure. ^{1}H NMR spectra taken over time showed that equilibrium was reached after a few hours at 120 °C. A filling factor of 23% was estimated by comparing the integrated intensity of the endohedral water signal with the integrated intensity of the exohedral protons taken as reference. Due to the strong magnetic shielding effect of the fullerene cage, the endohedral water resonates at negative chemical shift and is easily detectable by ^{1}H NMR (Figure 7).

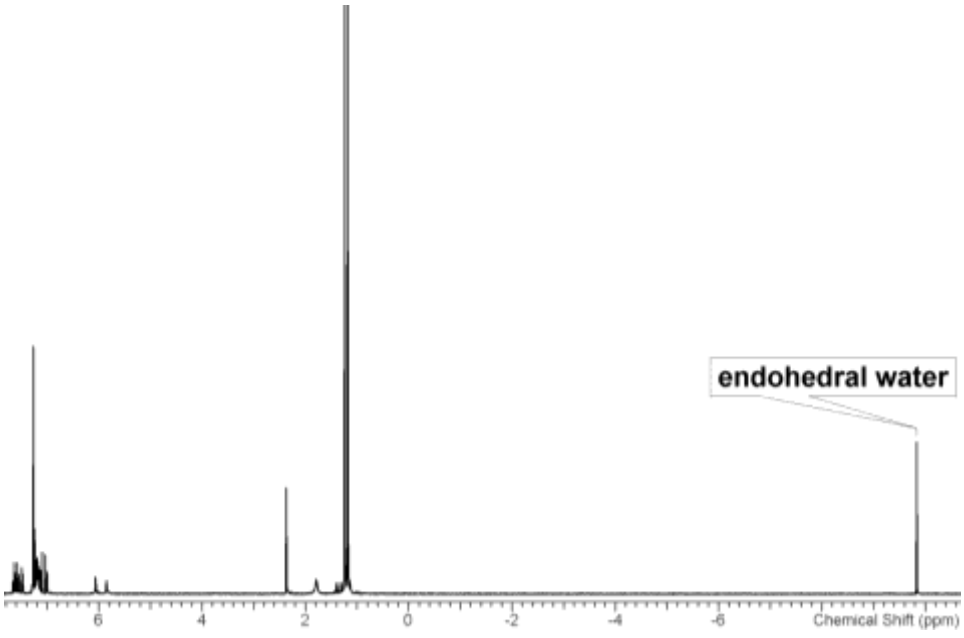

Figure 7: ^{1}HNMR ($CDCl_3$, 400 MHz) spectrum of 78% filled **H_2O@29**.

The exohedral protons of **29** and those of **H_2O@29** give rise to the same signals in the ^{1}H NMR spectrum, and can therefore be used as an internal reference to estimate the filling factor. Equilibrating a solution of **29** in wet

toluene in the same conditions for 500 hours failed to give filling factor higher than 23%; once again demonstrating that the incorporation achieved was due to the establishment of equilibrium. During these experiments, heating the wet toluene solution caused the dissolved water to distil and condense over time on the cold sides of the tube. This limited the amount of water present in solution, and consequently, the filling factor achievable in these conditions. Saturating the reaction vessel with water vapour was envisioned as a way to counteract this phenomenon, since the amount of water dissolved in the organic solvent is dependent on the partial pressure of water vapor (Scheme 26).

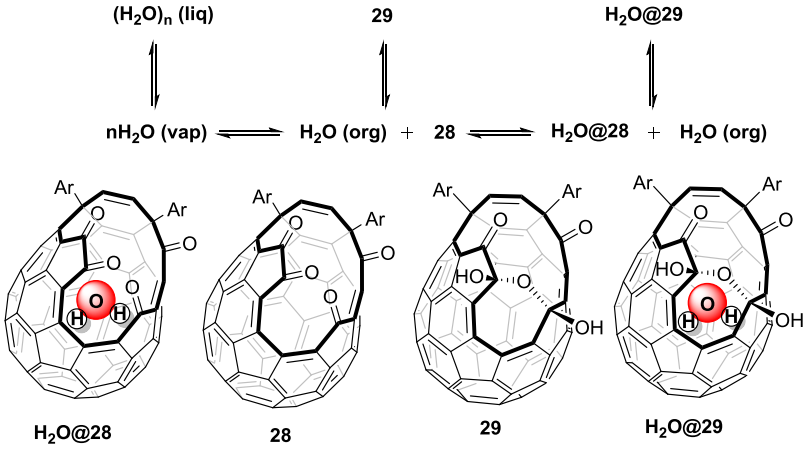

Scheme 26: Equilibria of formation of **H_2O@29** in the presence of liquid water.

A significantly higher filling factor (45%) was achieved in this case. Experimentally, this saturation could be produced in three different ways: (*i*) by periodically shaking the reaction vessel to allow the condensed water to come in contact with the hot solution, and vaporise again; (*ii*) by having a massive amount of water boiling inside the reaction vessel; or (*iii*) by completely immersing the reaction vessel inside the oil bath to keep the temperature constant all around the apparatus. The third set-up was the most practical, and was used in all the experiments that followed. A Schlenk tube fitted with a J.Young tap was used, which was filled with a 20mg/ml solution of **29**, and sufficient water (~5.6 equivalents) to saturate the head space with water vapour at 120 °C. The solution was thoroughly degassed and the tube was sealed under Ar gas (1 atm) to minimise decomposition; *circa* 90% of the starting material was recovered after flash chromatography. The effect of the solvent was investigated using this set-up. The filling factor reached at

equilibrium followed the trend: 1-chloronapthahalene (66%) > 1,2-dichlorobenzene (61%) > toluene (45%) > benzene (39%). A similar trend, where chlorinated aromatics tend to favour the encapsulation over their protonated counterparts, was also found by Frunzi *et al.* in their experiments on the formation of **H_2O@15**.[92] According to their measured thermodynamical data, the ΔH and ΔS for the incorporation equilibrium always assume negative values and both increase as the polarity of the solvent increases. In polar aromatic solvents however, a particularly large increase in the ΔS value makes up for the enthalpic destabilisation so that overall the incorporation is more favourable. As for any other chemical equilibrium, the filling of compound **29** will be affected by change in temperature. Indeed when the temperature was lowered from 120 °C to 100 °C, the filling factor in 1-chloronaphthalene increased from 66 to 78%, as it was expected for an entropically disfavoured process. Although the equilibrium was reached only after two days, this novel water encapsulation methodology provides a very practical alternative to the previous very high pressure procedure.

2.3 The case of deuterium oxide

In their original synthesis of **H_2O@C_{60}**, Kurotobi *et al.* reported that D_2O could be encapsulated quantitatively by the same high pressure method. However, their filling experiment was carried out using a mixture of H_2O and D_2O and therefore a mixture of **D_2O@C_{60}**, **HOD@C_{60}**, and **H_2O@C_{60}** was isolated at the end.[72] In order to extend the novel low pressure filling protocol to the synthesis of **D_2O@29**, a solution of **29** in 1-chloronaphthalene was heated at 100 °C inside a Schlenk tube saturated with D_2O vapour (cf. 2.2). After suturing the orifice (cf. 2.4) the endofullerene isolated contained D_2O, HOD and H_2O in relative ratio of 40:10:1, as determined by NMR (Figure 8).

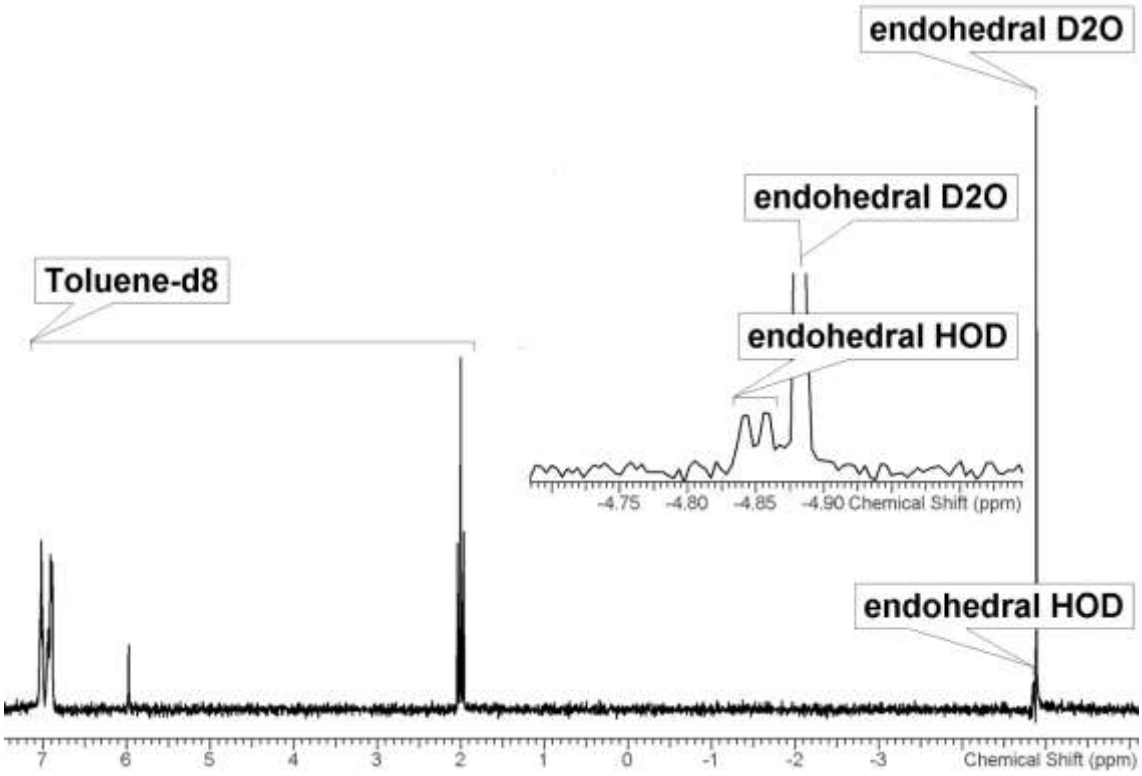

Figure 8: ^{2}H NMR (61 MHz, toluene) spectrum of a 40:10:1 sample of $D_2O/HOD/H_2O@C_{60}$.

The presence of H_2O and HOD inside the cage was thought to originate from the *in situ* dehydration of **29**, which released one equivalent of H_2O in the environment. The protons from the H_2O released by the substrate exchanged with the deuterons in D_2O, producing a D_2O, HOD, and H_2O mixture that was encapsulated in the cage. Alternatively, this mixture could originate from exchange with the protons of the solvent. The latter possibility was ruled out by running two parallel D_2O filling experiment, respectively using toluene, or toluene-d_8 as solvent. In both cases, the ^{1}H NMR spectrum showed the presence of H_2O and HOD in relative ratio of 1:10. On the other hand, when an excess (200 equivalents) of D_2O was used, a H_2O: HOD ratio of 0.07:1 was afforded. The large excess of D_2O diluted the H_2O and HOD present in the reaction environment, making their incorporation much less probable. Preforming tetraketone **28** represented the only way to avoid the release of H_2O during the filling. A solution of compound **29** in toluene was refluxed for one hour while the condensing solvent was desiccated through a column of activated 3Å molecular sieves. After evaporation to dryness by vacuum distillation, compound **28** was afforded in quantitative yield. The ^{1}H NMR spectrum still showed the same spin systems of its parent compound **29**; nevertheless, the

various protons displayed different chemical shift, reflecting the different structure. The broad singlets arising from the hydroxyl protons, visible in the ^{1}H NMR spectrum of **29,** were not present. Most importantly, the ^{13}C NMR spectrum of **28** clearly showed the presence of four carbonyl groups (Figure 9).

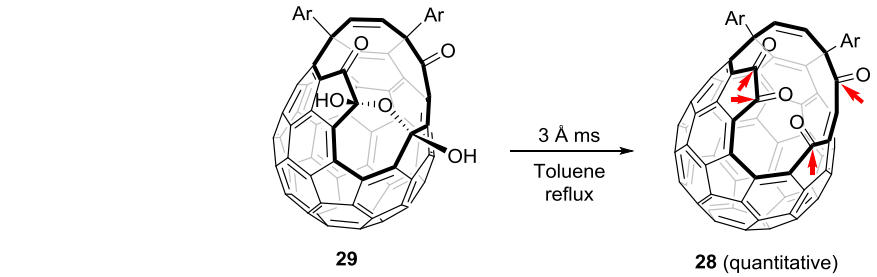

29 **28** (quantitative)

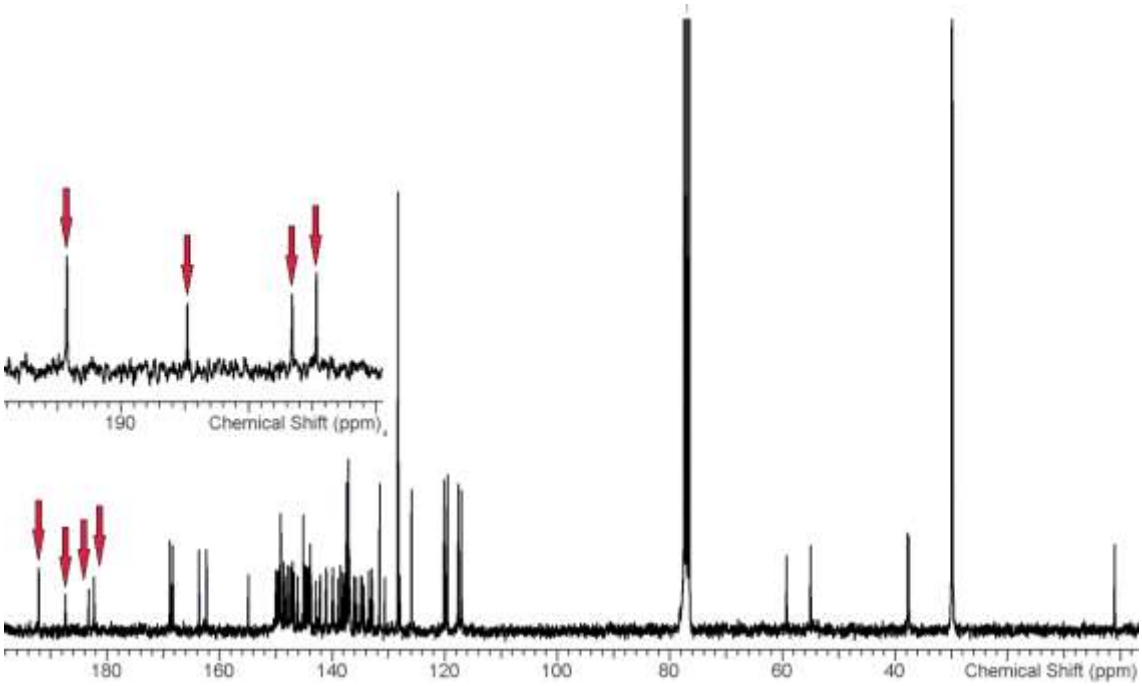

Figure 9: ^{13}C NMR (75 MHz, $CDCl_3$) spectrum of compound **28**. The peaks of the characteristic CO groups are indicated by red arrows.

The characterisation data agrees with the values reported by Futagoishi *et al.* which, roughly at the same time, independently isolated compound **28** using a different procedure.[73] OCF **28** was stable in anhydrous conditions, however it immediately hydrated to **29** in the presence of moisture. Likewise, addition of ethanol to **28** resulted in the formation of its ethyl hemiacetal. In theory, this nucleophilic attack could afford a mixture of regioisomers, but experimentally only a single compound was isolated. In the absence of x-ray data it is not possible to definitely determine the regiochemistry of fulleroid **29a**. However, the regioselectivity observed for this transformation is likely due to a structural

feature of **28**. In fact one of the carbonyl groups is bent towards the middle of the orifice so that its oxygen is just 2.6 Å away from the carbon atom of the carbonyl group across the orifice. Hence, a nucleophilic attack on this centre can trigger the formation of the oxygen bridge with minimal distortion of the structure (Scheme 27). An analogous regioselctive addition of alcohols to a structurally similar OCF has been reported by Hashikawa,[93] tough the transformation was not described in detail.

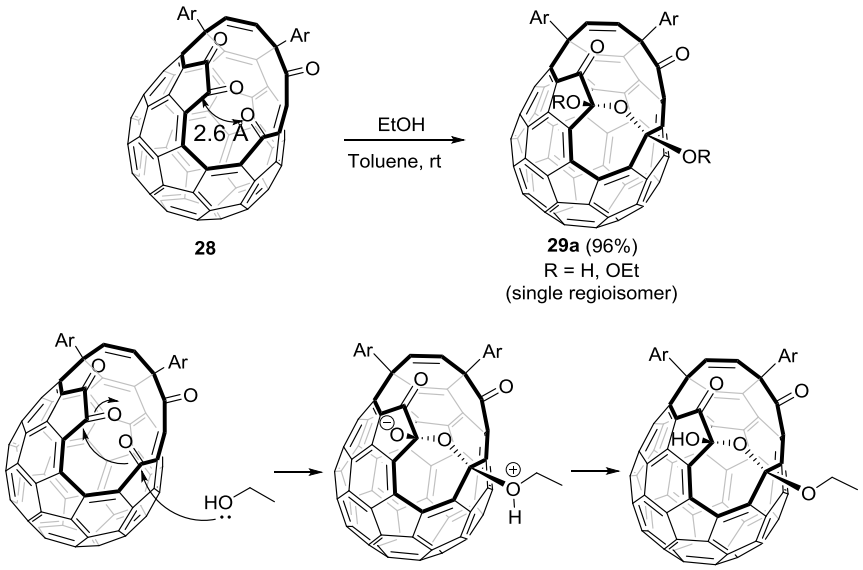

Scheme 27: Hypothetical mechanism for the addition of ethanol to OCF **28**.

Dissolution of **28** in 1-chloronaphthalene, addition of D_2O and heating at 100 °C for 48 hours gave 78% filled **D_2O@29**. This time no endohedral HOD or H_2O was visible by NMR (Figure 10).

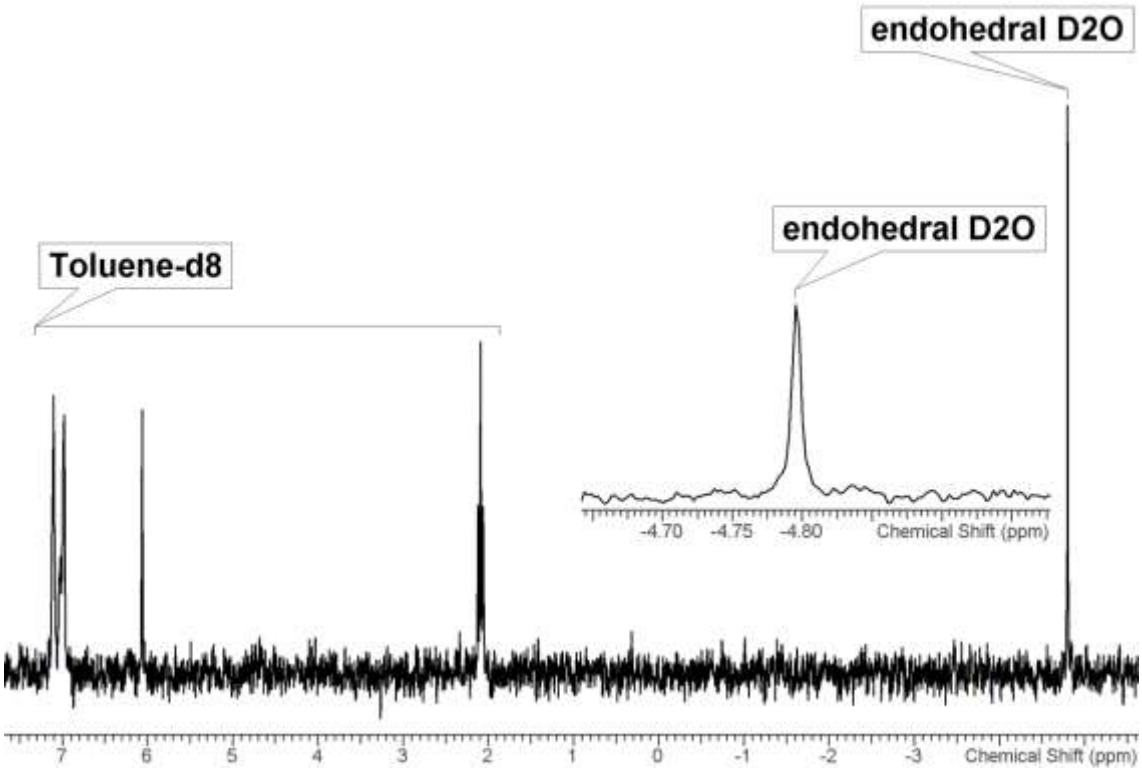

Figure 10: ^{2}H NMR (61 MHz, toluene) spectrum of 78% filled $D_2O@C_{60}$.

In conclusion, pre-forming OCF **28** allowed the application of the low pressure filling protocol to D_2O. The same protocol could be extended to the encapsulation of any other isotopologue of water.

2.4 Suturing the orifice of $H_2O@29$

In an effort to complete the synthesis of $\mathbf{H_2O@C_{60}}$, the attention was turned to suturing $\mathbf{H_2O@29}$. When compound $\mathbf{H_2O@29}$ was reacted with an excess of triisopropyl phosphite, the expected product $\mathbf{H_2O@26}$ was isolated only in 34% yield. A new endohedral derivative, compound $\mathbf{H_2O@35}$, was isolated from the reaction mixture in 31% yield as a single regioisomer (Scheme 28).

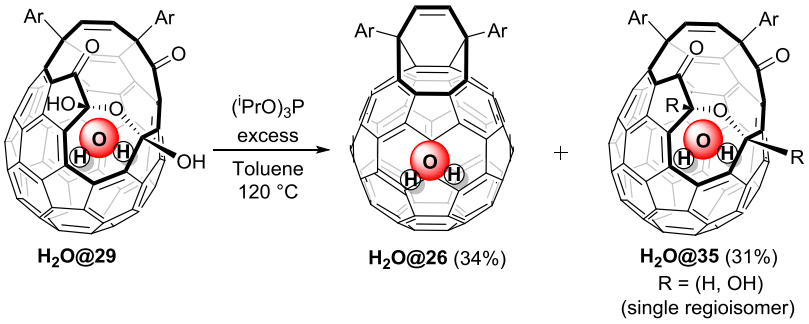

Scheme 28: Reduction of **H_2O@29** with triisopropyl phosphite.

The structure of **H_2O@35** was deduced by the appearance in the ^{1}H NMR spectrum of a new singlet at δ 7.80 ppm, which was assigned to the proton on the orifice, and a broad signal at δ 5.88 ppm attributable to the single hydroxyl group. The DFT-GIAO[94] simulations suggest the formation of OCF **35a** rather than its regioisomer **35b**; the ^{1}H and ^{13}C NMR spectra calculated for **35a** are consistent with the experimental data (Figure 11).

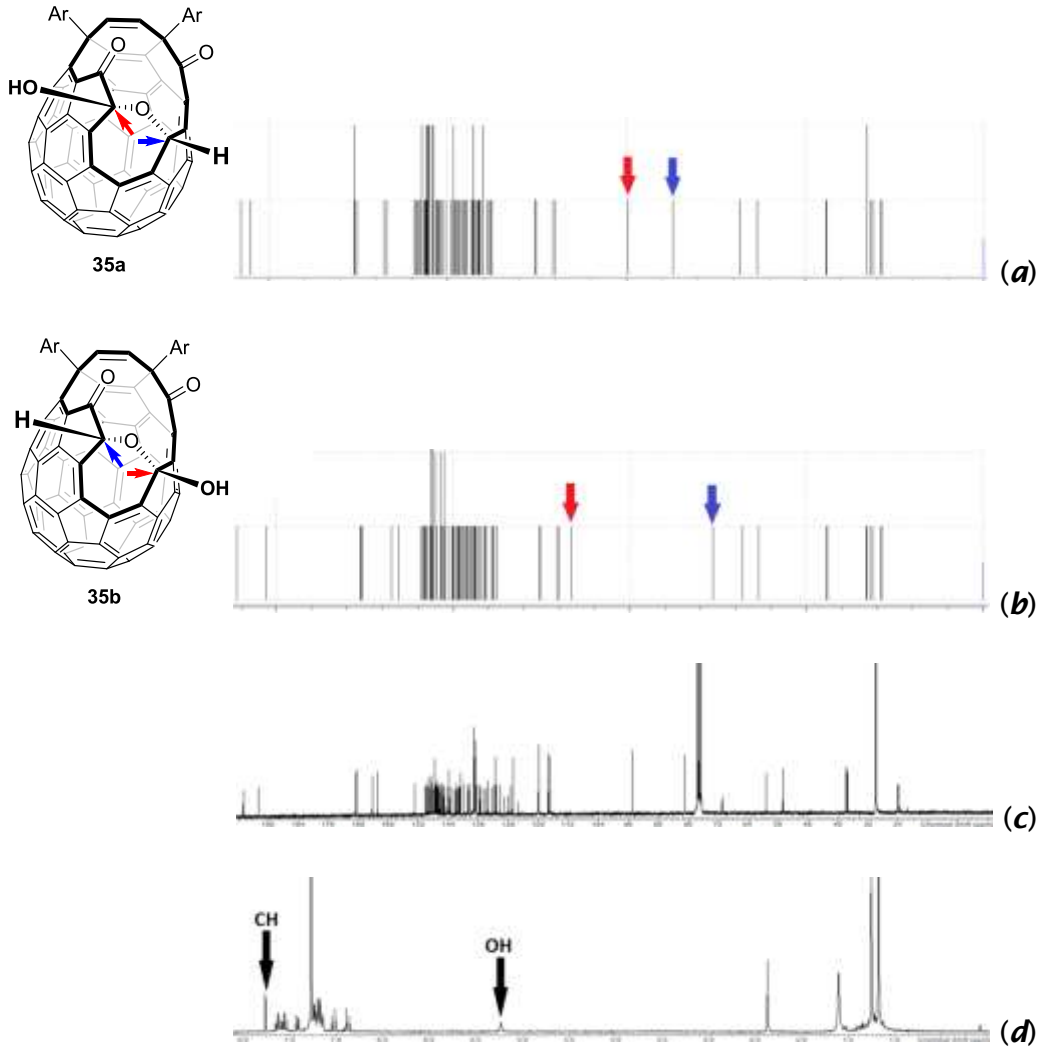

Figure 11: DFT-GIAO calculated ^{13}C spectra of **35a** (*a*) and **35b** (*b*). The peaks of the characteristic C-H and C-OH orifice carbons are respectively indicated by red and blue arrows . Experimental ^{13}C (75 MHz, $CDCl_3$) spectrum (*c*) and ^{1}H (300 MHz, $CDCl_3$) spectrum (*d*) of compound **35**.

Compound **35** was the only product isolated after chromatography (76% yield) when a solution of **29** in toluene was stirred at room temperature in the presence of triisopropyl phosphite or other trialkyl phosphites. Pre-formed tetra ketone **28** (cf. 2.3) reacted with triisopropyl phosphite in refluxing toluene to afford compound **26** in yield similar to the reported value.[72] The same reduction of pre-formed **28** with excess triisopropyl phosphite at room temperature produced OCF **26**, uncontaminated by **35** (Scheme 29).

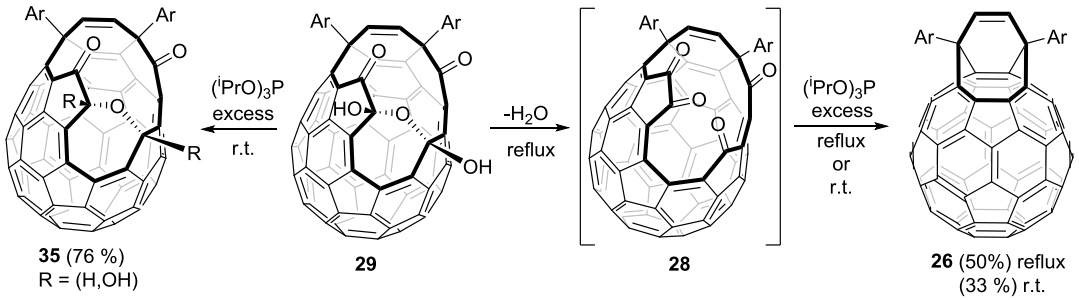

Scheme 29: Reactivity of **29** and **28** towards triisopropyl phosphite.

Very likely, under the reported conditions for the closure of **H_2O@29**, a mixture of **H_2O@29** and **H_2O@28** formed *in situ* reacted with triisopropyl phosphite to give a mixture of **H_2O@35** and **H_2O@26**. Compound **35** did not react with triisopropyl phosphite and **H_2O@35** did not lose the endohedral water upon refluxing in toluene. This side reaction of triisopropyl phosphite modified the orifice of OCF **29** irreversibly, and prevented the completion of the molecular surgery using the known route. Interestingly, Zhang *et al.* reported a similar reduction of OCF **18** with triethyl phosphite (Scheme 30).[95,96]

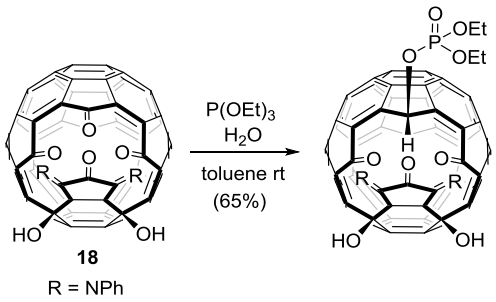

Scheme 30: Reactivity of OCF **18** towards triethyl phosphite.

The use of alternative phosphorus (III) reagents was considered in order to overcome this side reactivity. In particular, reaction of **H_2O@29** with excess triphenylphosphine in refluxing toluene, cleanly and selectively afforded **H_2O@27** in 84% yield. The endohedral water was not lost in the formation of **H_2O@27**, for which this reaction provides the first synthesis. Compound **H_2O@35** was not formed and triphenylphosphine, unlike trialkyl phosphites, did not react at all with compound **29** at room temperature. The selectivity of triphenylphosphine towards tetraketone **28** explains the high yield afforded with this reaction. Further reduction of **H_2O@27** to compound **H_2O@26** was not observed. This is likely accountable to the steric bulk of triphenylphosphine

that is unable to access the two carbonyl functions closer to the pyridyl groups on **H_2O@27** (Scheme 31).

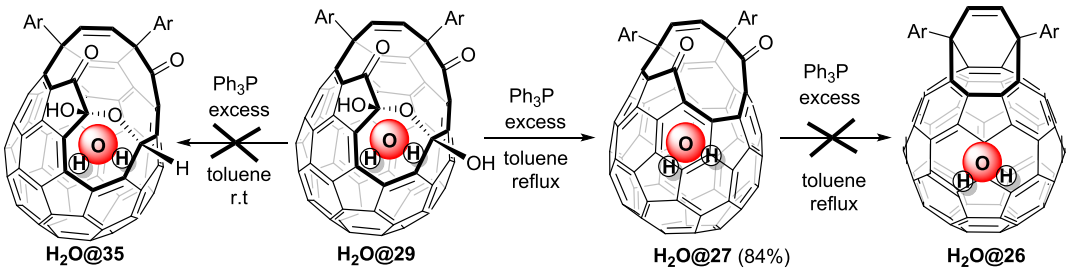

Scheme 31: Reactivity of **H_2O@29** towards triphenylphosphine.

TLC analysis of the reaction in course revealed the presence of an intermediate. In an attempt to isolate this unknown compound, OCF **29** was reacted with triphenylphosphine at lower temperature (60 ˚C); OCF **36** was isolated as the only product after chromatography. Compound **36** was formed as well when triphenylphosphine was reacted with pre-formed OCF **28** at room temperature (Scheme 32).

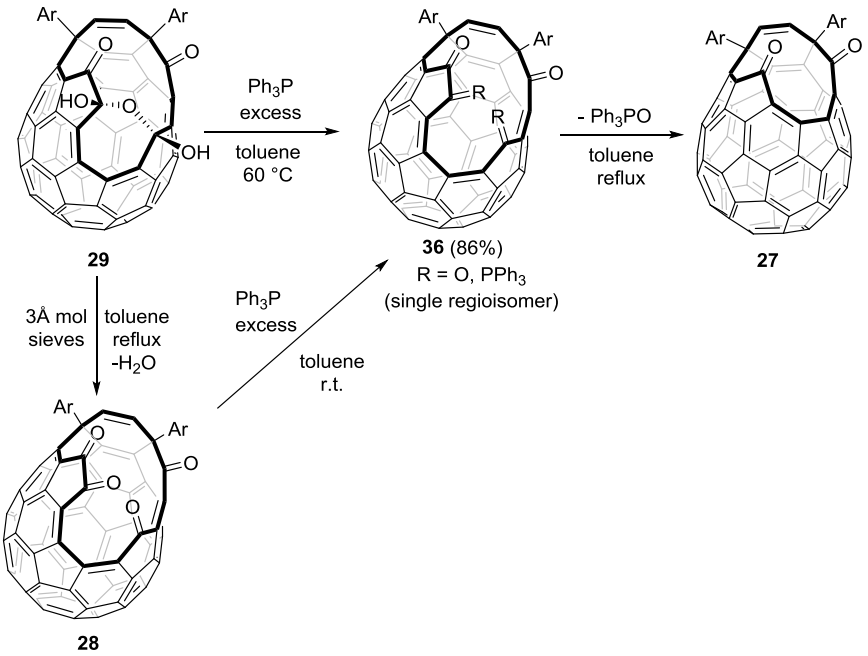

Scheme 32: Formation of ylide **36b**.

The structure of **36** was determined as follows. The ^{31}P NMR spectrum showed a single signal at δ 18.4 ppm (referenced to 85% H_3PO_4) which lied within the typical range of triphenylphosphonium ylides (δ 5-25 ppm). The ESI+ MS displayed a signal at *m/z* 1350, attributable to the molecular ion $[C_{100}H_{41}N_2O_3P+H]^+$ which suggested the displacement of one of the oxygen

atoms by triphenylphosphine. This hypothesis was reinforced by monitoring the reaction course via ^{31}P NMR; the spectra showed over time formation of **36** (δ = 18.4 ppm) and triphenylphosphine oxide (δ = 25 ppm). Upon heating at 100 °C or above, the ylide signal progressively disappeared over time with concomitant formation of more triphenylphosphine oxide. All these evidences strongly supported the formation of an intermediate triphenylphosphonium ylide which, upon heating, underwent an intramolecular Wittig reaction to afford compound **27**.

In the ^{13}C NMR spectrum, the signal of the ylide carbon was split into a doublet with a J_{CP} of 118 Hz due to one-bond coupling with the neighbouring phosphorus. Moreover, one of the carbonyl signals was split into a doublet with a J_{CP} of 9.6 Hz (Figure 12). It is reasonable to assume that this splitting would be present only in the spectrum of regioisomer **36b**, which has a carbonyl group only two bonds apart from the phosphorus nucleus.

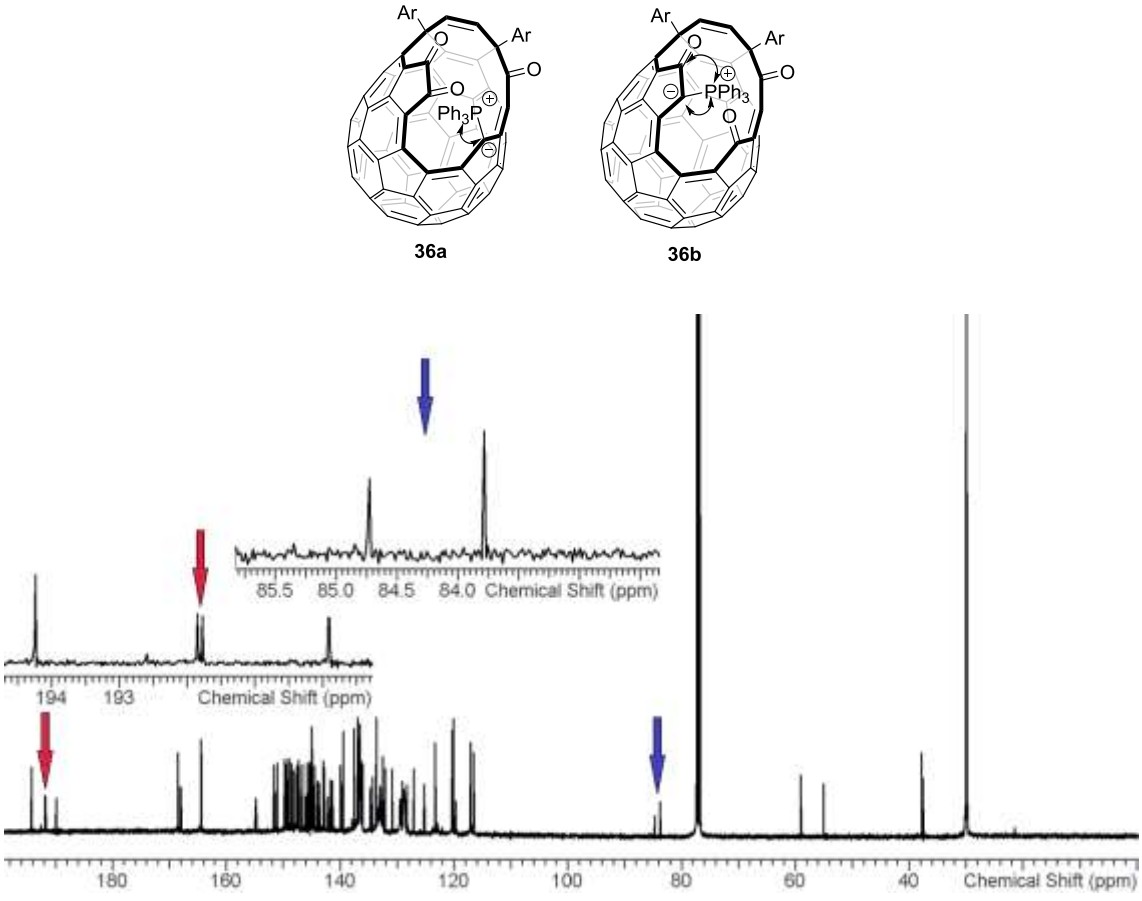

Figure 12: ^{13}C NMR (125 MHz, $CDCl_3$) spectrum of ylide **36**. The ylide carbon signal is indicated by a blue arrow. The signal of the CO group showing correlation to the phosphorus is indicated by a red arrow.

The values of these coupling constants are representative of triphenylphosphonium ylides.[97] The actual existence of these two splitting patterns was verified by recording two ^{13}C NMR spectra at different field; the values of the coupling constants measured coincided within experimental error.

The DFT-GIAO simulated ^{13}C NMR spectrum of ylide **36b** accords well with the experimental spectrum (Figure 13).

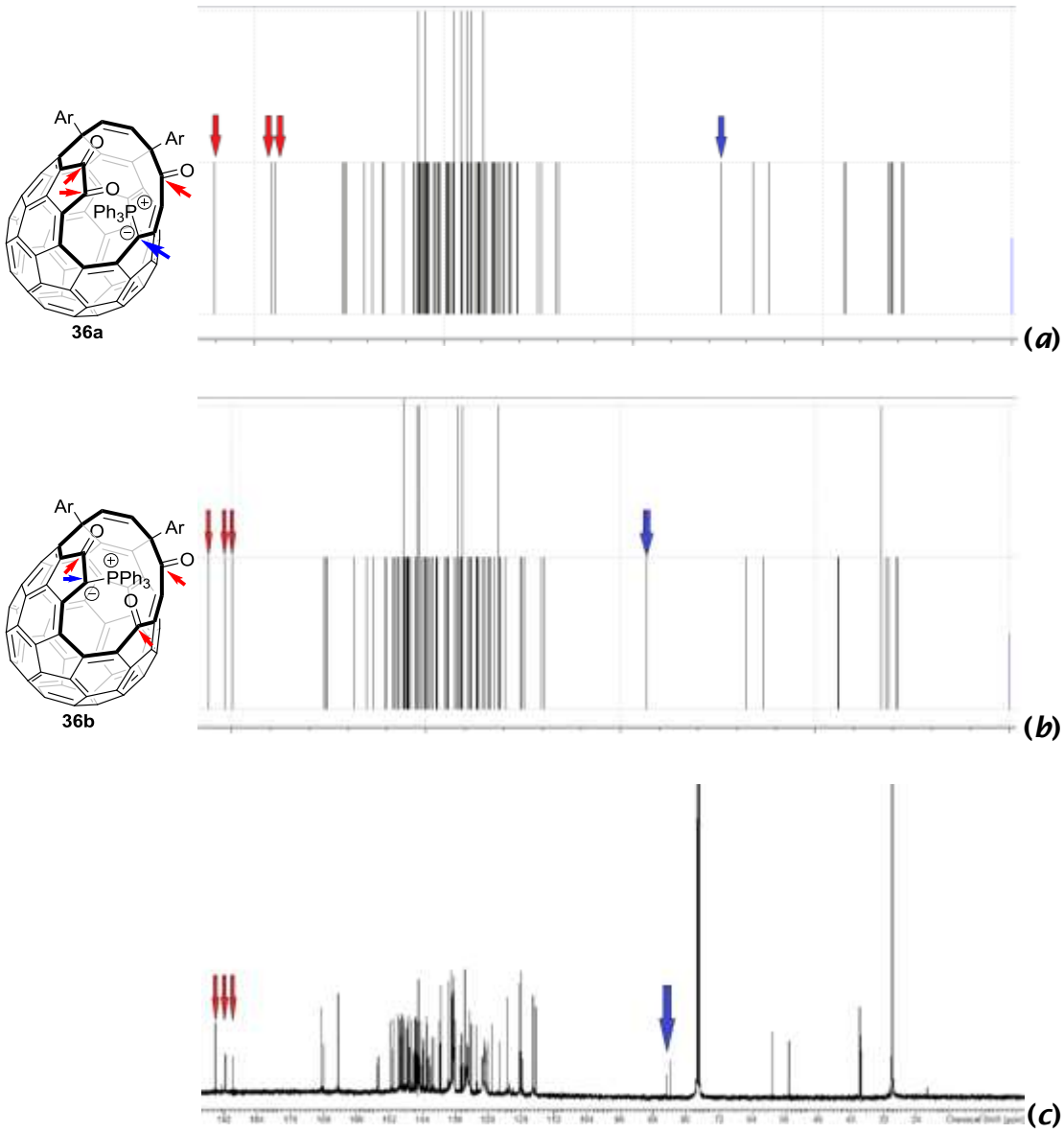

Figure 13: DFT-GIAO simulated ^{13}C spectra of ylides **36a** (*a*) and **36b** (*b*). Experimental ^{13}C (125 MHz, $CDCl_3$) spectrum of ylide **36** (*c*). The peaks of the characteristic CO and C-P orifice carbons are respectively indicated by red and blue arrows.

The reaction mechanism of this novel transformation was studied next. The experimental evidence clearly showed that compound **29** had to dehydrate to **28** in order to become reactive to triphenylphosphine; the successive formation of the ylide proceeded at room temperature. Finally, transformation of **36** into **27** required heating to 100 °C. A precedent works in the literature show that aromatic ketones are reactive towards phosphorus (III) reagents (Scheme 33).[98] For instance, fluorenone is reduced to 1,3-dioxaphosphorane **39**; this intermediate is formed from the attack of the 1,3-dipolar species **38** on a second molecule of fluorenone. In turn compound **38** forms either by attack of the phosphorus nucleophile on the oxygen atom of the carbonyl group or, through a 1,2-addition followed by phospha-Brook rearrangement of zwitterion **38a**. Most likely, the driving force behind the attack is the delocalization of the negative charge in an aromatic 6-π electrons system.

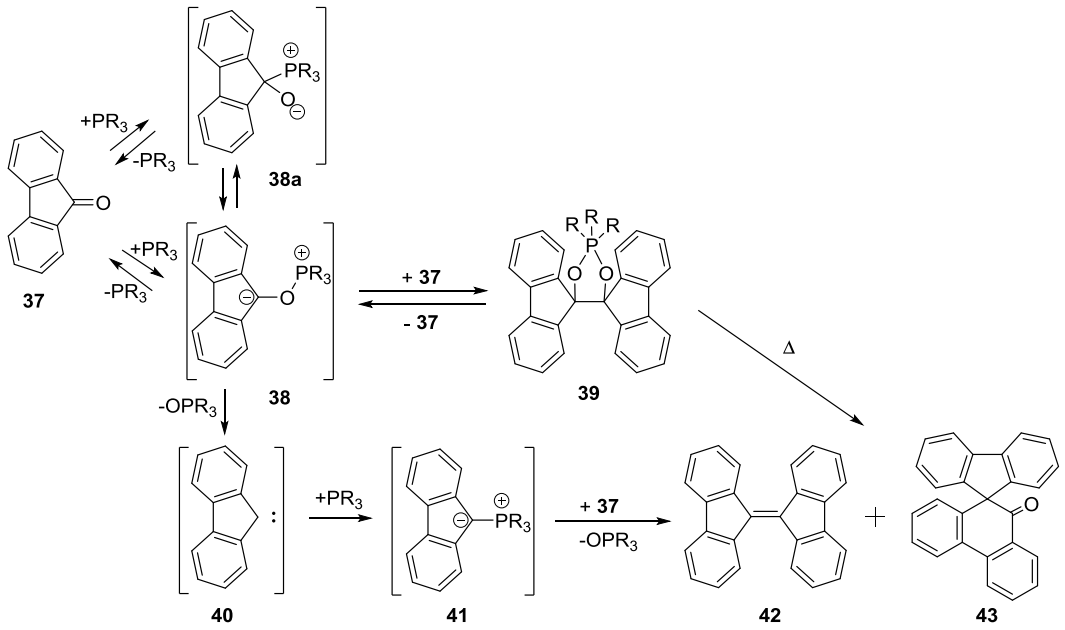

Scheme 33: Reactivity of fluorenone towards phosphorus (III) reagents.[98]

Upon heating, the intermediate **39** transforms into bifluorenylidene **42** and spirocycle **43**. The latter is the product of a pinacol-like rearrangement of **39**. The formation of **42** can instead be interpreted as the result of: (*i*) the decomposition of **39** into its components **38** and **37**, (*ii*) formation of carbene **40**, (*iii*) formation of ylide **41** by reaction of a second equivalent of phosphorus reagent with carbene **40**, (*iv*) final Wittig reaction of ylide **41** with fluorenone **37**.

This reactivity study suggested that a similar path could be taken for the reduction of OCF **28** with triphenylphosphine. This possibility was investigated by DFT calculations. Theoretically, all of the four carbonyl groups of OCF **28** can be attacked by a nucleophile; however, two are shielded by the nearby aryl rings. This limits the attack to the two more accessible carbonyl groups, belonging to the acenaphthenequinone- and cyclopentaphenanthrenone-like moieties (Figure 14).

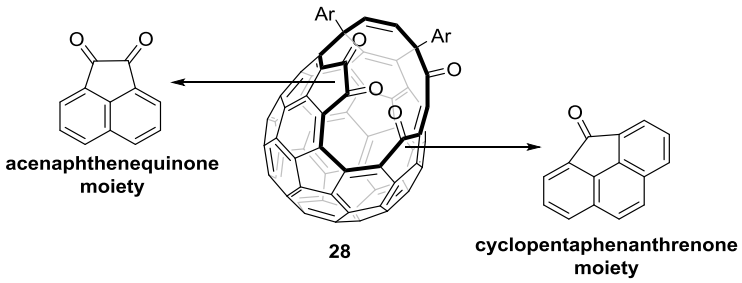

Figure 14: Structural motifs on OCF **28**.

The bulky fullerene cage precludes nucleophilic 1,2-addition on these two carbonyls, however direct attack on the oxygen is possible. Such addition can produce regioisomers **44a** (Scheme 34, route *a*) and **44b** (Scheme 34, route *b*).

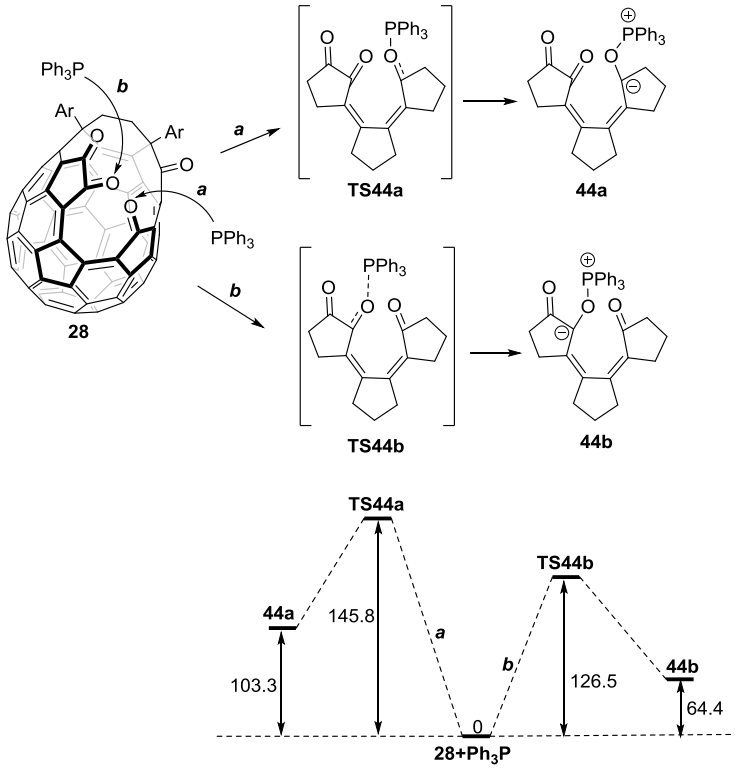

Scheme 34: Free energy profile for the attack of triphenylphosphine on **28**. Energies are reported in KJ/mol. Only the reacting portion of the OCF structures has been represented.

The formation of **44b** over **44a** is favoured both kinetically and thermodynamically. In fact, the activation energy for the formation of **44b** is 19.3 KJ/mol lower and this intermediate is 38.9 KJ/mol more stable than **44a**. Theoretically, compounds **44a** and **44b** can eliminate triphenylphosphine oxide to form the two regioisomeric carbenes **45a** and **45b**. Calculations gave a high activation energy (*circa* 200 KJ/mol) for the formation of **45a** from **44a**. A similar computational experiment performed on **44b** did not result in the encounter of a transition state. Moreover, optimisation of the geometry of **45b** produced oxepin **47** as an energy minimum (Scheme 35).

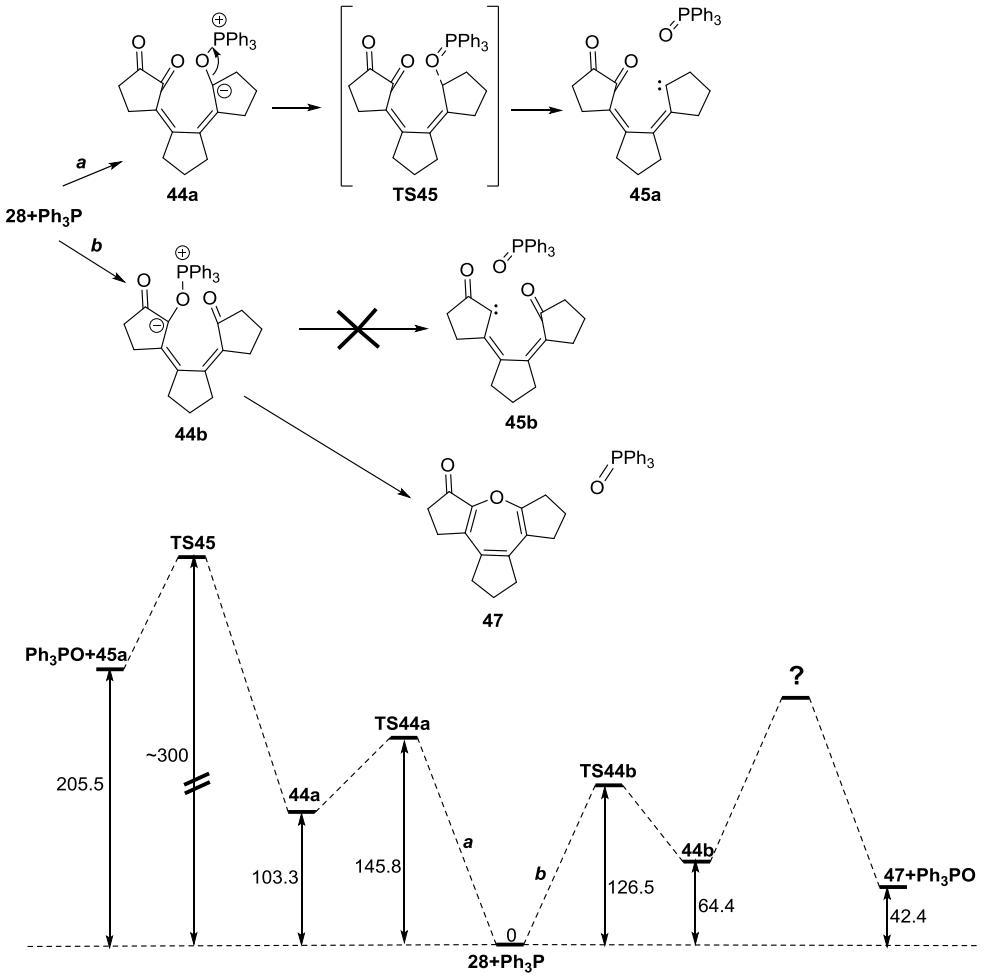

Scheme 35: Free energy profile for the direct elimination of triphenylphosphine oxide from **44a** and **44b**. Energies are reported in KJ/mol. Structures are drawn following the convention used in Scheme 34.

Unlike its structural isomer carbene **45a**, oxepin **47** does not have a free valence; consequently, **47** is 163.1 KJ/mol more stable than **45a**. The reorganisation of the geometry of **45b** to oxepin **47** is due to the proximity of the oxygen atom of the cyclopentaphenanthrenone motif of **45b** to the electron-deficient carbon across the rim. This feature allows the formation of an oxygen bridge with minimal distortion of the initial geometry. On the contrary, the oxygen atom on the acenaphthenequinone motif of **45a** points away from the electron-deficient carbon across the rim and, consequently, cannot form the bridge.

In the light of these discoveries, an alternative mechanism for the formation of oxepin **47** from compound **44b** was conceived. Thus, electrocyclisation of **44b**

first affords intermediate **46**, which in turn eliminates triphenylphosphine oxide to form the stable oxepin **47** (Scheme 36).

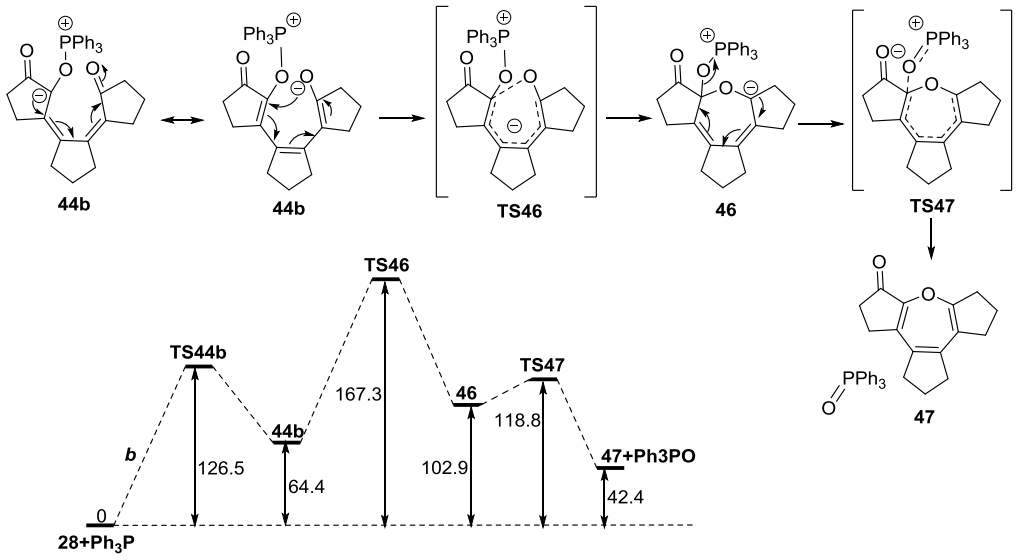

Scheme 36: Free energy profile for the elimination of triphenylphosphine oxide from intermediate and **44b**. Energies are reported in KJ/mol. Structures are drawn following the convention used in Scheme 34.

The formation of **44b**, with activation energy of 126.5 KJ/mol, is the rate limiting step of the sequence of reactions leading to **47**. An analogous reaction profile is available to **44a** but is overall higher in energy.

The rearrangement of oxepin **47** into epoxide **48** was then investigated. Calculations gave activation energies of 3.9 and 23.9 KJ/mol respectively for the forward and reverse transformation. Epoxide **48** is 20.0 KJ/mol more stable than oxepin **47**. These figures suggest that the two molecules are in rapid equilibrium, with epoxide **48** being the predominant specie (Scheme 37). The closely related equilibrium between oxepin and benzene oxide is well known.[99]

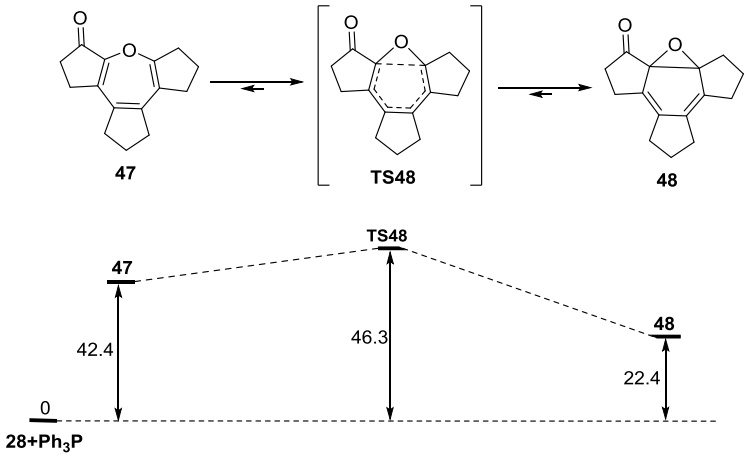

Scheme 37: Free energy profile for the interconversion of **47** and **48**. Energies are reported in KJ/mol. Structures are drawn following the convention used in Scheme 34.

The mechanism of formation of the ylide was investigated next. The fullerene cage shields the trajectory of attack to the electrophilic carbons of **48**, impeding the nucleophilic substitution of the epoxide ring. Simulations in which the carbon-oxygen bonds on the epoxide ring of **48** were broken to produce an electrophilic carbocation, did not lead to the formation of stable intermediates. Nucleophilic attack of triphenylphosphine on the oxide bridge of **48** and concerted elimination of triphenylphosphine oxide is also possible. This pathway affords directly the reaction product **27**, and does not explain the formation of the ylide observed experimentally. Simulations gave activation energy of 162.7 KJ/mol for **TS48o** (Scheme 38).

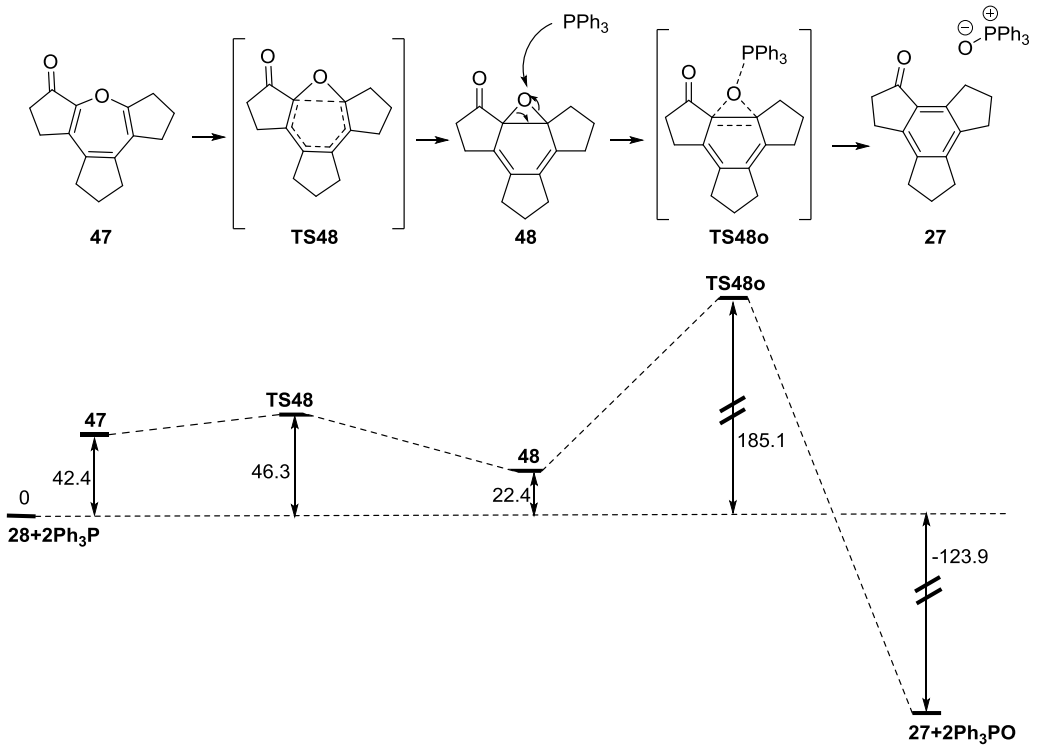

Scheme 38: Reduction of epoxide **48** to OCF **27**. Free energies are reported in KJ/mol. Structures are drawn following the convention used in Scheme 34.

The final option consisted in the attack of triphenylphosphine on the electrophilic carbons of oxepine **47**. Such attack can take place on either C-7 (Scheme 39, route *a*), or C-2 (Scheme 39, route *b*) of the oxepine ring to form respectively the two regioisomeric tetrahedral intermediates **49a** and **49b**. Breaking of the oxygen bridge, via electrocyclic ring-opening, finally leads to the formation of ylides **36a** and **36b**.

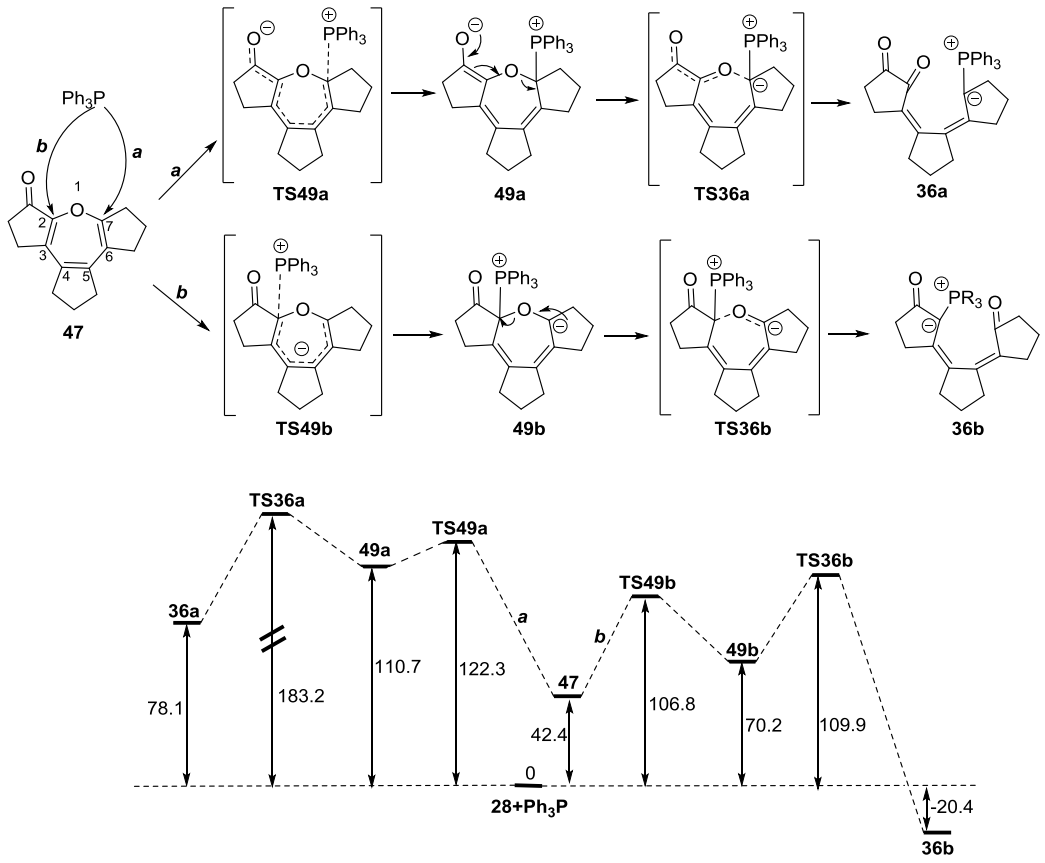

Scheme 39: Free energy profile for the formation of **36a** and **36b**. Energies are reported in KJ/mol. Structures are drawn following the convention used in Scheme 34.

The energy figures showed that both kinetics and thermodynamics favour the formation of **36b** over **36a**, or the direct reduction of epoxide **48** described above. Indeed, the reaction profile leading to **36b** features the lowest energy barriers and leads to the formation of the thermodynamically more stable ylide. Overall this mechanism supports the regioselective formation of ylide **36b** observed experimentally.

Lastly, the Wittig reaction of ylides **36a** and **36b** was investigated. Calculations gave similar energies for the two transition states **TS27a** and **TS27b**. The activation energy for the reaction of **36b** (161.4 KJ/mol) is much higher than the one calculated for its regioisomer **36a** (67.5 KJ/mol), due to the difference in energy of the starting ylides (Scheme 40). The activation energy for this last step is also the highest of the entire reaction sequence. This figure accords with the high temperature (100 °C) necessary to carry out this last transformation experimentally.

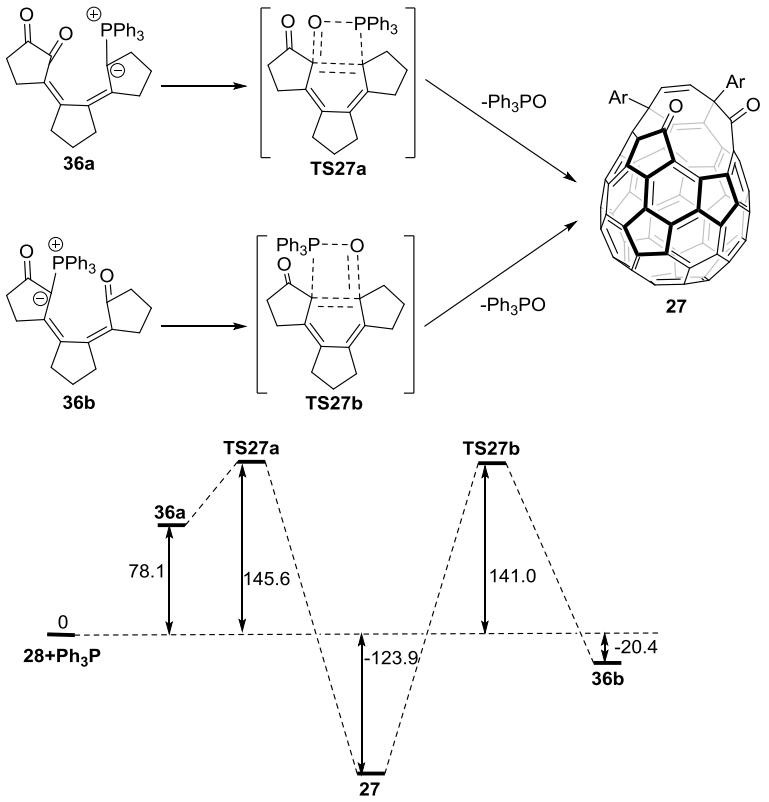

Scheme 40: Free energy profile for the formation of **27**. Energies are reported in KJ/mol. Structures are drawn following the convention used in Scheme 34.

It can be assumed that a similar reaction path involving the intermediate oxepine **47** might be followed, in opposite direction, in the oxidation of OCF **27** with NMO (cf. 1.3, Scheme 41).

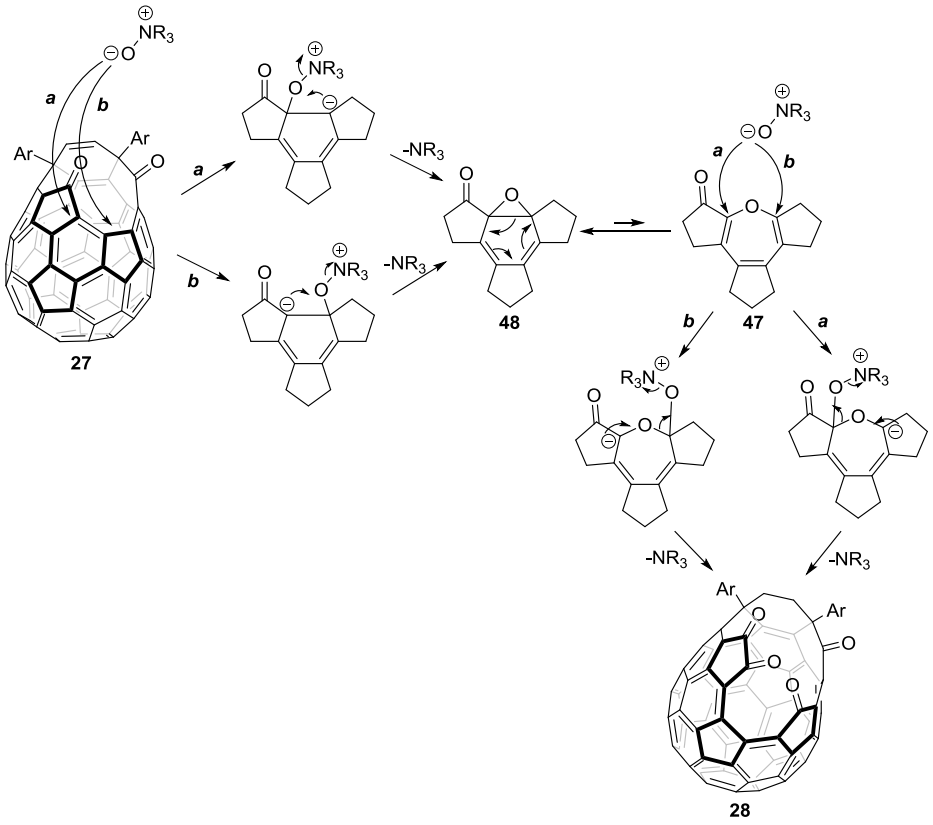

Scheme 41: Hypothetic mechanism for the oxidation of OCF **27** with NMO. Structures are drawn following the convention used in Scheme 34.

Compound **H_2O@27** was then reacted with excess triisopropyl phosphite to give **H_2O@26** in 84% yield (Scheme 42). In comparison with the reported direct reaction,[72] the yield of **H_2O@26** afforded in the two step process, was overall higher.

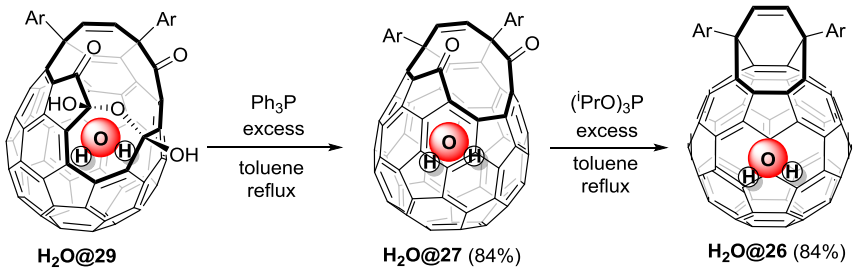

Scheme 42: Novel reduction of **H_2O@29**.

Then the attention was turned to the last step of the suturing procedure, the conversion of **H_2O@26** into **H_2O@C_{60}**. This transformation was originally[72] afforded in 29% yield by vacuum thermolysis at 360˚C of **H_2O@26** dispersed on

dry neutral alumina. When this protocol was repeated on empty **26**, HPLC analysis showed only minimal transformation of the substrate into C_{60} (Figure 15).

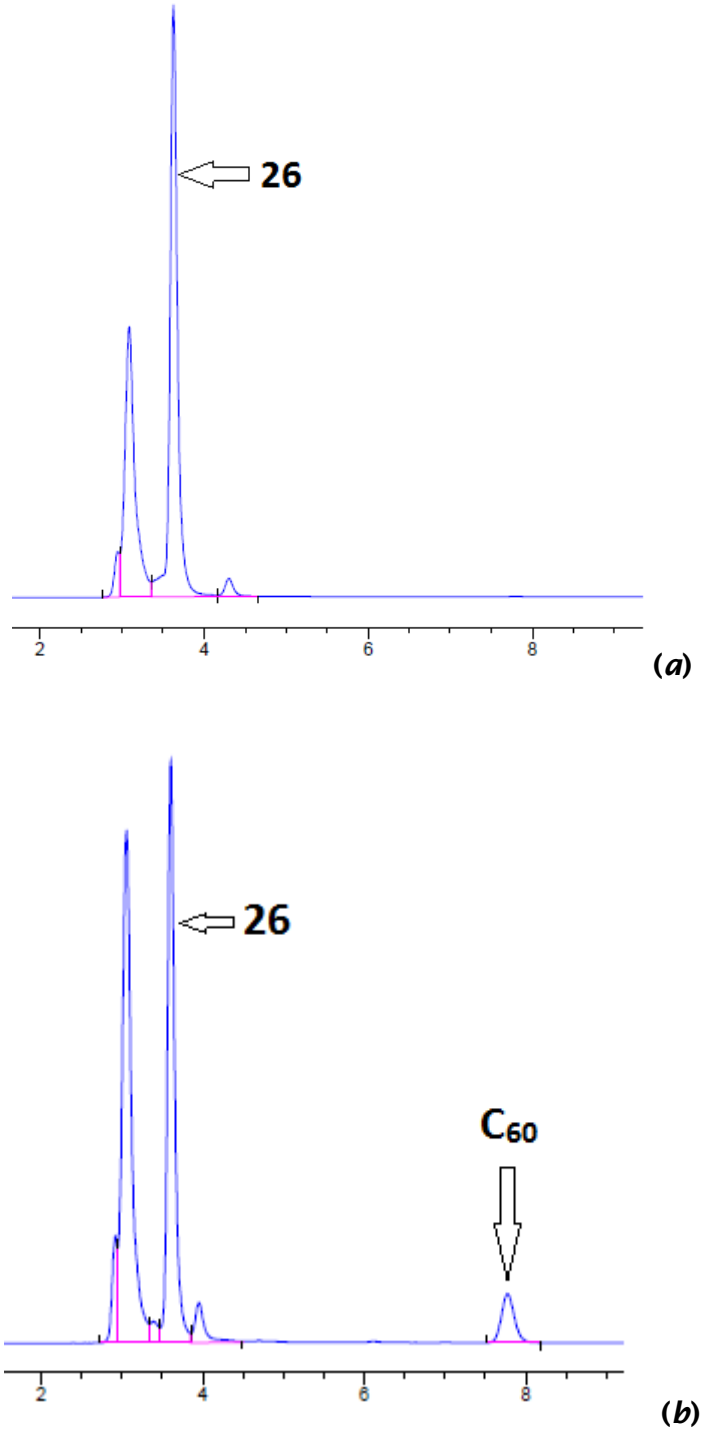

Figure 15: HPLC chromatogram of the vacuum pyrolysis of OCF **26** after 0 (*a*) and 1 hour (*b*) at 360 °C.

According to the proposed reaction mechanism (cf. 1.3), the final retro [2+2+2] cycloaddition involves the breaking of three σ-bonds and therefore, most likely possesses the highest activation energy of the entire series of transformations. Precedent studies showed that retro [4+2] cycloadditions were very effective in removing functional groups from fulleroids. For instance, as early as 1996, the group of Rubin discovered a way to de-functionalise fulleroid **4**. At that time the molecular surgery approach was still just an intriguing concept and this reaction was developed as part of a technique of reversible functionalisation of C_{60}.[69] Their results showed that while the straight retro [2+2+2] cycloaddition of **4** to C_{60} was energetically too demanding, a lower energy [4+2]/retro [4+2] course could be followed in the presence of a strong dieonophile. In particular reaction of **4** with N-phenyl maleimide or maleic anhydride at room temperature afforded the [4+2] adducts. Those fulleroids decomposed into C_{60} upon heating. Similarly, reaction of **4** with dimethyl acetylenedicarboxylate in refluxing toluene cleanly gave C_{60} in 75% yield (Scheme 43).

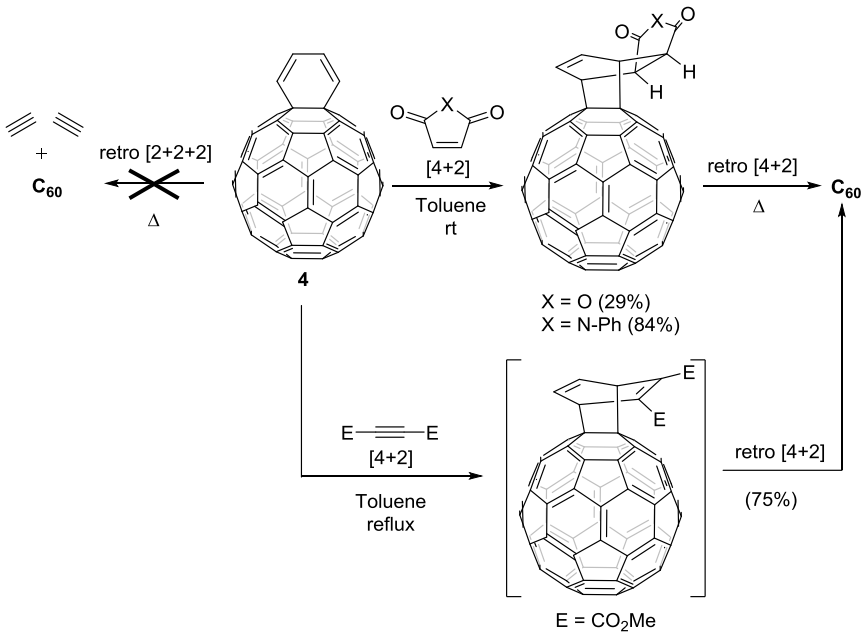

Scheme 43: Rubin's studies on the defunctionalisation of **4**.[69]

On these premises, it was envisioned that the same reactivity could be exploited to carry out the transformation of endofullerene **26** into C_{60} (Scheme 44)

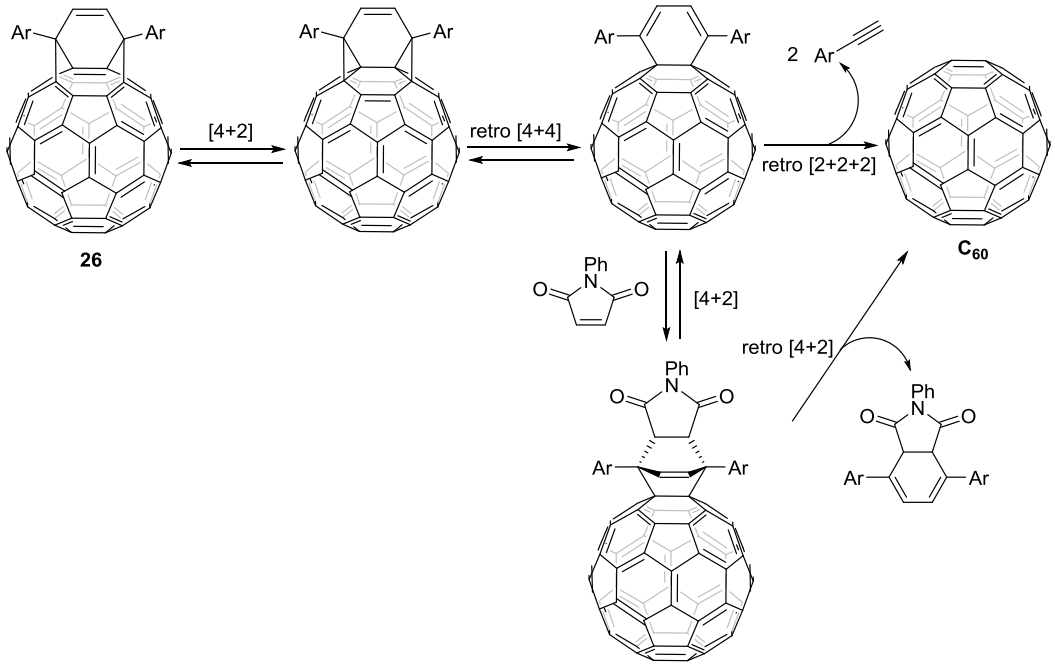

Scheme 44: Proposed mechanism for the alternative defunctionalisation of **26**.

This expectation was confirmed experimentally. Refluxing a solution of **H_2O@26** and N-phenyl maleimide in 1-chloronaphthalene for 24 hours, cleanly afforded **H_2O@C_{60}** in *circa* 90% yield after chromatography and removal of the solvent by vacuum distillation. The HPLC chromatogram of the isolated endofullerene showed that the material still contained minor impurities, consisting mainly of 1-chloronaphthalene. These apolar contaminants could not be removed by chromatography over silica gel as the polar stationary phase cannot retain them, or the product. Further purification was therefore achieved by vacuum sublimation, ultimately affording a very pure and solvent free **H_2O@C_{60}** and **D_2O@C_{60}** in ~70% yield (Figure 16). This is the first example of purification of small molecule endofullerenes via vacuum sublimation. The endofullerenes are stable under the sublimation conditions (550 °C, 10^{-5} torr) and completely retain the endohedral molecules. Mixtures of 78% filled **H_2O@C_{60}** and C_{60} can be co-sublimed by the same method to afford homogenous **H_2O@C_{60}** samples of lower filling factor.

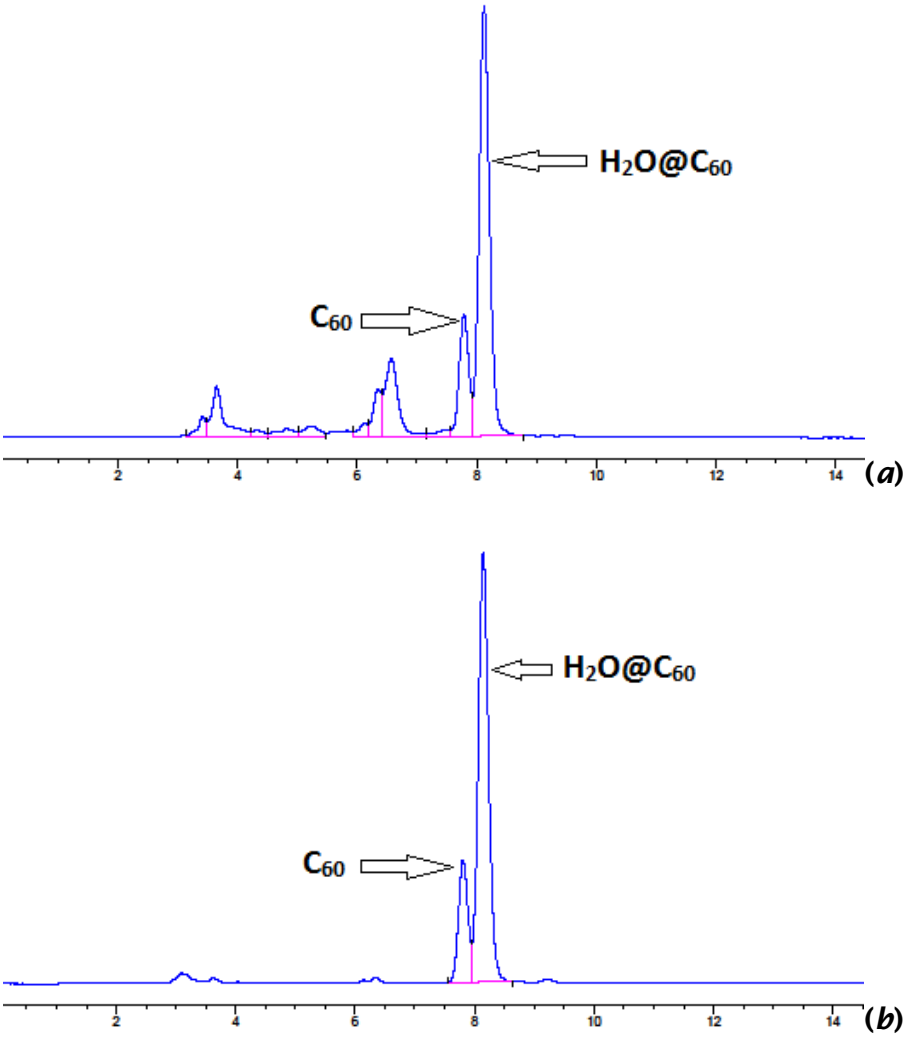

Figure 16: HPLC chromatograms of 78% filled chromatographed (*a*) and sublimed $H_2O@C_{60}$ (*b*).

The encapsulated water molecule imparts a dipole moment of 0.5 D to $H_2O@C_{60}$.[100] This characteristic allows the separation of $H_2O@C_{60}$ (RT = 8.14 min) from C_{60} (RT = 7.81 min) by HPLC (Buckyprep, toluene). Therefore, even if the low pressure water filling protocol does not afford quantitative incorporation of water, 100% filled $H_2O@C_{60}$ can still be produced at this stage.[72]

2.5 Ortho-para conversion study of water inside C_{60}

Small symmetrical molecules, such as hydrogen and water display spin isomerism. These molecules, depending on the different relative orientation of the proton spins, exist in isomeric forms that exhibit distinct properties. For example water, and hydrogen likewise, subsist as the spin parallel form ortho-

water (o-H_2O), and the spin anti-parallel form para-water (p-H_2O). This differentiation arises from the strict correlation existing between spin and rotational states; in order to preserve the overall antisymmetry of the molecular wavefunction, the spin symmetric o-H_2O is strictly confined to antisymmetric rotational states, and the spin antisymmetric p-H_2O to symmetric rotational states (Figure 17).

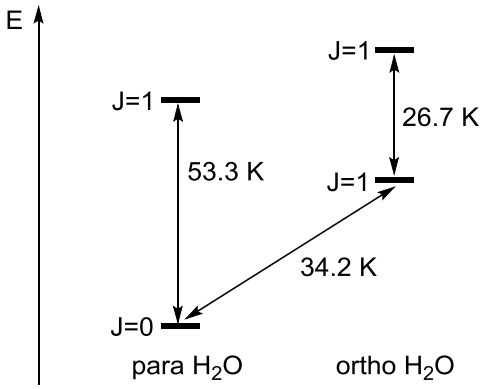

Figure 17: Energy levels of the spin isomers of water.

The equilibrium repartition between the ortho and para states depends on the temperature; the o/p ratio is roughly 3:1 at room temperature and tends to zero at low temperature limit. This 3:1 distribution at room temperature is statistical, due to the triple degeneracy of the o-state. The ortho state has nuclear spin $I = 1$ and therefore $(2I+1) = 3$ spin states; whereas the para state has nuclear spin $I = 0$ and therefore only $(2I+1) = 1$ spin state. The interconversion of the two spin isomers is slow in the absence of catalysts. Indeed, p-H_2 can be produced by cooling hydrogen at cryogenic temperatures in the presence of a spin catalyst. After removal of the catalyst, a sample of p-H_2 kept at room temperature will take several days to reach the 3:1 equilibrium distribution.

Spin isomerism finds an important application in NMR. Hydrogenation of a substrate with p-H_2 leads to intensification of the NMR signal by several orders of magnitude; this effect is known as para hydrogen induced polarisation (PHIP).[101] This technique finds an important application in the sensitivity enhancement of magnetic resonance imaging (MRI).[102] On similar grounds p-H_2O could be used to enhance the NMR signal. The conversion and isolation of spin isomers of water in the condensed phase is complicated by the fast proton exchange. These interactions subsist even when water is dispersed in a

matrix, given that this approach still does not rule out the formation of water clusters. From this point of view **$H_2O@C_{60}$** is an ideal system to study the spin isomers of water since the encapsulated molecules are physically separated from each other by the highly symmetric fullerene cages and organised in a homogeneous and physically very stable matrix. **$H_2O@C_{60}$** samples, produced by the low pressure improved synthesis (cf. 2.2 and 2.4) developed in this work, were used to study the spin isomer conversion of water molecules by NMR spectroscopy. This research was done in collaboration with the group of Prof. M. H. Levitt at the University of Southampton. The o/p conversion was followed by monitoring the ^{1}H NMR signal at constant temperature; o-H_2O, having $I = 1$, is NMR active while p-H_2O, having $I = 0$, is NMR inactive. Therefore a change in the proton signal at constant temperature is indicative of spin isomer conversion. Kinetics experiments, executed by following the ^{1}H NMR signal of an **$H_2O@C_{60}$** sample gradually cooled to cryogenic temperature, demonstrated that the spin isomer conversion process follows a bimolecular mechanism in which two adjacent o-H_2O molecules interact and transform into two p-H_2O molecules.[103] Further o/p conversion experiments were carried out on endofullerene **H_2O @50-d_{60}**, functionalised with exohedral malonate groups arranged in an octahedral symmetric pattern (Figure 18).

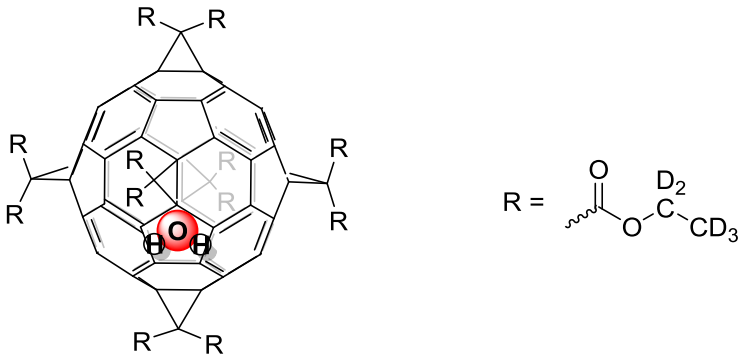

$H_2O@50-d_{60}$

Figure 18: structure of **$H_2O@50-d_{60}$**.

In this case o/p conversion was not observed. Most probably the exohedral appendages increase the distance between the cages, consequently inhibiting the interaction between neighbouring water molecules. Endofullerene **$H_2O@50-d_{60}$** was synthesised from **$H_2O@C_{60}$** using the Bingel-Hirsch methodology.[104] This reaction consists in the addition of a malonic ester to the [6,6]double bond of C_{60}. The malonic ester nucleophile can be formed by deprotonation of an α-

bromomalonate;[105] the latter can be in turn conveniently generated *in situ* by reacting the malonate ester with a stoichiometric amount of base in the presence of tetrabromomethane.[104] The addition of the carbon nucleophile on the fullerene [6,6] bond is followed by the intramolecular substitution of the halide atom by the fullerene anion to form a methano bridge (Scheme 45 route *a*). Also plausible is that the reaction might proceed via concerted addition of carbene to the double bond (Scheme 45, route *b*).

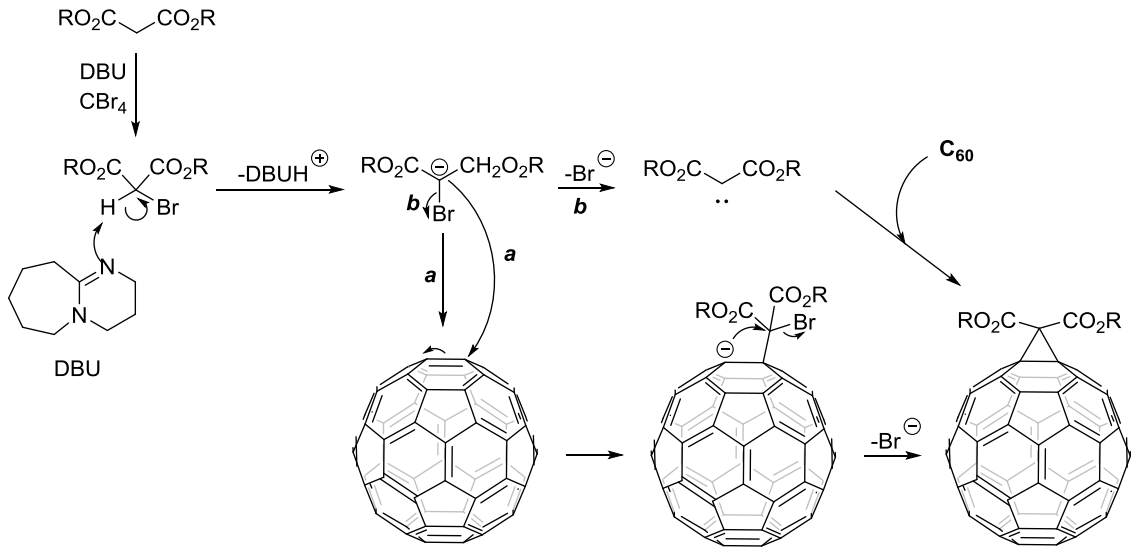

Scheme 45: mechanism of the Bingel cyclopropanation via nucleophilic attack (route *a*) or addition of carbene (route *b*).

Since the bare C_{60} contains a total of 30 [6,6] double bonds, several different regioisomers can form by addition of multiple malonate groups (Figure 19).

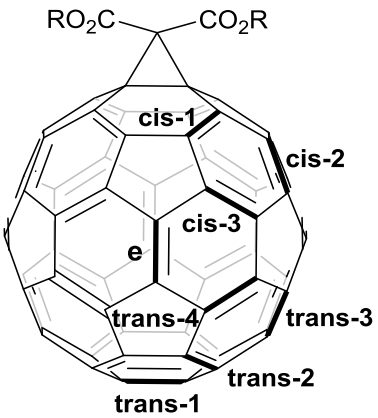

Figure 19: Different [6,6] double bonds of a C_{60}-monomalonate.

However the second insertion is slightly selective: kinetics and thermodynamics favour the attack on the [6,6] double bonds lying on the

mirror plane perpendicular to the malonate ("e" double bond).[106] Attack on this position produces a C_{60}-dimalonate with an incomplete, but correct, octahedral substitution pattern. The alternative attacks lead to a non-octahedral substitution pattern. The regioselectivity of the third and successive attacks increases as the number of addends already bound in "e" positions grows. Thus, the one pot-reaction of C_{60} with 8 equivalents of diethyl bromomalonate affords the T_h symmetric **50** in 14% yield.[107] The ability of 9,10-dimethylanthracene (DMA) to undergo a reversible [4+2] cycloaddition with C_{60} at room temperature has been employed to further enhance the regioselectivity of the Bingel reaction. Equilibration of C_{60} with ten equivalents of DMA yields a mixture of regioisomers $C_{60}(DMA)_n$ (n = 1-3), having predominantly an incomplete octahedral addition pattern.[107] Upon addition of the carbon nucleophile the substitution pattern is completed, and then the DMA molecules are irreversibly replaced by the malonate groups.

Using this methodology, T_h symmetric **50** and **H_2O @50-d_{60}** were synthesised in *circa* 30% yield. The ^{13}C NMR spectra of these adducts show just 7 resonances, four belonging to the six equivalent malonate groups, and the remaining three belonging to the non-equivalent carbons on the T_h symmetrically functionalised fullerene cage (Figure 20). The ^{1}H NMR spectrum of **H_2O @50-d_{60}** displays a single resonance for the endohedral water as it would be expected from a regioisomerically pure sample.

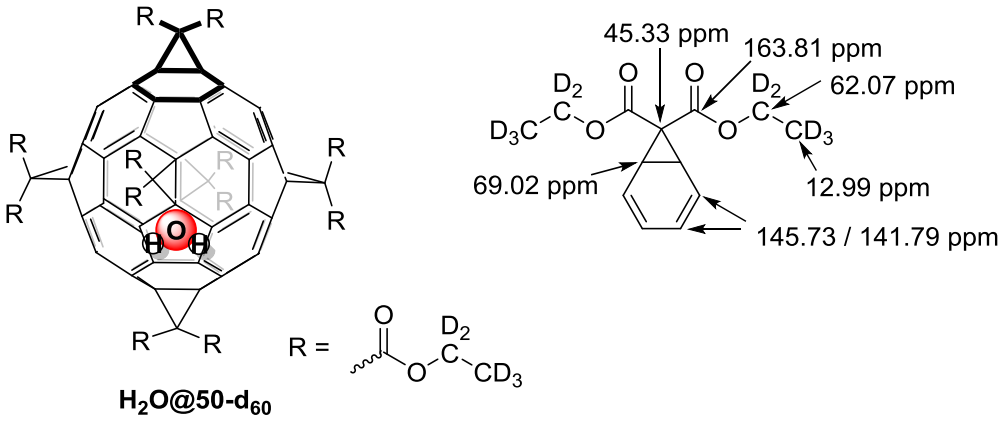

Figure 20: ^{13}C NMR (100 MHz, $CDCl_3$) chemical shift values of **H_2O@50-d_{60}**.

The Bingel-Hirsch reaction provides a very useful way to decorate the C_{60} scaffold maintaining a high degree of symmetry. This is the first application of the reaction to endofullerene **H_2O@C_{60}**.

2.6 A new synthesis of $H_2@C_{60}$

As previously discussed (cf. 1.3), Komatsu was the first to accomplish the synthesis of $\mathbf{H_2@C_{60}}$ in 2005. This first complete example of molecular surgery employed OCF **23** and afforded 91% filled $\mathbf{H_2@C_{60}}$ in 5% overall yield from pristine C_{60}. Even if the high pressure used to fill **23** allowed the quantitative insertion of hydrogen,[67] *circa* 9% of the endohedral molecule was lost in the final thermolysis step.[70] The practicality of the more recent $\mathbf{H_2O@C_{60}}$ molecular surgery (only 6 steps overall), and the efficiency of the optimised closure (cf. 2.3), encouraged the research for an alternative route to $\mathbf{H_2@C_{60}}$. The use of OCF **28** to carry out the incorporation of hydrogen was attractive. The size of the orifice of OCF **28** (16-members), relative to OCF **23** (13-members), meant that lower temperature and pressure could be used. On the other hand, the larger opening of OCF **28** presented the challenge of keeping the endohedral molecule inside during the closure phase (Figure 21).

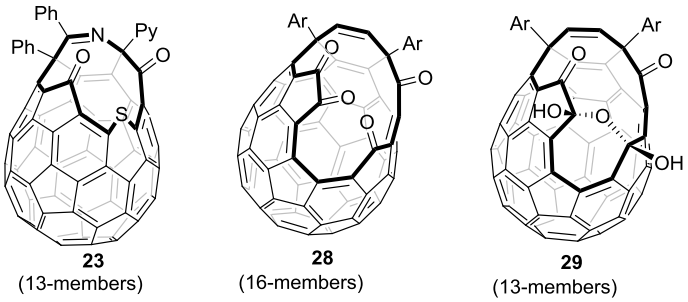

Figure 21: structures of OCFs **23**, **28** and **29**.

Refluxing a solution of **29** in toluene under hydrogen atmosphere produced a new signal at δ -7.17 ppm in ^{1}H NMR spectrum; this was attributed to encapsulated hydrogen. The filling factor, derived from the integration of the peak, did not exceed 3%. This very low figure was due to the low pressure used which limited the fraction of hydrogen dissolved in the solvent. Therefore, this process was repeated using a steel reactor that was charged with 120 atm of hydrogen gas. A filling factor of 48% was achieved under these conditions. Surprisingly, the isolated sample also contained a substantial amount (22%) of encapsulated water. Similar to the case of deuterium oxide (cf. 2.2), the encapsulated water was likely originating from the *in situ* dehydration of **29**. Even at low concentration, the water molecule still competed effectively for the cage. These experimental results can be interpreted by assuming that the

supramolecular complex **H_2O@28** is more stable than **H_2@28**. Indeed, the attractive force between the endohedral molecule and the cage experienced by water and hydrogen are different. In the first case, the attraction results from a dipole-induced dipole interaction, while in the latter, the attraction results from a weaker interaction between two induced-dipoles. Theoretical data from DFT calculations interprets well the experimental result as the calculated binding energy for **H_2O@28** (-39.9 KJ/mol) is substantially greater than the calculated binding energy for **H_2@28** (-21.0 KJ/mol). The use of pre-formed **28** was once again envisioned to solve this issue. Experimentally, the most practical solution consisted in carrying out the filling process in the presence of activated 3Å molecular sieves to mop up the water generated from the *in situ* dehydration of **29**, and any moisture present inside the reactor. In these conditions, 60% filled **H_2@29** was isolated and in 90% yield after 20 hours at 120 °C and 120 atm. The lower temperature used (120 *vs.* 200 °C for the incorporation of hydrogen inside **23**), allowed reasonable incorporation at moderate pressures and testifies the advantage of using OCF bearing large orifices in the encapsulation step. Changing the solvent did not lead to variation of the filling factor; this was likely due to the similar solubility of hydrogen in aromatic solvents. When the filling was attempted at lower temperature (100 °C), the hydrogen molecule was not incorporated. This result agrees with theoretical data which gave higher activation energy for the entry of hydrogen (64.3 KJ/mol), rather than for the entry of water (52.2 KJ/mol). This difference might sound contradictory due to the smaller volume of hydrogen relative to water; nonetheless, a polar molecule can undergo more favourable interactions with the polar groups on the orifice, lowering the energy of the transition state.

The closure of **H_2@29** was attempted next. Initially, a mixture of **H_2O@29** and **H_2@29** in toluene was refluxed in the presence of excess triisopropyl phosphite. In these conditions the endohedral hydrogen was completely lost; only **H_2O@26** was isolated after chromatography. At this point it was noticed that the filling and the initial reduction of the orifice were carried out under similar conditions. Conceivably, the filling and reduction of the orifice could be carried under pressure of hydrogen in a one-pot experiment. In this case, the hydrogen would take on two functions: (*i*) blocking the filling equilibrium to avoid loss of the endohedral molecule, and (*ii*) providing the inert atmosphere necessary for the closure. Compound **29** was heated to 120 °C in o-

dichlorobenzene under hydrogen pressure (120 atm) in the presence of 3 Å molecular sieves to give 60% filled **H_2@28**. The reaction mixture was cooled to room temperature, and the pressure released in order to add triisopropyl phosphite, or triphenylphosphine. Finally, the reactor was once again charged with 120 atm of hydrogen gas and heated to 120 °C overnight. After work up and chromatography, 60% filled **H_2@26** and 60% filled **H_2@27**, were isolated respectively when triisopropyl phosphite or triphenylphosphine were used (Scheme 46).

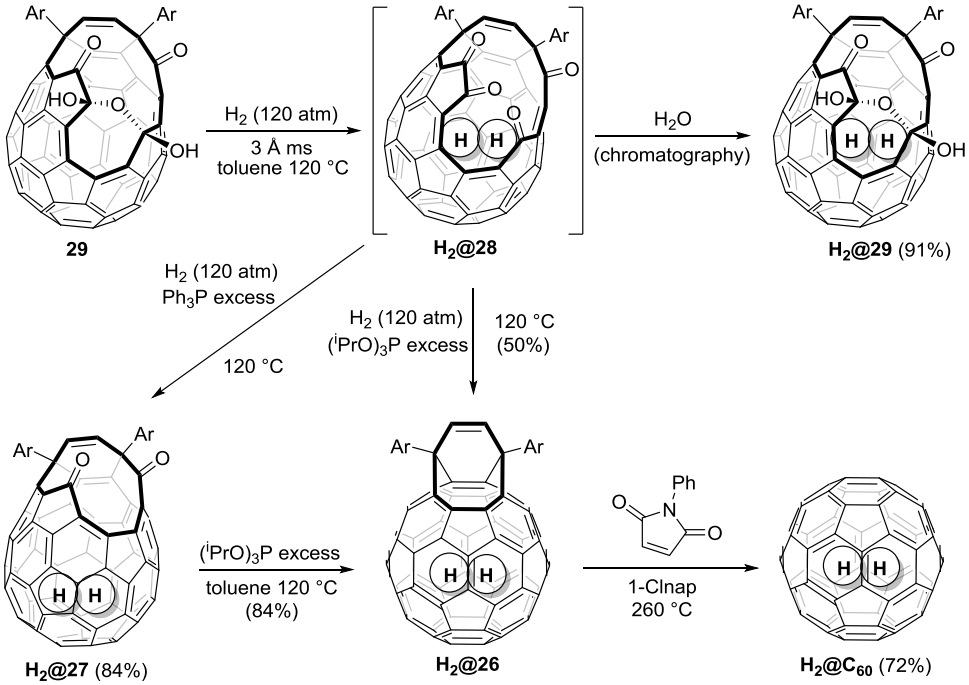

Scheme 46: Synthesis of **H_2@C_{60}** from **29**.

H_2@26 and **H_2@27** can be reacted analogously as previously described for **H_2O@26** and **H_2O@27** to isolate 60% filled **H_2@C_{60}**. Compounds **35** or **H_2@35** were not isolated in the hydrogen-filling/ triisopropyl phosphite-closure one-pot reaction. Here, the phosphite is added to a reaction mixture containing exclusively **28** and **H_2@28**, therefore the side reaction of triisopropyl phosphite with **29** cannot take place. Reduction of the orifice size from 16- (**H_2@28**) to 12-members (**H_2@27**) was sufficient to trap the hydrogen molecule in the fullerene cage. In fact further reduction of **H_2@27** or **H_2@26** was carried out at ambient pressure without loss of the endohedral molecule. Likewise, **H_2@C_{60}** was sublimed at 550 °C without appreciable loss of the endohedral molecule.

This new synthesis of $\mathbf{H_2@C_{60}}$ via OCF **28** is shorter and higher yielding than that via OCF **23**. Unfortunately, the equipment available during this work prevented the use of pressures higher than 120 atm. This in turn limited the filling factor to 60%. $\mathbf{H_2@C_{60}}$ and C_{60} can be separated by recycling HPLC,[70] but the process is extremely laborious and unsuitable to scale-up. Therefore, realistically, the use of high pressure is necessary to increase the filling factor. Under this point of view, the larger OCF **28** encapsulates hydrogen at lower temperature than the smaller **23**, so lower pressure will be needed for its quantitative filling. In fact incorporation of hydrogen inside **23** under 180 atm resulted only in 51% filling factor.

2.7 Filling the fullerene cavity with hydrogen fluoride

The successful extension of Murata's molecular surgery to $\mathbf{H_2@C_{60}}$ encouraged further experiments, aimed at encapsulating other species inside OCF **28**. Density functional theory calculations gave activation energy of 29.8 KJ/mol for the entry of HF into **28**. By comparison, the activation energy for the incorporation of H_2 and H_2O inside **28** was respectively 64.3 and 52.2 KJ/mol. Probably H_2O and HF are encapsulated more easily than H_2 due to the more favourable interactions between the polar molecules and the groups on the orifice of the OCF. In fact, experimentally, the filling of OCF **28** with H_2 required a higher temperature compared to the filling with H_2O (respectively 120 and 100 °C). The calculated binding energy for HF inside **28** (-25.9 KJ/mol) and the barrier for the release of HF from **HF@28** (55.7 KJ/mol) suggested that the loss of HF from **HF@28** would be slow at room temperature. Overall the calculations suggested that HF could be encapsulated inside the cage of OCF **28** and trapped by forming hemiacetal **29**. **HF@29** was therefore considered a viable target.

On these premises the filling of OCF **28** with HF was attempted. Gaseous hydrogen fluoride forms relatively stable polymeric adducts with several organic bases;[108,109] therefore such compounds were envisioned as a convenient source of anhydrous hydrogen fluoride. When a solution of **28** or **29** was treated with a large excess of 70% hydrogen fluoride in pyridine (HF-Py), **HF@29** was isolated after basic work-up and chromatography (Scheme 47).

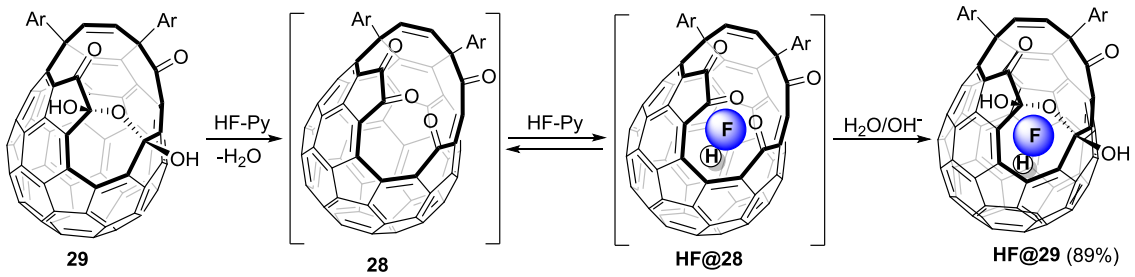

Scheme 47: synthesis of **HF@29**.

The signals from the endohedral HF molecule inside **HF@29** are clearly visible in the ^{1}H and ^{19}F NMR spectra at negative chemical shift. The ^{1}H NMR spectrum shows a doublet centred at δ = -6.55 ppm with a J_{HF} of 508 Hz (Figure 22).

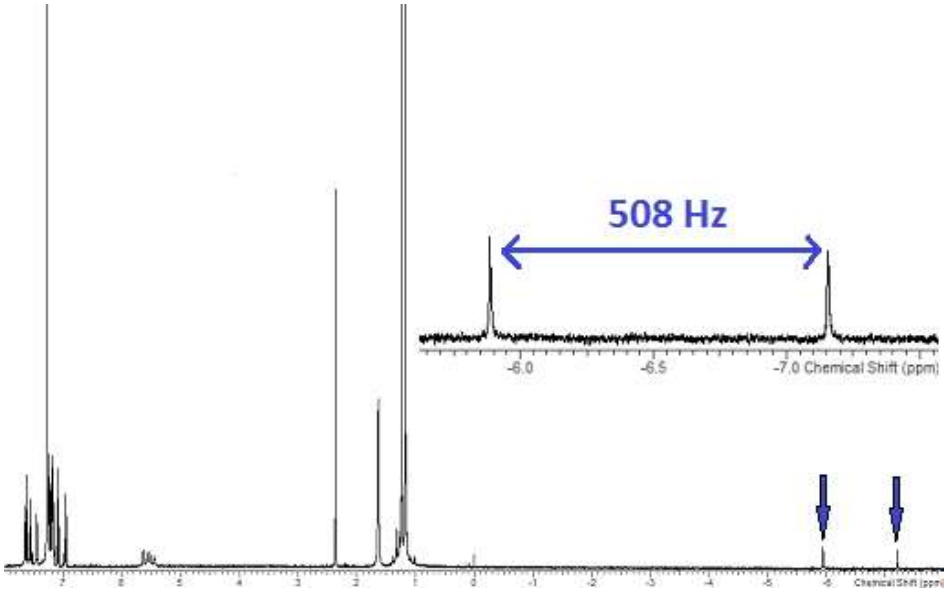

Figure 22: ^{1}H NMR (400 MHz, $CDCl_3$) spectrum of **HF@29**.

This chemical shift is similar to those reported for the endohedral protons of **H_2@29** and **H_2O@29**, which resonate at δ -7.17 and -9.84 ppm respectively. The large J value is comparable to that reported for HF in the gas phase.[110–112] A doublet with a J_{HF} of 508 Hz is present in the ^{19}F NMR at δ -223.91 ppm (Figure 23); the two lines coalesce into a singlet in the proton decoupled spectrum.

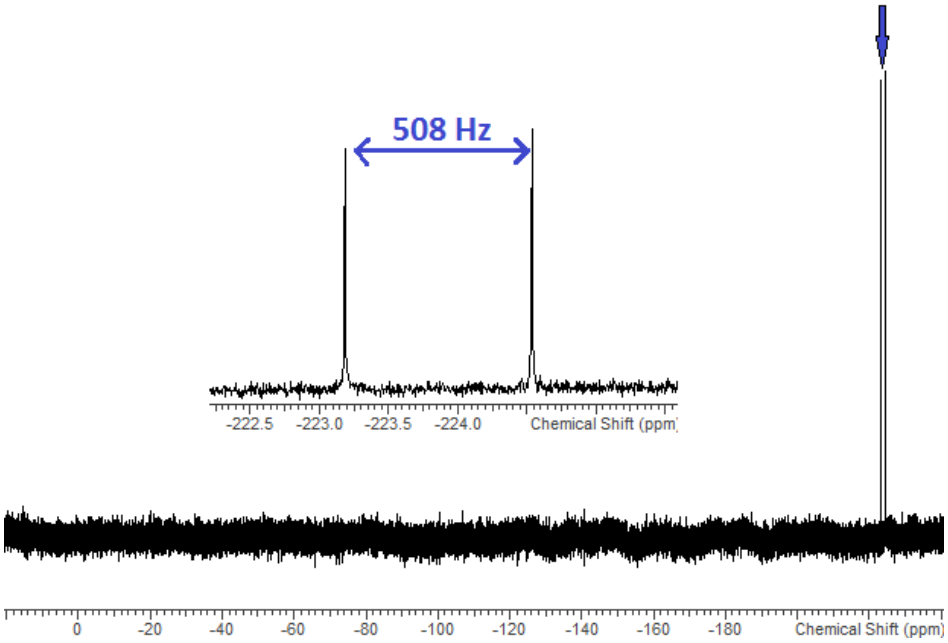

Figure 23: ^{19}F NMR (376 MHz, $CDCl_3$) spectrum of **HF@29**.

The MS spectrum displays signals at m/z 1121 and 1141 respectively for the molecular ions [**29**+H]$^+$, and [**HF@29**+H]$^+$. The filling factor of **HF@29** was established by ^1H NMR spectrometry, comparing the intensity of the peaks belonging to the endohedral HF and exohedral groups. The highest filling factor (50%) was achieved by equilibrating a solution of **29** or **28** in dichloromethane with an excess (200eq) of HF-Py at room temperature. In these conditions, the equilibrium was reached within 24 hours, and prolonged reaction time did not afford a higher filling factor; 50% filled **HF@29** was isolated after work up and chromatography in 89% yield. When a lower excess (100 eq) of HF-Py was used in similar conditions, a lower filling factor (40%) was achieved after equilibration. On the other hand a larger excess of HF-Py (400 eq) still produced 50% filled **HF@29** in comparable conditions. Both compounds **28** and **29** can be used as substrate, given that the acidic reaction medium is evidently able to afford the dehydration of **29** to form **28**. The filling at 4 ˚C proceeded at a much slower rate (~6 days), and did not afford a filling factor higher than 50% once the equilibrium was reached. When the process was carried out at 80 ˚C, a lower filling factor (30%) was achieved as it would be expected for an entropically disfavoured process; decomposition of the substrate also occurred and 30% filled **HF@29** was isolated in slightly lower yield (80%). When the filling was carried out in non-chlorinated solvents such as benzene, after the addition of excess HF-Py a biphasic system was formed and

the substrate was quantitatively extracted in the ionic liquid. Nonetheless, after work and chromatography, 50% filled **HF@29** was still isolated in very good yield (88%). Unexpectedly, other amine/poly(hydrogen fluoride) complexes such as triethylamine trihydrofluoride, poly[4-vinylpyridinium poly(hydrogen fluoride)], and anhydrous hydrogen fluoride[113] formed by reaction of H_2SO_4 with CaF_2, failed to afford any HF incorporation in comparable conditions.

2.8 Trapping hydrogen fluoride inside C_{60}

Suturing an endohedral OCF is the most challenging part of the molecular surgery approach. While several opening sequences have been reported and many molecules have been encapsulated inside various OCFs (cf. 1.3), only Komatsu and Murata have succeeded in completing the synthesis of closed endofullerenes. The reported routes to $H_2@C_{60}$ and $H_2O@C_{60}$ relied on the use of OCFs having orifices just wide enough to let the guest molecule through; in both cases this design allowed the use of high temperatures to force the closure without incurring in the loss of the encapsulated molecule. When the suturing of OCF **HF@29** was first evaluated, it was clear that the procedure was going to be complicated by the small size of HF in relation to the orifice of **28**. Calculations gave activation energies of 92.1, 85.3 and 55.7 KJ/mol respectively for the exit of H_2O, H_2 and HF from the cavity of **28**; consequently the release of HF from **HF@28** was expected to be fast in the conditions previously employed for suturing the orifice. The rapid hydration of **HF@28** to **HF@29** provides a very convenient way to shrink the size of the orifice and trap the endohedral molecule after the filling step (cf. 2.7). However, dehydration of **29** to **28** is a prerequisite for the successive reduction of the orifice. **H_2O@29** was dehydrated and reduced to **H_2O@27** by triphenylphosphine in refluxing toluene. When the same conditions were applied to **HF@29**, all of the endohedral HF was lost and only empty OCF **27** was isolated (Scheme 48).

To avoid the loss of HF, a new protocol for the dehydration of **HF@29** and the successive reduction of **HF@28** at lower temperature had to be developed.

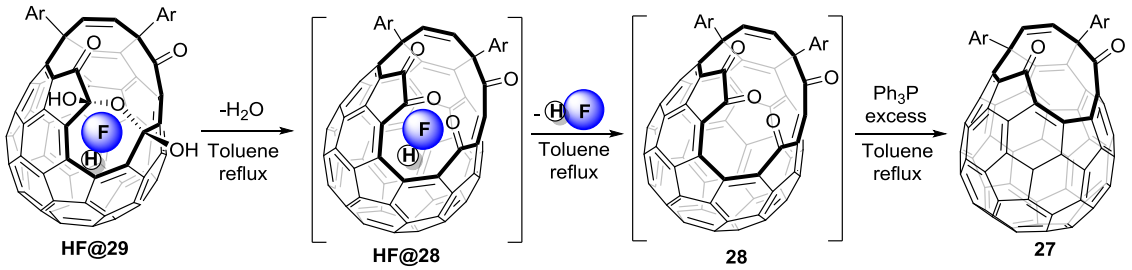

Scheme 48: Reduction of **HF@29** with triphenylphosphine in refluxing toluene.

The dehydration of OCF **29** using strong dehydrating reagents such as diisopropyl azodicarboxylate/triphenylphosphine,[114] triflic anhydride, and triphenylphosphonium anhydride trifluoromethane sulfonate[115] was attempted; however, none of these experiments were successful. The problems encountered were due to the dehydrating reagent which was either reacting destructively with the substrate, or causing unwanted side reactions that led to complex mixtures. Due to these complications, non-reactive desiccants such as magnesium sulphate, calcium sulphate, and molecular sieves were contemplated as well. In particular, activated 3 Å molecular sieves afforded the dehydration of **29** in toluene at room temperature. In order to easily follow the reaction, the process was carried out in the presence of an excess of triphenylphosphine. In these conditions, the dehydration product **28** was rapidly trapped as ylide **36b** (cf. 2.4) which showed a characteristic signal in the HPLC chromatogram (Figure 24).

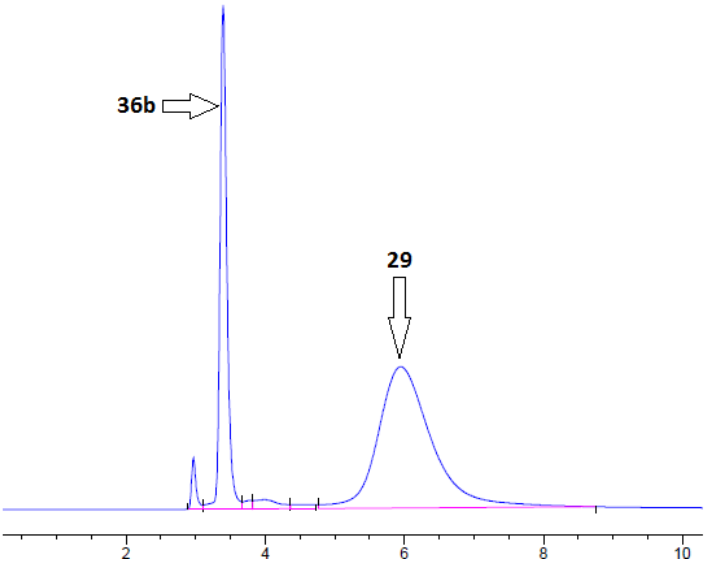

Figure 24: HPLC chromatogram showing formation of **36b** from **29** and triphenylphosphine in the presence of molecular sieves.

In these conditions the dehydration was extremely slow, requiring days of equilibration at room temperature to achieve complete transformation of **29** into **36b**. Unexpectedly, the addition of Brønsted and Lewis acids, which were presumed to catalyse the dehydration, completely inhibited the process. Preformed OCF **28** is reduced to **26** by triisopropyl phosphite at room temperature (cf. 2.4); however, the slow rate of the dehydration in the presence of molecular sieves precluded the use of this reducing reagent due to its side reactivity (cf. 2.4) towards OCF **29** (Scheme 49).

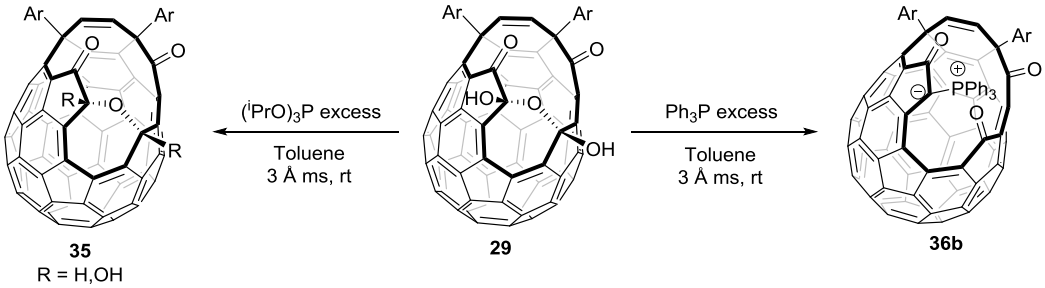

Scheme 49: Reactivity of **29** towards triphenylphosphine and triisopropyl phosphite at room temperature in the presence of molecular sieves.

Nonetheless, stirring a solution of **HF@29** and excess triphenylphosphine in dry toluene at room temperature over activated molecular sieves, afforded **HF@36b** as the only product. At this stage, the endohedral HF molecule was completely retained inside the cage (Scheme 50).

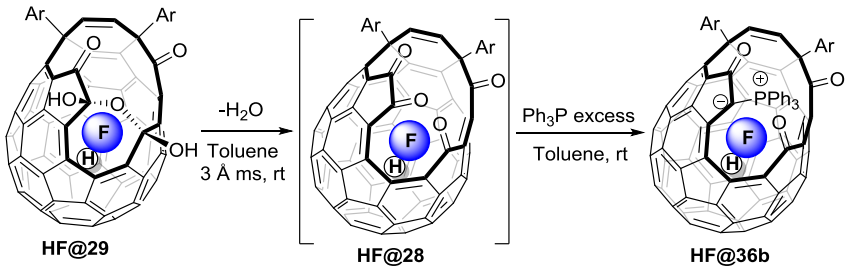

Scheme 50: Reactivity of **HF@29** towards triphenylphosphine at room temperature in the presence of molecular sieves.

Next step, **HF@36b** was refluxed in toluene to reduce the orifice via the intramolecular Wittig reaction. This transformation afforded OCF **27**, but the endohedral HF molecule was completely lost. The 16-membered orifice of ylide **36b** still allowed the escape of the guest molecule at the relatively high temperature needed for its reduction. The addition of excess HF-Py during this step was envisioned as an option to counteract the loss of HF from

endofullerene **HF@36b**. However, in the presence of excess HF-Py, ylide **36b** was reduced to OCF **51** (Scheme 51).

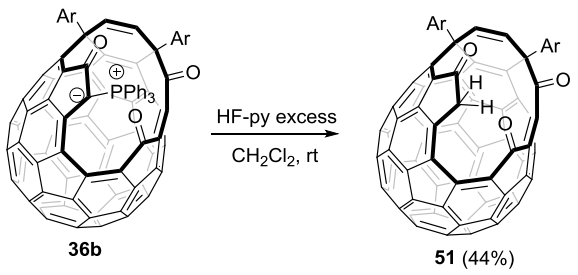

Scheme 51: Formation of OCF **51**.

The structure of compound **51** was supported by the appearance of two new doublets in the ^{1}H NMR spectrum at δ 4.75 and 4.15 ppm, showing a J_{HH} of 23 Hz (AX spin system); these signals were assigned to the diastereotopic protons of the new methylene group. The sp^{3} methylene carbon produced a new diagnostic signal at δ 45.84 ppm in the ^{13}C NMR spectrum. The DFT – GIAO calculated spectra further supported the regiochemistry of **51**. Particularly, an AX spin system was calculated for the methylene group of **51**. In fact, one of its protons falls within the anisotropy cone of the carbonyl group across the orifice and, consequently, is strongly deshielded. In contrast, calculations gave an AB spin system for the methylene protons of regioisomer **51a**, which are affected by similar environment (Figure 25). The loss of the triphenyl phosphonium group was supported as well by ^{31}P NMR and MS. The reduction of the ylide to OCF **51** is an indirect evidence of the regiochemistry of ylide **36b**.

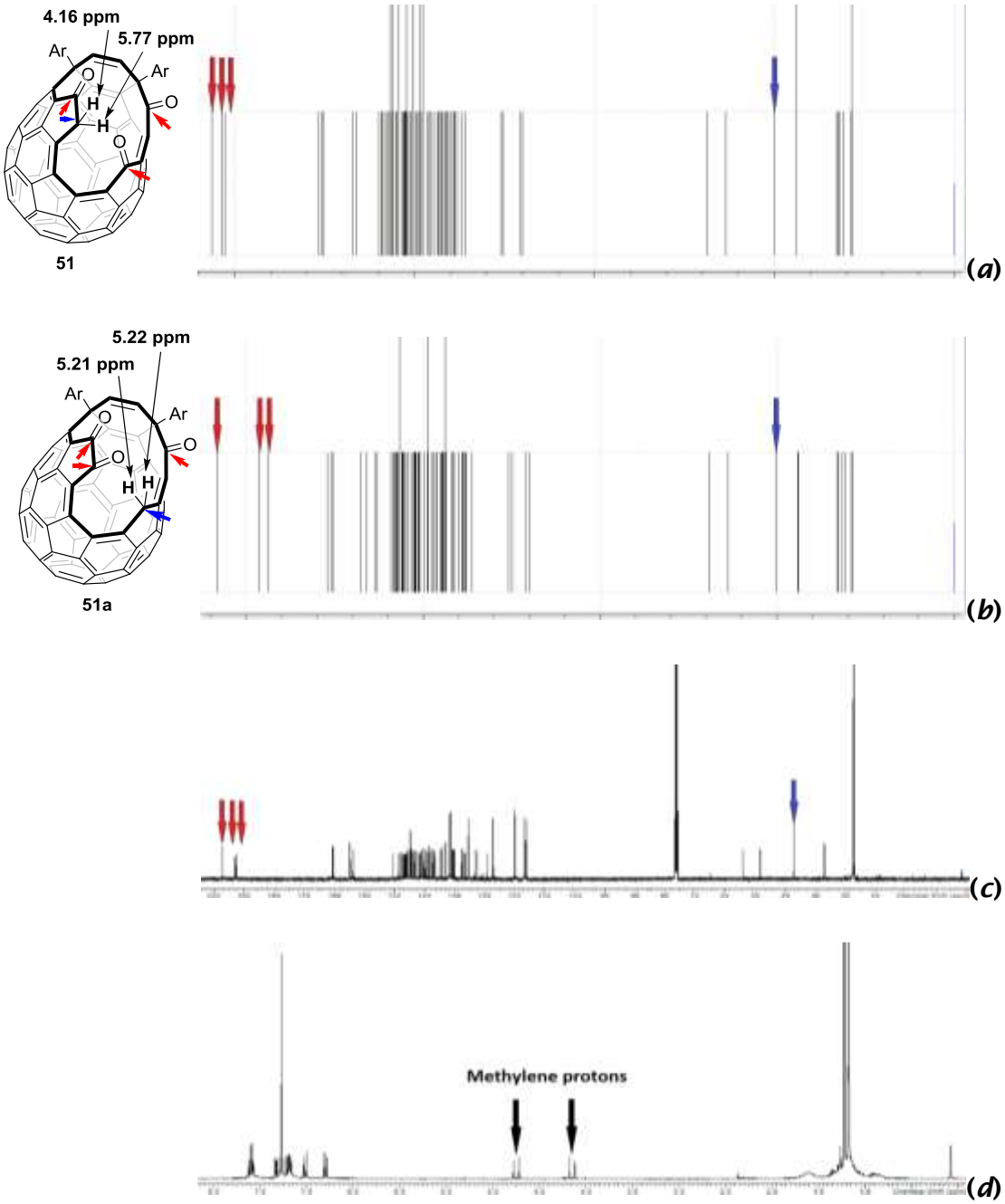

Figure 25: DFT-GIAO calculated ^{13}C spectra of **51** (*a*) and **51a** (*b*). The peaks of the characteristic CO and CH_2 orifice carbons are respectively indicated by red and blue arrows. Experimental ^{13}C (125 MHz, $CDCl_3$) spectrum (*c*) and ^{1}H (400 MHz, $CDCl_3$) spectrum (*d*).

The isolation of **HF@36b** in the aforementioned conditions suggested that a different ylide, which would undergo the intramolecular Wittig reaction at room temperature, could be used to trap the HF molecule inside the cavity of **27**. It has been reported that electron-withdrawing groups on the phosphorus atom affect the selectivity and rate of the Wittig reaction.[116-119] The furyl group has

been studied more than others, given that furyl phosphines can be easily synthesised from inexpensive precursors. Treating the 2-furyl group as electron-withdrawing can sound counterintuitive; after all, the furyl fragment is an electron-rich aromatic ring expected to have a mesomeric (+M) effect on its substituents. Nonetheless, experimental evidence shows its electron-withdrawing character relative to the phenyl ring, likely due to the strong inductive (-I) effect of the electronegative oxygen atom.[120,121] In particular, 2-furyl substituted ylides were expected to eliminate phosphine oxide more easily, and therefore lower the activation energy for the intramolecular Wittig step. To test this hypothesis, a solution of 50% filled **HF@29** in toluene was reacted at room temperature with excess tri(2-furyl)phosphine in the presence of molecular sieves. HPLC analysis showed conversion of the substrate **29** in the product **27** over time; no substantial build-up of the ylide signal was noticed (Figure 26).

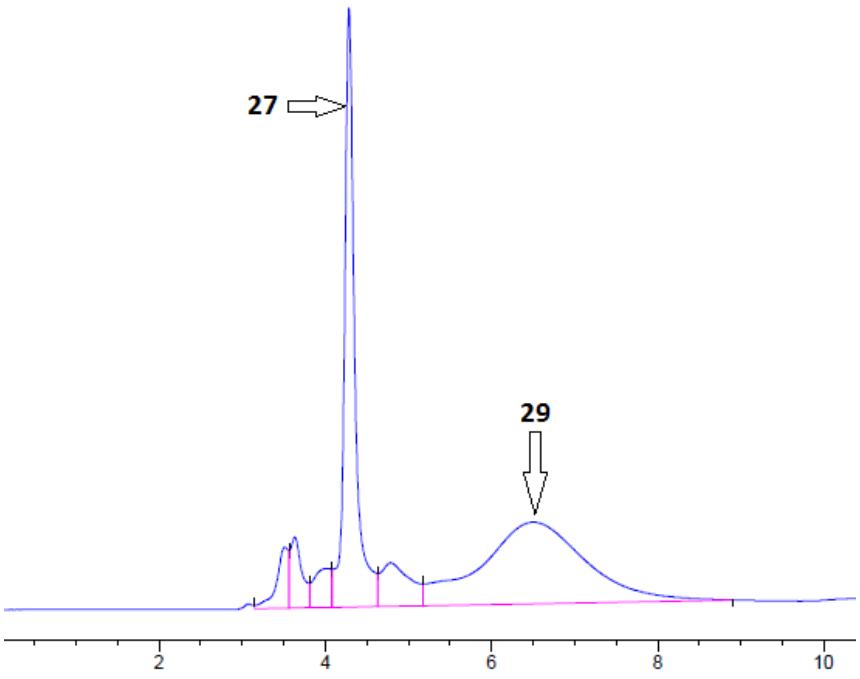

Figure 26: HPLC chromatogram of the reaction between **29** and tri(2-furyl)phosphine after 89 hours at room temperature.

Flash chromatography of the reaction mixture afforded **27** in 30% yield, with traces of endohedral HF barely detectable by ^{1}H NMR. The unreacted substrate **HF@29** was the only other component recovered, and showed a substantial loss of the endohedral HF molecule (-12% filling factor). The outcome of this experiment was interpreted on the basis of the previously studied (cf. 2.4)

mechanism of formation of triphenylphosphonium ylide **36b**. An analogous trifurylphosphonium ylide was formed *in situ* from **28** and tri(2-furyl)phosphine following the same reaction, followed by spontaneous extrusion of tri(2-furyl)phosphine oxide at room temperature, resulting in the formation of the reaction product **27**. The stability of the endohedral HF inside the cavity of triphenylphosphonium ylide **36b** at room temperature suggested that, in the case of tri(2-furyl)phosphine, the guest molecule was lost before the ylide was formed.

The free energy profile for the reaction of **28** with tri(2-furyl)phosphine was calculated. The figures suggested a mechanism analogous to the case of triphenylphosphine, with kinetics and thermodynamics favouring the formation of tri(2-furyl)phosphonium ylide **36b**. The calculated activation barrier for the Wittig reaction of tri(2-furyl)phosphonium ylide **36b** was 29.1 KJ/mol lower (Scheme 52) than the activation barrier of triphenylphosphonium ylide **36b** (cf. 2.4). This accorded with the lower temperature required to carry out this step experimentally.

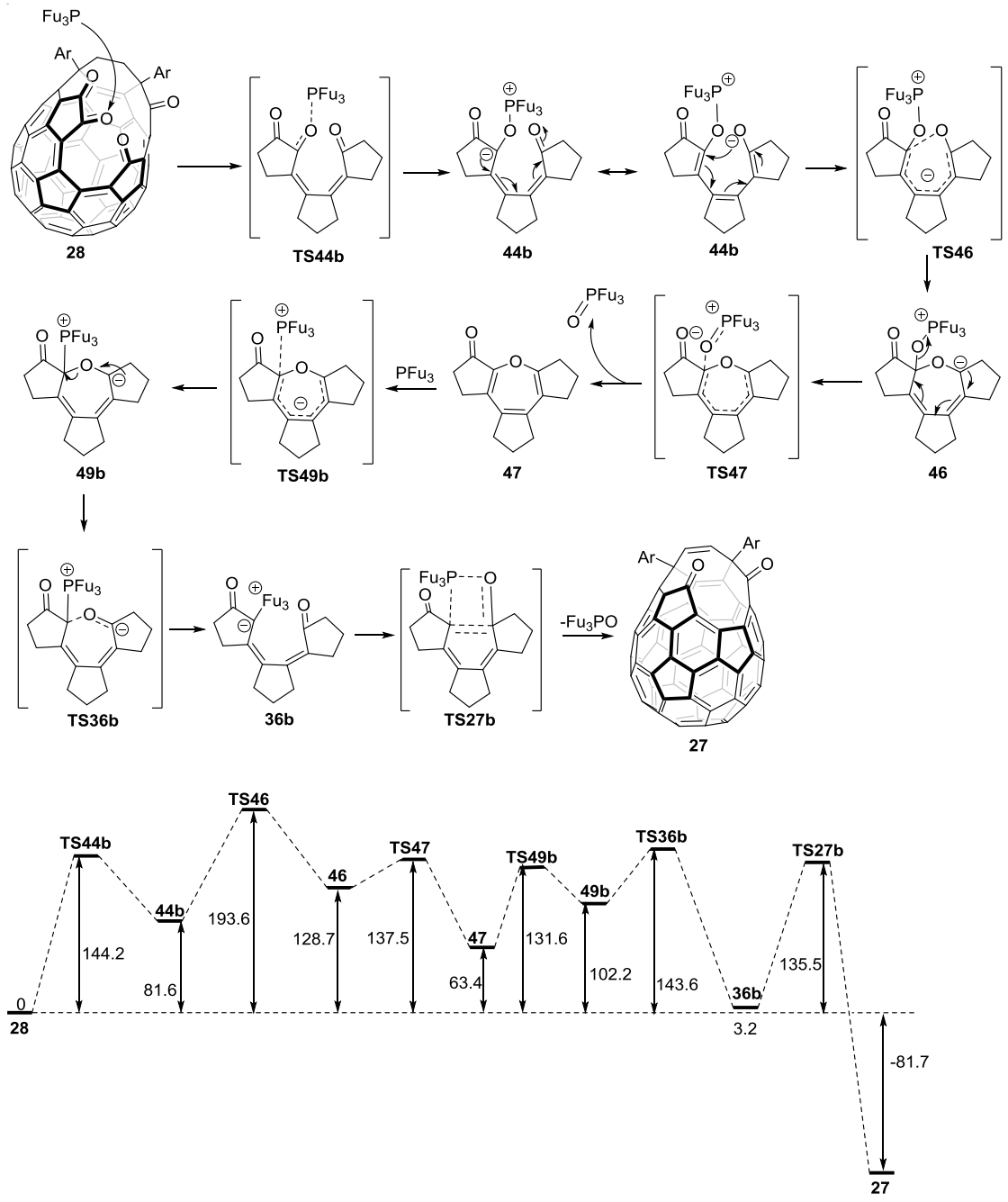

Scheme 52: Free energy profile for the reaction of **28** with tri(2-furyl)phosphine. Energies are reported in KJ/mol. Structures are drawn following the convention used in Scheme 34.

At the opposite end of the reaction profile, the barrier for the attack of tri(2-furyl)phosphine on **28** was 17.7 KJ/mol higher than for the attack of triphenylphosphine. This difference reflects the less nucleophilic character of the phosphorus atom of tri(2-furyl)phosphine in relation to triphenylphosphine. Moreover, the intermediate **44b** formed from this initial attack, was 17.2 KJ/mol less stable in the case of tri(2-furyl)phosphine. Similarly, the following

formation of tetrahedral intermediate **46** involved a higher energy barrier (+ 26.3 KJ/mol), and the intermediate was significantly less stable (+25.8 KJ/mol) for tri(2-furyl)phosphine. Experimentally, these factors translated into a slower attack on OCF **28** by tri(2-furyl)phosphine, and in a shift of the equilibrium of formation of the key intermediates **44b** and **46** towards the starting materials. Consequently, the HF molecule was almost completely lost from **HF@28** before the tri(2-furyl)phosphonium ylide was formed.

Similar calculations suggested that a compromise between the nucleophilicity of the phosphine and the reactivity of the ylide, could be reached using di(2-furyl)phenylphosphine. This mixed phosphine showed an intermediate nucleophilicity and could produce *in situ* a ylide showing similar reactivity to the tri(2-furyl)phosphonium one (Scheme 53).

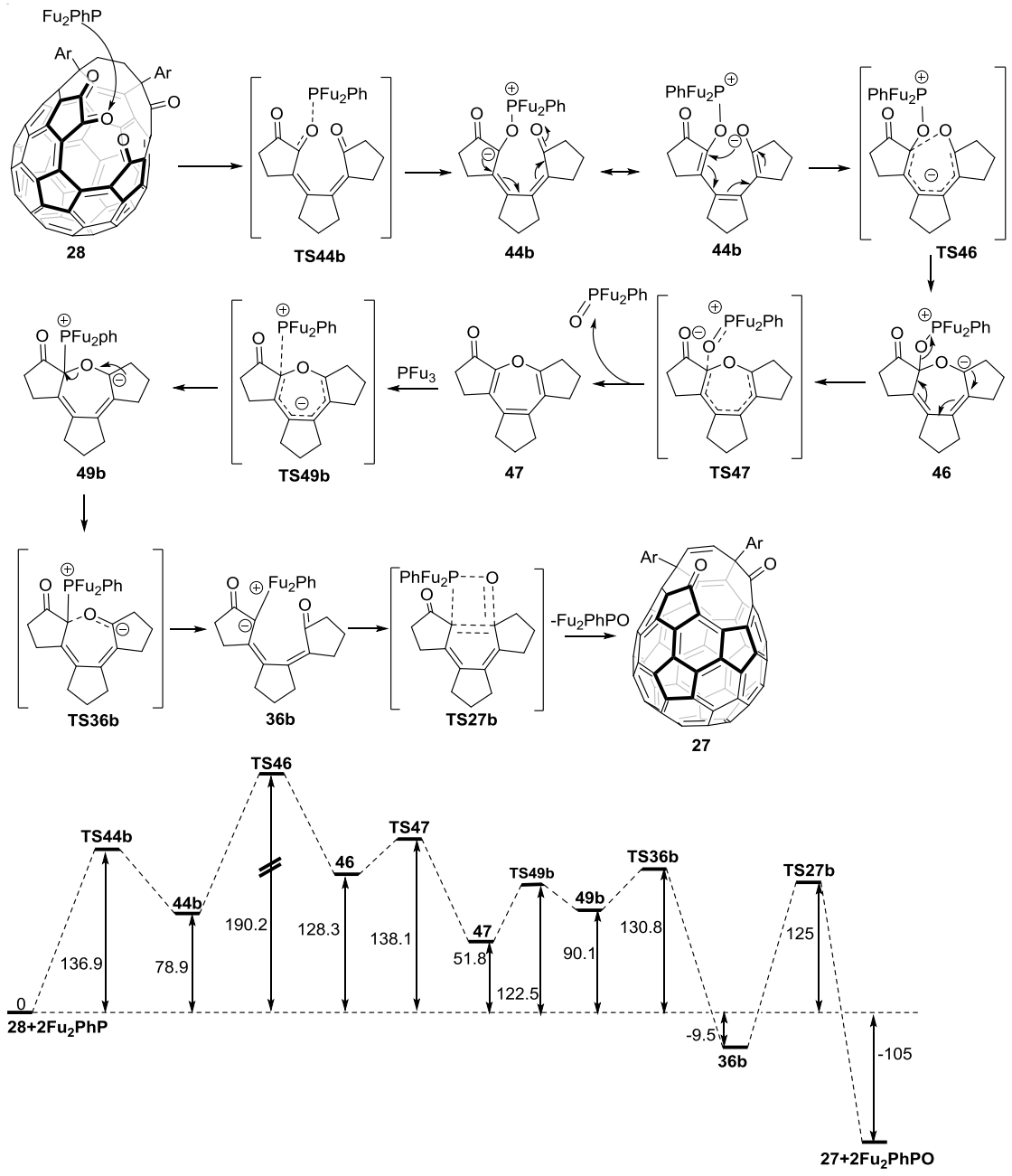

Scheme 53: Free energy profile for the reaction of **28** with di(2-furyl)phenylphosphine. Energies are reported in KJ/mol. Structures are drawn following the convention used in Scheme 34.

Therefore a solution of 50% filled **HF@29** in toluene was reacted at room temperature with excess di(2-furyl)phenylphosphine, in the presence of 3 Å molecular sieves. HPLC analysis showed conversion of the substrate **29** in the ylide **36d**, followed by its slow transformation into product **27** over time (Figure 27).

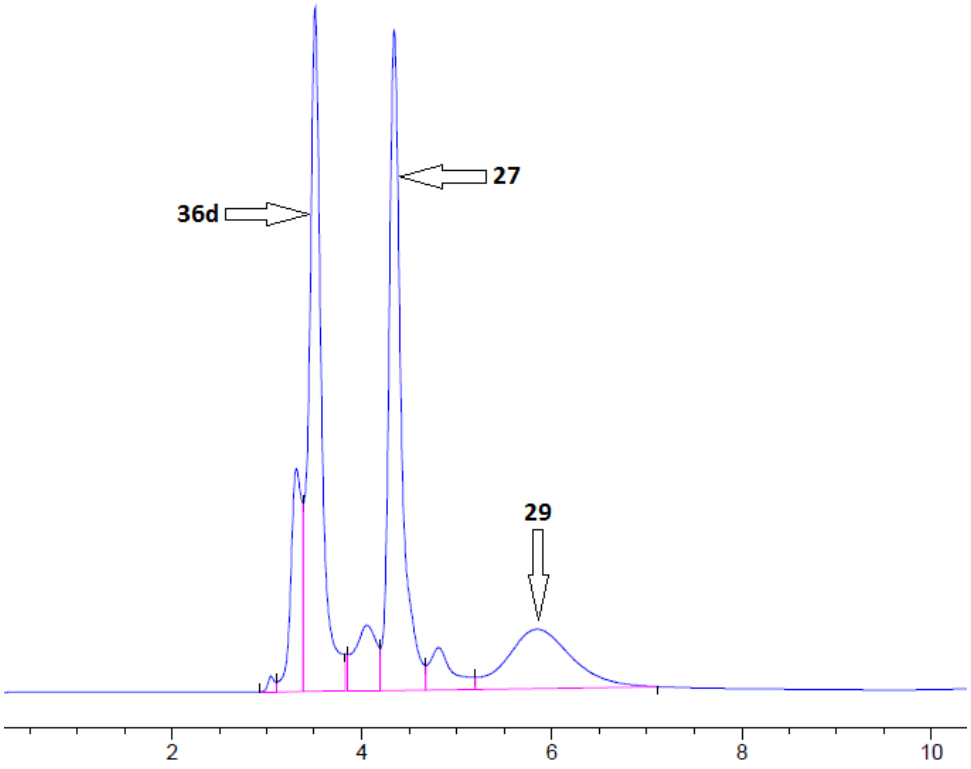

Figure 27: HPLC chromatogram of the reaction between **29** and di(2-furyl)phenylphosphine after 48 hours at room temperature.

After chromatography 30% filled **HF@27** was isolated in 64% yield. As the calculation suggested, the greater nucleophilicity of di(2-furyl)phenylphosphine was key to closing the cavity of **HF@28**, and trapping part of the endohedral HF inside the cavity of OCF **27**. Unfortunately, a significant part of the encapsulated HF is still lost on the way to the ylide.

The 12-membered orifice of **HF@27** was sutured as described for $\mathbf{H_2@C_{60}}$ and $\mathbf{H_2O@C_{60}}$ without appreciable loss of the endohedral molecule. Thus, 30% filled $\mathbf{HF@C_{60}}$ was isolated after reduction of **HF@27** with triisopropyl phosphite, and reaction of **HF@26** with N-phenylmaleimide (Scheme 54).

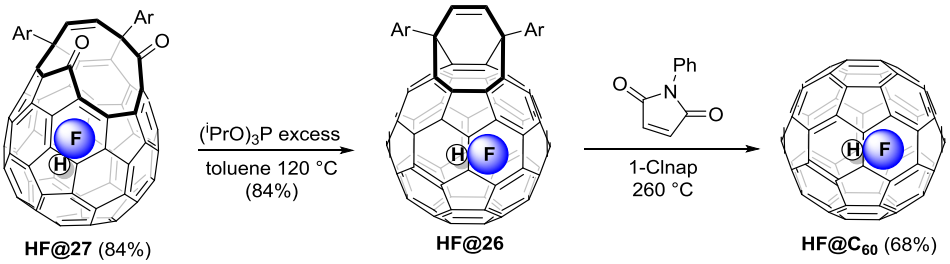

Scheme 54: synthesis of $\mathbf{HF@C_{60}}$ from **HF@27**.

Overall, 30% filled **HF@C$_{60}$** is produced in three steps, and 36% yield form 50% filled **HF@29**. The endohedral HF molecule inside OCFs **HF@27**, **HF@26**, and endofullerene **HF@C$_{60}$**, resonates at negative δ in the ^{1}H and ^{19}F NMR spectra due to the shielding effect of the C$_{60}$ cage; similarly to the case of **HF@29** (cf. 2.7). The ^{1}H and ^{19}F NMR spectra of **HF@C$_{60}$** display a doublet respectively centred at δ = -2.51 and -219.94 ppm, with a J_{HF} of 506 Hz. The latter doublet coalesces into a singlet in the proton decoupled ^{19}F spectrum. The ^{13}C NMR spectrum of 30% filled **HF@C$_{60}$** shows a sharp singlet at δ = 142.76 that is 0.04 ppm upshifted from empty C$_{60}$.This value lies between the 0.02 ppm upshift[71] of **He@C$_{60}$** and the 0.07 ppm upshift[70,122] of **H$_2$@C$_{60}$**, and follows the increase in the van der Waals radius of the endohedral guest (Figure 28).[123]

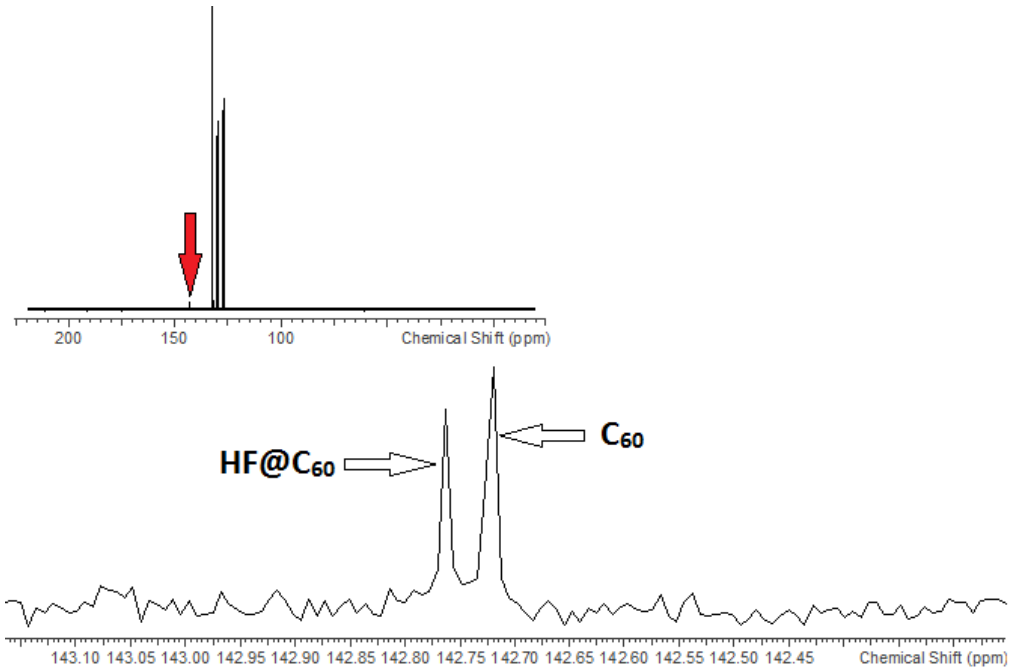

Figure 28: ^{13}C NMR (odcb-d$_4$, 100 MHz) spectrum of 30% filled HF@C$_{60}$.

The dipole moment calculated for **HF@C$_{60}$** is slightly lower than the dipole moment of **H$_2$O@C$_{60}$**.[124] This property affects the separation by HPLC (Buckyprep, toluene) of C$_{60}$ (RT = 7.81 min) from **HF@C$_{60}$** (RT = 8.02 min). In fact **H$_2$O@C$_{60}$** was separated from C$_{60}$ in a single stage, while two cycles were needed to completely separate **HF@C$_{60}$** from C$_{60}$ (Figure 29).

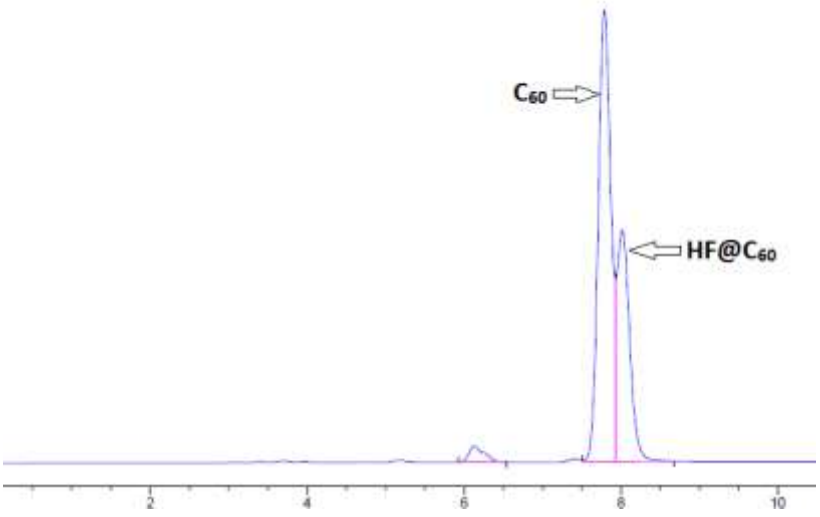

Figure 29: HPLC chromatogram (Buckyprep, toluene) of 30% filled HF@C_{60}.

Empty C_{60} was not detected by HPLC, ^{13}C NMR or MS analysis of the 100% **HF@C_{60}** sample.

Chapter 3: Conclusion

This work investigated the synthesis of small molecule endofullerenes. In particular, a systematic study of the $H_2O@C_{60}$ synthesis developed by the group of Murata,[72] was carried out. It demonstrated that H_2O can be encapsulated inside the hydrophobic cavity of OCF **29** without the need of high pressure, achieving a 78% filling using traditional laboratory glassware. Dehydration of **29** to form OCF **28** allowed the incorporation of D_2O in similar conditions, without contamination of HOD and H_2O. Theoretically, the same protocol can be extended to the encapsulation of any isotopologue of water avoiding contamination. Similarly, dehydration of **29** allowed the incorporation of hydrogen without contamination by water. The large size of the orifice of compound **29** relative to OCF **23** enabled 60% incorporation of hydrogen at relatively low temperature and pressure.

A novel reduction of the orifice of **28** with triphenylphosphine was developed, affording the first isolation of **H_2O@27** and **H_2@27**. This reaction was studied theoretically. A reaction mechanism involving the formation of intermediate phosphonium ylide **36b** and its subsequent intramolecular Wittig reaction was proposed. Successive reduction of **H_2O@27** and **H_2@27** with triisopropyl phosphite afforded **H_2O@26** and **H_2@26**.

A new method for the synthesis of C_{60} endofullerenes from filled OCF **26** was developed using a Diels–Alder/retro-Diels–Alder sequence, which gave substantially higher yields than the known pyrolysis method. Overall, pure sublimed **$H_2O@C_{60}$** (78% incorporation), **$D_2O@C_{60}$** (78% incorporation, uncontaminated by HOD or H_2O) and **$H_2@C_{60}$** (60% incorporation) were synthesised in 15% yield from pristine C_{60}.

All these advances will help meet the demand for **$H_2O@C_{60}$**, **$H_2@C_{60}$** and their isotopologues needed for physical studies. This improved synthesis has already provided **$H_2O@C_{60}$** for the study of spin conversion between ortho and para water by NMR.[103] Investigation of ortho-para conversion via dielectric constant measurement is currently underway.

A convenient protocol for the encapsulation of hydrogen fluoride inside the cavity of **29** was as well discovered; **HF@29** is the first example of endofullerene enclosing a molecule of HF inside its cavity. The solution NMR

data showed a large ^{1}H-^{19}F J-coupling of 508 Hz, similar to that obtained for HF in the gas phase. The solid-state NMR spectra indicated that the HF molecule rotates rapidly, and almost isotropically, in the supramolecular complex.

Reaction of **HF@29** with di(2-furyl)phenylphosphine in the presence of molecular sieves allowed partial closure to **HF@27** at room temperature, thus avoiding complete escape of the encapsulated molecule. Reduction with triisopropyl phosphite and reaction with N-phenylmaleimide resulted in the first synthesis of HF@C_{60}. This novel endofullerene is the ideal candidate for the study of HF at a molecular level, and is also anticipated to display interesting properties such as ferroelectricity.[125]

Chapter 4: Experimental

4.1 General

All reactions were carried out under argon or nitrogen atmosphere, unless otherwise stated. All glassware was dried overnight at 160 °C and cooled down to room temperature in a desiccator over Drierite before assembly, or assembled under nitrogen flow while still hot. Sublimation tubes were degreased with aqua regia, and then rinsed with water, acetone, and finally oven dried. When needed, solutions were degassed under reduced pressure (1 mmHg) until the evolution of gas stopped. All additions were performed using regular air-free techniques. Reactions involving hydrogen fluoride/pyridine were carried out in polytetrafluoroethylene (PTFE) or polyethylene (PE) tubes, fitted with screw caps. Hydrogen fluoride pyridine was handled using PE or PTFE containers and tubing. Reactions under high pressure (120 atm) were performed using a Parr reactor. The course of reaction was monitored by TLC using Merck silica gel 60 F254 plates, detecting the spots using an UV lamp. Alternatively, HPLC performed on a Cosmosyl Bukyprep analytical column with detection at 326nm was used. Flash column chromatography was run using Merck silica gel Geduran Si60 (40-63 μm) as stationary phase. NMR spectra were recorded on Bruker AV300, DPX400 or 500 spectrometers. Chemical shifts are reported in ppm and referenced to the residual solvent peak for ^{1}H and ^{13}C, or $CFCl_3$ and H_3PO_4, for ^{19}F and ^{31}P respectively. Due to partial filling factor, peaks of reduced intensity belonging to the empty cages were displayed in the ^{13}C spectra of endofullerenes; these signals are not listed. FT-IR spectra were recorded on a Bruker Alpha-T instrument. UV spectra were recorded on an Ocean Optics USB2000+ UV/Vis spectrometer. Electrospray mass spectra were recorded in the positive ion mode. The expected peaks due to natural abundance ^{13}C were present, but not reported. Note that due to the noise-reducing threshold used in processing, relative intensities of weak peaks are reduced. High resolution mass spectra were recorded using a solariX (Bruker Daltonics, Bremen, Germany) mass spectrometer equipped with Fourier Transform Ion Cyclotron Resonance (FT-ICR), using positive ion atmospheric pressure photoionisation.

4.2 Materials

Molecular sieves type 3 Å (beads, 8-12 mesh) were purchased from Sigma-Aldrich Company Ltd., activated by heating at 220 °C under dynamic vacuum (1 mmHg) for 4 hours, cooled, and stored under nitrogen atmosphere. Toluene, benzene, and o-dichlorobenzene were distilled over sodium under nitrogen atmosphere. Dichloromethane was distilled over calcium hydride under nitrogen atmosphere. Tetrahydrofuran was distilled over sodium/benzophenone under nitrogen atmosphere once the indicator had turned to a deep blue colour. Triisopropyl phosphite (≥95%) was purchased from Sigma-Aldrich Company Ltd. and distilled over sodium under reduced pressure before use. Technical 1-chloronaphthalene (≥85%) was purchased from Sigma-Aldrich Company Ltd. and distilled under nitrogen before use. All other solvents and reagents were directly employed as received from the supplier without any further purification. di(2-furyl)phenylphosphine was synthesised according to literature.[126]

4.3 Experimental procedures and characterisation data

4.3.1 Preparation of precursors

4.3.1.1 Synthesis of 33

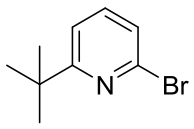

33

2,6-Dibromopyridine (15.089 g, 63.7 mmol) and copper(I) iodide (3.639 g, 19.1 mmol) were suspended in distilled THF (70 ml) under argon atmosphere. The suspension was cooled inside an ice bath and t-butylmagnesium chloride 1.7 M in THF (56 ml) was slowly added during 1 hour. Upon completion of the addition, the mixture was stirred for 2 hours. The reaction mixture was diluted with diethyl ether (120 ml) and later quenched with NH_4Cl saturated solution. The mixture was filtered and the two layers separated. The organic layer was washed with brine while the aqueous layer was extracted with diethyl ether. The organic extracts were then combined, dried over $MgSO_4$, filtered, and evaporated to dryness to afford a dark yellow oil. This crude was purified by flash column chromatography over a short silica plug (eluent: hexane) to afford **33** as a pale yellow oil (9.325 g, 68%).

^{1}H NMR: (400 MHz, $CDCl_3$, δ): 7.48 (t, J = 7.9 Hz, 1H, H-4), 7.28 (d, J = 7.8 Hz, 2H, H-3 and H-5), 1.36 (s, 9H, t-butyl).

^{13}C NMR: (75 MHz, $CDCl_3$, δ): 171.22, 141.18, 135.45, 124.93, 117.76, 37.59, 29.97.

Known compound; values consistent with reported data.[72]

4.3.1.2 Synthesis of 25

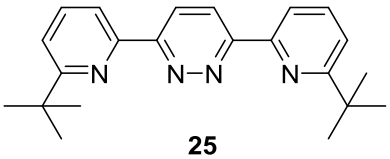

25

2-Bromo-6-t-butylpyridine **25** (9.183 g, 42.9 mmol) was dissolved in distilled THF (43 ml) under argon atmosphere. The reaction mixture was cooled in a liquid N_2/acetone bath, then n-buthyllithium 2.5 M in hexanes (17 ml) was slowly added. Upon completion of the addition, the reaction mixture was stirred for 15 minutes; a solution of anhydrous $ZnCl_2$ in distilled THF (43 ml) was added next. The solution was allowed to warm up to room temperature and then stirred for 30 minutes. 3,6-dichloropyridazine and $Pd(PPh_3)_4$ were added and the reaction mixture was refluxed for 15 hours. The reaction mixture was quenched with saturated $NaHCO_3$ (150 ml) and the two layers were separated. The organic layer was washed with brine while the aqueous layer was exhaustively extracted with dichloromethane. The combined organic extracts were dried over $MgSO_4$, filtered and evaporated to dryness to isolate a brown oil. This crude was purified by flash column chromatography over silica gel (eluent 10% ethyl acetate in hexanes). The fractions containing the spot located at at R_f 0.27 (eluent: 10% ethyl acetate in hexanes) were collected and evaporated to yield **25** as an off white solid (3.390 g, 68%).

^{1}H NMR: (400 MHz, $CDCl_3$, δ): 8.78 (s, 2H, H-3), 8.57 (d, J = 7.9 Hz, 2H, H-3'), 7.82 (t, J = 7.9 Hz, 2H, H-4'), 7.44 (d, J = 7.9 Hz, H-5'), 1.48 (s, 18H, t-butyl).

^{13}C NMR: (100 MHz, $CDCl_3$, δ): 168.89, 158.56, 151.90, 137.22, 125.10, 119.98, 118.24, 37.70, 30.20.

Known compound; values consistent with reported data.[72]

4.3.1.3 Synthesis of 27

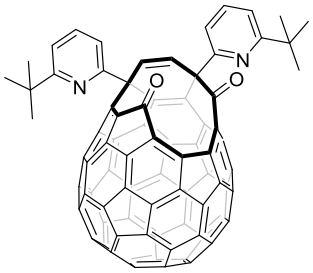

27

C_{60} (3.590 g, 4.98 mmol) and **25** (1.726 g, 4.98 mmol) were placed inside a round-bottom flask under argon atmosphere. 1-chloronaphthalene (180 ml) was added and the mixture was degassed under dynamic vacuum. The apparatus was then put under argon atmosphere and the reaction mixture was refluxed for 26 hours. The mixture was diluted with CS_2 (100 ml) and transferred to a 500 ml jacketed cylindrical flask. Water was circulated in the outer jacket for cooling and oxygen was bubbled in the reaction mixture using a needle at a flow of approximately 20 ml/min. The mixture was irradiated using a 400W halogen light placed at a distance of 20 cm from the bottom of the reactor for 24 hours. The mixture was poured over a short silica column. The column was eluted with 1:1 toluene/hexanes to remove unreacted C_{60} and 1-chloronaphthalene and then the column was flushed with toluene. The fraction containing the spot located at Rf 0.43 (toluene) were collected and evaporated to afford a black solid (2.811 g, 53%).

^{1}H NMR: (400 MHz, $CDCl_3$, δ): 7.69 (t, J = 7.8 Hz, 1H, H-4 or H-4' of pyridyl), 7.66 (t, J = 7.8 Hz, 1H, H-4 or H-4' of pyridyl), 7.52 (d, J = 7.8 Hz, 1H, H-3/3' or H-5/5' of pyridyl), 7.40 (d, J = 7.8 Hz, 1H, H-3/3' or H-5/5' of pyridyl), 7.24 (d, J = 8.1 Hz, 2H, H-3/3' or H-5/5' of pyridyl), 7.22 (d, J = 10.0 Hz, 1H, alkenyl), 7.18 (d, J = 9.8 Hz, 1H, alkenyl), 1.27 (s, 9H, t-butyl), 1.19 (s, 9H, t-butyl).

^{13}C NMR: (125 MHz, odcb-d_4, δ): 199.2, 191.42, 168.84, 168.52, 165.44, 162.44, 154.46, 149.59, 148.33, 147.45, 147.41, 147.24, 146.97, 146.47, 146.33, 146.22, 146.04, 145.89, 145.62, 145.48, 145.43, 145.39, 145.31, 145.18, 144.96, 144.69, 144.63, 144.28, 144.25, 143.92, 143.83, 143.57, 142.54, 142.23, 142.08, 141.81, 141.54, 141.51, 141.31, 140.69, 140.57, 140.31, 140.1, 139.76, 139.69, 139.56, 139.29, 139.25, 138.38, 138.35, 137.32, 137.12, 137.02, 136.09, 135.83, 135.42, 134.77, 133.74, 132.6, 132.53, 131.31, 130.24, 129.87, 129.02, 128.2, 127.39, 120.09, 119.71, 117.44, 116.72, 61.03, 54.84, 37.6, 37.51, 29.85.

UV: (CH_2Cl_2, λ_{max}, nm): 257.11, 322.41.

Known compound; values consistent with reported data.[72]

4.3.1.4 Synthesis of 29

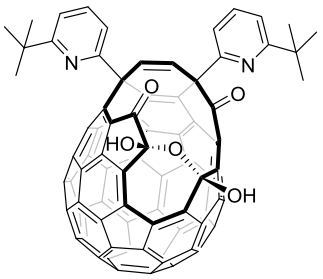

29

Compound **27** (3.355 g, 3.13 mmol) was dissolved in distilled THF (335 ml) under argon atmosphere. N-methylmorpholine-N-oxide (0.843 g, 7.20 mmol) was added followed by distilled water (57 μl). The reaction mixture was stirred at room temperature for 3 hours. Silica gel (25 ml) was added and the mixture was evaporated to dryness to afford a black solid. This material was purified by flash column chromatography (eluent gradient: 10 to 15% ethyl acetate in toluene). The fractions containing the spot located at Rf 0.21 (10% ethyl acetate in toluene) were collected and evaporated to afford compound **29** as a black solid (3.070 g, 88%).

^{1}**H NMR:** (400 MHz, $CDCl_3$, δ): 7.64 (t, J = 7.9 Hz, 1H, H-4 or H-4' of pyridyl), 7.57 (t, J = 7.8 Hz, 1H, H-4 or H-4' of pyridyl), 7.44 (d, J = 7.8 Hz, 1H, H-3/3' or H-5/5' of pyridyl), 7.23 (d, J = 7.2 Hz, 1H, H-3/3' or H-5/5' of pyridyl), 7.22 (d, J = 7.8 Hz, 1H, H-3/3' or H-5/5' of pyridyl), 7.16 (d, J = 7.1 Hz, 1H, H-3/3' or H-5/5' of pyridyl), 7.09 (d, J = 10.2 Hz, 1H, alkenyl), 6.94 (d, J = 10.1 Hz, 1H, alkenyl), 5.42 (s, 1H, hydroxyl), 5.34 (s, 1H, hydroxyl), 1.24 (s, 9H, t-butyl), 1.18 (s, 9H, t-butyl).

^{13}**C NMR:** (125 MHz, odcb-d_4, δ): 198.88, 194.33, 168.71, 168.29, 164.53, 162.89, 153.59, 149.79, 149.27, 149.22, 148.97, 148.92, 147.77, 148.28, 148.18, 148.12, 147.89, 147.59, 147.34, 146.95, 146.87, 146.51, 146.40, 145.92, 145.10, 144.93, 144.78, 144.28, 144.17, 143.52, 143.37, 142.61, 142.52, 142.10, 141.85, 140.97, 140.57, 140.46, 140.08, 139.78, 138.71, 137.85, 137.82, 137.52, 137.32, 137.06, 137.00, 136.93, 136.77, 136.12, 135.89, 135.44, 134.62, 134.42, 133.92, 133.76, 131.98, 131.60, 130.97, 129.42, 129.22, 129.02, 128.21, 125.32, 120.00, 119.85, 117.42, 116.83, 110.23, 96.75, 59.73, 54.88, 37.65, 37.46, 29.94, 29.81.

UV: (CH_2Cl_2, λ_{max}, nm): 256.73, 326.09.

Known compound; values consistent with reported data.[72]

4.3.1.5 Synthesis of 28

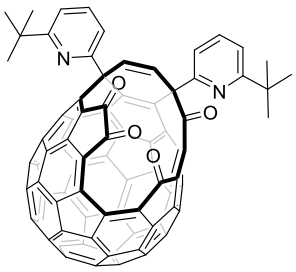

28

Compound **29** (60 mg, 0.053 mmol) was placed inside 50 ml Schlenk flask. The flask was connected to a 5 ml dropping funnel with a pressure regulating arm. The funnel was completely filled with 3Å activated molecular sieves. The top of the dropping funnel was connected to a straight condenser linked to a vacuum/argon inlet. The system was put under argon atmosphere and then toluene was added (20 ml). The apparatus was placed inside an oil bath heated to 120 °C, and the tap of the dropping funnel was closed so that the solvent vapours could start refluxing through the pressure regulating arm and then condense and accumulate inside the dropping funnel. The tap was opened and the system was refluxed for 2 hours. The reaction mixture was allowed to cool down to room temperature. The solution was transferred to a distillation apparatus under argon atmosphere. The solvent was distilled off under argon to afford compound **28** as a black solid (59 mg, quantitative yield).

^{1}H NMR: (300 MHz, $CDCl_3$, δ): 7.55 (t, J = 7.5 Hz, 1 H, H-4 or H-4' of pyridyl), 7.49 (t, J = 7.9 Hz, 1 H, H-4 or H-4' of pyridyl), 7.31 (d, J = 7.2 Hz, 1 H), 7.12 (d, J = 10.2 Hz, 1 H), 7.15 (d, J = 7.9 Hz, 1 H), 7.13 (d, J = 7.2 Hz, 1 H), 7.09 (d, J = 7.9 Hz, 1 H), 6.90 (d, J = 10.2 Hz, 1 H), 1.09 (s, 9 H), 1.06 (s, 9 H).

^{13}C NMR: (75MHz, $CDCl_3$, δ): 192.11, 187.38, 183.26, 182.32, 168.86, 168.32, 163.66, 162.31, 154.89, 150.01, 149.85, 149.7, 149.39, 149.17, 149.15, 149.12, 148.62, 148.59, 148.17, 147.99, 147.46, 147.4, 147.33, 147.09, 147.02, 146.97, 146.73, 146.14, 145.09, 144.74, 144.68, 144.57, 144.43, 144.19, 143.94, 143.77, 142.9, 142.21, 142.1, 141.12, 140.99, 140, 139.87, 138.98, 138.54, 138.37, 137.96, 137.83, 137.42, 137.12, 137.08, 136.87, 136.81, 136.12, 135.68, 134.9, 134.7, 134.35, 133.47, 133, 132.93, 132.82, 131.57, 130.62, 127.98, 125.9, 120.09, 119.52, 117.59, 117.06, 59.22, 55.04, 37.76, 37.61, 29.93, 29.81.

UV: (CH_2Cl_2, λ_{max}, nm): 257.48, 319.83.

Known compound; values consistent with reported data.[73]

4.3.2 Preparation of water open-cage endofullerenes

4.3.2.1 Synthesis of H_2O@29

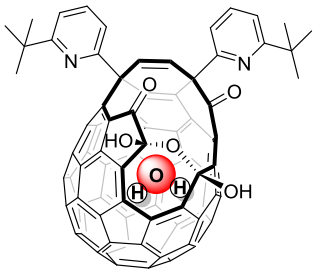

H_2O@29

Compound **29** (600 mg, 0.536 mmol) was placed inside a 40 ml tube equipped with a J.Young valve. The tube was put under an argon atmosphere and 1-chloronaphthalene (17 ml) was added followed by distilled water (54 μl). The solution was degassed and the tube was charged with argon gas (1 atm). The tube was completely immersed inside an oil bath preheated to 100 ˚C for 48 hours. After this time had elapsed the tube was cooled to room temperature and the solution was poured directly over a silica column packed with toluene. The column was eluted with toluene until all 1-chloronapthalene was removed. The eluent polarity was then gradually increased to 15% AcOEt in toluene to collect 78% filled **H_2O@29** (546 mg, 90%).

^{1}H NMR: (300 MHz, $CDCl_3$, δ): 7.64 (t, J = 7.8 Hz, 1H, H-4 or H-4' of pyridyl), 7.57 (t, J = 7.8 Hz, 1H, H-4 or H-4' of pyridyl), 7.48 (d, J = 7.8 Hz, 1H, H-3 or H-3' of pyridyl), 7.21 (d, J = 7.8 Hz, 2H, H-5 and H-5' of pyridyl), 7.16 (d, J = 7.8 Hz, 1H, H-3 or H-3' of pyridyl), 7.11 (d, J = 10.0 Hz, 1H, alkene), 7.01 (d, J = 10.0 Hz, 1H, alkene), 6.06 (br s, 1H, OH), 5.85 (br s, 1H, OH), 1.24 (s, 9H, t-butyl group), 1.18 (s, 9H, t-butyl group), -9.84 (s, 1.56H, endohedral H_2O).

^{13}C NMR: (75 MHz, $CDCl_3$, δ): 198.21, 193.6, 168.93, 168.43, 164.11, 162.54, 153.82, 150.24, 149.93, 149.84, 149.69, 149.4, 149.26, 148.92, 148.76, 148.38, 148.18, 148.13, 148, 147.52, 147.48, 147.39, 147.09, 146.59, 146.54, 145.55, 145.46, 145.33, 145.06, 144.79, 144.29, 143.96, 143.69, 143.14, 142.87, 142.62, 142.57, 141.48, 141.36, 140.98, 140.14, 140.1, 140.08, 139.74, 139.17, 138.63, 138.37, 137.31, 137.25, 137.08, 136.94, 136.65, 136.16, 134.96, 134.85, 134.54, 133.76, 133.35, 131.7, 131.62, 130.06, 127.18, 126.86, 119.94, 119.67, 117.49, 116.9, 110.2, 96.37, 59.57, 54.74, 37.81, 37.61, 30.00, 29.85.

MS: *m/z* (relative intensity, ion): 1139 (100%, $[M+H]^+$ **H_2O@29**), 1121 (5%, $[M+H]^+$ **29**).

Known compound; values consistent with reported data.[72]

4.3.2.2 Synthesis of D_2O@29

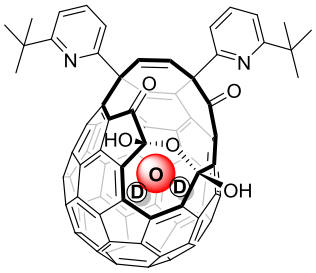

D_2O@29

Compound **28** (143 mg, 0.130 mmol) was dissolved in distilled 1-chloronapthalene (5ml). The solution was transferred to a 40ml Schlenk tube fitted with a J.Young tap under argon atmosphere. D_2O (99.990 %D, 100 μl) was added and the tube was sealed and completely immersed inside an oil bath preheated to 100 °C. After 48 hours the tube was cooled to room temperature and the solution was poured directly over a silica column packed with toluene. The column was eluted with toluene until all the 1-chloronapthalene was removed. The eluent polarity was then gradually increased to 15% AcOEt in toluene to collect 78% filled **D_2O@29** (133 mg, 90%).

All spectra look identical to those of **H_2O@29**, except for the absence of the signal at δ -9.84 ppm in the ^{1}H NMR spectrum.

^{1}H NMR: (400 MHz, $CDCl_3$, δ): 7.64 (t, J = 7.8 Hz, 1H, H-4 or H-4' of pyridyl), 7.57 (t, J = 7.8 Hz, 1H, H-4 or H-4' of pyridyl), 7.47 (d, J = 7.8 Hz, 1H, H-3 or H-3' of pyridyl), 7.21 (d, J = 7.8 Hz, 2H, H-5 and H-5' of pyridyl), 7.16 (d, J = 7.8 Hz, 1H, H-3 or H-3' of pyridyl), 7.10 (d, J = 10.1 Hz, 1H, alkene), 6.99 (d, J = 10.1 Hz, 1H, alkene), 5.79 (br s, 1H, OH), 5.66 (br s, 1H, OH), 1.24 (s, 9H, t-butyl), 1.18 (s, 9H, t-butyl).

4.3.3 Synthesis of 29a

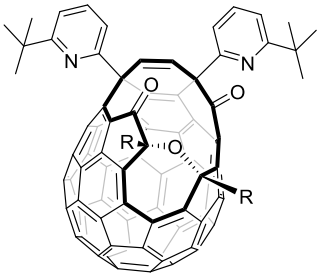

29a
R = OH, OEt
(single regioisomer)

Compound **29** (50 mg, 0.045 mmol) was placed inside an oven dried Schlenk flask connected to a pressure equalised dropping funnel filled with 3 Å activated molecular sieves. The top of the dropping funnel was fitted with a straight condenser and the system was put under nitrogen atmosphere. Distilled toluene (15 mL) was added and the solution was refluxed for 2 hours, forcing the condensed solvent to pass through the molecular sieves before being returned to the flask. After this time the solution was allowed to cool down to room temperature and ethanol (0.5 ml) was added. The solution was stirred at room temperature for 2.5 hours. The

solution was evaporated to dryness to isolate a black solid that was purified by flash column chromatography over silica gel (eluent: 5% ethyl acetate in toluene). The fractions containing the spot running at R_f 0.37 (eluent: 5% ethyl acetate in toluene) were collected and evaporated to afford compound **29a** as a black solid (50 mg, 96%).

^{1}H NMR (400 MHz, $CDCl_3$, δ): 7.63 (t, J = 7.9 Hz, 1H, H-4 of pyridyl), 7.55 (t, J = 7.8 Hz, 1H, H-4 of pyridyl), 7.23 (d, J = 7.8 Hz, 1H, H-3 or H-5 of pyridyl), 7.21 (d, J = 7.8 Hz, 1H, H-3 or H-5 of pyridyl), 7.19 (d, J = 7.5 Hz, 1H, H-3 or H-5 of pyridyl), 7.16 (d, J = 7.9 Hz, 1H, H-3 or H-5 of pyridyl), 7.10 (d, J = 10.2 Hz, 1H, alkenyl), 6.93 (d, J = 10 Hz, 1H, alkenyl), 5.07 (s, 1H, hydroxyl), 4.98 – 4.90 (m, 1H, methylene) 4.72 – 4.65 (m, 1H, methylene), 1.58 (t, J = 3.3 Hz, 3H, methyl), 1.22 (s, 9H, t-butyl), 1.17 (s, 9H, t-butyl).

^{13}C NMR: (125 MHz, odcb-d_4, δ): 195.93, 193.66, 168.79, 168.26, 164.45, 162.99, 154.08, 149.68, 149.25, 149.16, 148.95, 148.91, 148.69, 148.19, 148.16, 147.81, 147.48, 147.4, 147.21, 147.15, 146.89, 146.63, 146.36, 146.09, 145.98, 144.93, 144.81, 144.74, 143.87, 143.83, 143.36, 142.14, 141.7, 141.38, 141.11, 141.04, 140.6, 140.57, 140.19, 139.55, 138.43, 137.82, 137.71, 137.2, 137.11, 136.96, 136.7, 136.15, 135.99, 135.47, 135.41, 135.18, 134.73, 133.21, 131.81, 131.65, 130.34, 130.24, 129.54, 129.42, 129.22, 127.64, 127.39, 120, 119.61, 117.3, 116.8, 114.25, 95.93, 66.6, 59.63, 54.84, 37.62, 37.44, 29.89, 29.8, 15.86.

IR: (ν_{max}, cm^{-1}): 2959, 1756, 1704, 1572, 1515, 1444, 1123, 1081 1000.

UV: (CH_2Cl_2, λ_{max}, nm): 257.48, 326.09.

MS: *m/z* (relative intensity, ion): 1149 (100%, $[M+H]^+$ **29**).

4.3.4 Partial closure of water endofullerenes

4.3.4.1 Synthesis of H_2O@27

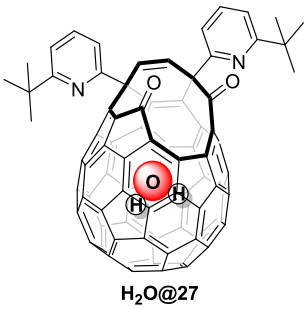

H_2O@27

78% filled **H_2O@29** (73 mg, 0.064 mmol) and triphenylphosphine (269 mg, 1.03 mmol) were placed inside a round-bottom flask equipped with a straight condenser. The system was put under argon atmosphere. Distilled toluene (6 ml) was added. Once a homogeneous solution was afforded the mixture was refluxed for 15 hours. The reaction mixture was then concentrated and purified by flash column chromatography (eluent gradient: 1:1 toluene/hexane to toluene). The fractions containing the spot at R_f 0.48 (eluent: toluene) were collected and evaporated to afford 78% filled **H_2O@27** as a black solid (64 mg, 84%).

^{1}H NMR: (300 MHz, $CDCl_3$, δ): 7.69 (t, J = 7.8 Hz, 1H, H-4 of pyridyl), 7.66 (t, J = 7.8 Hz, 1H, H-4 of pyridyl) 7.52 (d, 1H, J = 7.8 Hz, H-2 or H-3 of pyridyl) 7.40 (d, 1H, J = 7.8 Hz, H-2 or H-3 of pyridyl), 7.25-7.21 (m, 2H, H-2 or H-3 of pyridyl), 7.21-7.17 (m, 2H, H of alkene) 1.27 (s, 9H, t-butyl), 1.19 (s, 9H, t-butyl), -8.78 (s, 1.56H, endohedral H_2O).

^{13}CNMR: (125 MHz, odcb-d_4, δ): 199.09, 191.38, 168.83, 168.53, 165.34, 162.34, 154.52, 150, 148.66, 147.78, 147.69, 147.57, 147.3, 146.43, 146.25, 146.16, 146.12, 145.98, 145.66, 145.58, 145.54, 145.49, 145.37, 145.3, 144.93, 144.54, 144.51, 144.43, 144.1, 143.78, 143.72, 142.57, 142.52, 141.99, 141.84, 141.73, 141.52, 140.69, 140.35, 140.2, 140.17, 140.08, 139.99, 139.47, 139.38, 139.29, 138.52, 138.35, 138.24, 137.33, 137.27, 137.15, 136.39, 135.85, 135.64, 134.8, 133.63, 132.66, 132.54, 132.48, 132.1, 131.03, 130.22, 129.01, 128.19, 127.37, 125.31, 120.09, 119.7, 117.47, 116.76, 61.07, 54.81, 37.61, 37.52,29.97 29.86.

IR: (ν_{max}, cm^{-1}): 2956, 1745, 1697, 1571, 1477, 1444.

UV: (CH_2Cl_2, λ_{max}, nm): 257.11, 324.62.

MS: *m/z* (relative intensity, ion): 1152 (17% $[M+MeCN+Na]^+$, **H_2O@27**), 1089 (100%, $[M+H]^+$, **H_2O@27**), 1071 (16% $[M+H]^+$, **27**).

An analogous experiment run on **D_2O@29** afforded **D_2O@27** as a black solid. All spectra look identical to those of **H_2O@27**, except for the absence of the signal at δ -8.78 ppm in the ^{1}H NMR spectrum.

^{1}H NMR: (300 MHz, $CDCl_3$, δ): 7.69 (t, J = 7.8 Hz, 1H, H-4 of pyridyl), 7.66 (t, J = 7.8 Hz, 1H, H-4 of pyridyl) 7.52 (d, 1H, J = 7.8 Hz, H-2 or H-3 of pyridyl) 7.40 (d, 1H, J = 7.8 Hz, H-2 or H-3 of pyridyl), 7.25-7.21 (m, 2H, H-2 or H-3 of pyridyl), 7.21-7.17 (m, 2H, H of alkene) 1.28 (s, 9H, t-butyl), 1.19 (s, 9H, t-butyl).

4.3.4.2 Synthesis of H_2O@26 from H_2O@27

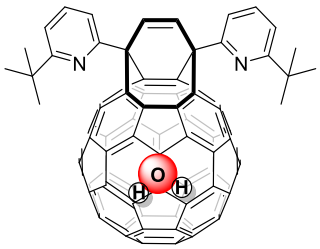

H_2O@26

Compound **H_2O@27** (420 mg, 0.386 mmol) was placed inside a round-bottom flask connected to a straight condenser under argon atmosphere. Distilled toluene was added (42 ml) followed by triisopropyl phosphite (1.5 ml). The reaction mixture was refluxed for 26 hours and then allowed to cool to room temperature. The mixture was concentrated and purified by flash column chromatography (eluent: toluene). The fractions containing the spot at R_f 0.95 were collected and evaporated to dryness to afford **H_2O@26** as a black solid (349 mg, 84%).

^{1}H NMR: (400 MHz, $CDCl_3$, δ): 7.79 (t, J = 7.8 Hz, 2H, H-4 of pyridyl), 7.72 (d, J = 7.8 Hz, 2H, H-2 or H-3 of pyridyl), 7.33 (d, J = 7.8 Hz, 2H, H-2 or H-3 of pyridyl), 6.48 (s, 2H, alkene), 1.37 (s, 18H, t-butyl groups), -6.08 (s, 1.56H, endohedral H_2O).

^{13}C NMR: (75 MHz, $CDCl_3$, δ): 168.87, 164.78, 152.47, 149.74, 145.71, 145.64, 145.58, 144.76, 144.56, 144.49, 144.35, 144.33, 144.04, 143.99, 143.97, 143.74, 143.57, 142.12, 141.32, 140.69, 140.65, 140.5, 140.14, 138.33, 137.3, 137.16, 137.08, 136.96, 136.76, 135.28, 135.07, 130.73, 127.47, 120.77, 117.16, 57.48, 37.74, 30.01.

Upon contact with air in solution **H_2O@26** started to transform into **H_2O@27** which was visible as an impurity in the ^{13}C NMR and MS spectra.

MS: *m/z* (relative intensity, ion): 1089 (23%, $[M+H]^+$ **H_2O@27**), 1057 (39%, $[M+H]^+$ **H_2O@26**), 536 (100%, $[M+2H]^{2+}$ **27**), 529 (38%, $[M+2H]^{2+}$ **H_2O@26**).

Known compound; values consistent with reported data.[72]

An analogous experiment run on **D_2O@27** afforded **D_2O@26** as a black solid. All spectra look identical to those of **H_2O@26**, except for the absence of the signal at δ -6.08 ppm in the ^{1}H NMR spectrum.

^{1}H NMR: (400 MHz, $CDCl_3$, δ): 7.78 (t, J = 7.8 Hz, 2H, H-4 of pyridyl), 7.72 (d, J = 7.8 Hz, 2H, H-2 or H-3 of pyridyl), 7.33 (d, J = 7.8 Hz, 2H, H-2 or H-3 of pyridyl), 6.47 (s, 2H, alkene), 1.37 (s, 18H, t-butyl groups).

4.3.4.3 Reduction of H_2O@29 with triisopropyl phosphite

Compound **H_2O@29** (323 mg, 0.288 mmol) was placed inside an oven dried Schlenk tube fitted with a J. Young tap. The tube was filled with argon gas and distilled toluene (32 ml) was added. The mixture was degassed and the tube charged with argon gas. Triisopropyl phosphite was added under argon then the tube was sealed and heated to 120 °C for 17 hours. The reaction mixture was allowed to cool down to room temperature and concentrated under vacuum. The mixture was purified by flash column chromatography (eluent: toluene) to collect two bands at R_f 0.95 and 0.3 (toluene). The solvent was evaporated to afford respectively **H_2O@26** (106 mg, 34%) and **H_2O@35** (100 mg, 31%) as black solids.

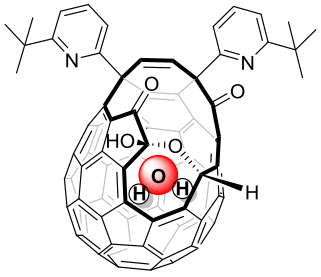

H_2O@35

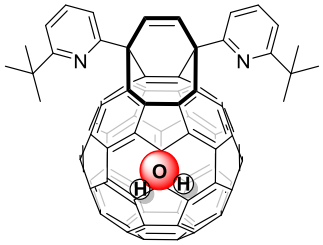

H_2O@26

H_2O@35: ^{1}H NMR: (400 MHz, $CDCl_3$, δ): 7.80 (s, 1 H), 7.62 (t, J = 7.9 Hz, 1 H), 7.56 (t, J = 7.9 Hz, 1 H), 7.42 (d, J = 7.9 Hz, 1 H), 7.23 (d, J = 7.9 Hz, 1 H), 7.22 (d, J = 7.9 Hz, 1 H), 7.16 (d, J = 7.9 Hz, 1 H), 7.04 (d, J = 10.2 Hz, 1 H), 6.89 (d, J = 10.2 Hz, 1 H), 5.88 (s, 1H), 1.25 (s, 9 H), 1.17 (s, 9 H), -9.75 (s, 1.32 H).

MS: *m/z* (relative intensity, ion): 1123 (100%, $[M+H]^+$, **H_2O@35**), 1105 (23%, $[M+H]^+$, empty **35**).

4.3.4.4 Synthesis of 35

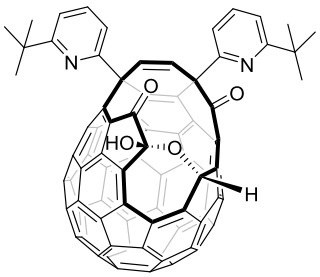

35

Compound **29** (30 mg, 0.027 mmol) was placed inside a 5 ml Schlenk tube fitted with a Rotaflo valve under argon atmosphere. Distilled toluene (3 ml) was added. Once the substrate had dissolved triisopropyl phosphite (0.450 ml) was added. The mixture was reacted at room temperature for 24 hours and then purified by flash column chromatography (eluent: toluene). The fractions containing the spot located at R_f 0.3 (toluene) were collected and evaporated to afford compound **35** as a black solid (22 mg, 76%).

^{1}H NMR: (300 MHz, $CDCl_3$, δ): 7.76 (s, 1 H), 7.62 (t, J = 7.9 Hz, 1 H), 7.55 (t, J = 7.9 Hz, 1 H), 7.42 (d, J = 7.9 Hz, 1 H), 7.23 (d, J = 7.9 Hz, 1 H), 7.22 (d, J = 7.9 Hz, 1 H), 7.16 (d, J = 7.9 Hz, 1 H), 7.03 (d, J = 10.2 Hz, 1 H), 6.88 (d, J = 10.2 Hz, 1 H), 5.20 (s broad, 1H), 1.25 (s, 9 H), 1.17 (s, 9 H).

^{13}C NMR: (75 MHz, $CDCl_3$, δ): 198.63, 194.6, 168.77, 168.32, 164.25, 162.91, 152.98, 150.15, 149.84, 149.66, 149.26, 149.24, 148.89, 148.74, 148.58, 148.38, 148.35, 147.8, 147.65, 147.44, 147.19, 147.05, 146.94, 146.9, 146.57, 146.16, 145.96, 145.93, 145.55, 145.16, 144.37, 143.96, 143.86, 143.79, 143.38, 142.29, 141.8, 141.28, 141.15, 140.98, 140.68, 139.92, 138.7, 138.65, 138.45, 137.12, 136.95, 136.86, 136.7, 136.56, 135.7, 135.47, 134.65, 133.87, 133.5, 132.38, 131.56, 131.24, 130.26, 129.01, 128.2, 127.27, 126.77, 125.27, 119.87, 119.79, 117.38, 116.8, 94.91, 80.87, 59.26, 54.73, 37.77, 37.56, 29.97, 29.83.

IR: (ν_{max}, cm^{-1}): 2958, 1765, 1695, 1573, 1516, 1445.

UV: (CH_2Cl_2, λ_{max}, nm): 257.11, 325.36.

MS: *m/z* (relative intensity, ion):1105 (17%, $[M+H]^+$ **35**), 167 (100%).

4.3.4.5 Synthesis of 26

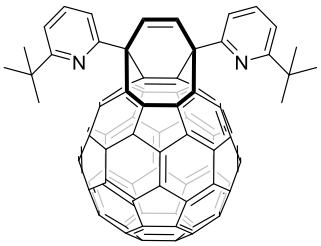

26

Compound **27** (32 mg, 0.0299 mmol) was placed inside a Schlenk flask fitted with a straight condenser under nitrogen atmosphere. Distilled toluene (4 ml) was added followed by triisopropyl phosphite (118 µl). The solution was refluxed under nitrogen atmosphere for 22 hours. The solution was allowed to cool down to room temperature, concentrated and purified by flash column chromatography over silica gel. The fractions containing the spot running with the eluent front (eluent: toluene) were collected and evaporated to dryness to afford compound **26** as a black solid (25 mg, 81%).

^{1}H NMR (400 MHz, $CDCl_3$, δ): 7.78 (t, J = 7.7 Hz, 2H, H-4 of pyridyl), 7.72 (d, J = 7.7 Hz, 2H, H-3 or H-5 of pyridyl), 7.33 (d, J = 7.7 Hz, 2H, H-3 or H-5 of pyridyl), 6.47 (s, 2H, alkenyl), 1.36 (s, 18H, t-butyl).

^{13}C NMR: (125 MHz, $CDCl_3$, δ): 168.87, 164.86, 152.35, 149.86, 145.75, 145.69, 145.31, 144.58, 144.4, 144.34, 144.26, 144.16, 144.05, 143.87, 143.79, 143.72, 143.67, 143.64, 143.55, 143.31, 142.2, 141.49, 140.47, 140.12, 138.09, 137.23, 137, 136.94, 136.83, 135.33, 134.91, 130.77, 127.72, 120.77, 117.13, 57.48, 37.75, 30.01.

IR: (ν_{max}, cm^{-1}): 2959, 1573, 1515, 1447, 811, 749.

UV: (CH_2Cl_2, λ_{max}, nm): 263.45, 327.01.

MS: m/z (relative intensity, ion): 1039 (12%, $[M+H]^+$, **12**), 520 (100%, $[M+2H]^{2+}$, **12**).

Note: compound **26**, uncontaminated by **35**, was also synthesised from **28** and triisopropyl phosphite in toluene at room temperature (*a*) or under reflux (*b*).

> **(*a*)** A solution of compound **28** (10 mg, 0.09 mmol) in distilled toluene (1 ml) was placed inside a 5 ml Schlenk tube fitted with a J.Young tap. Triisopropyl phosphite (0.15 ml) was added under argon and the mixture was reacted at room temperature for 24 hours. The reaction mixture was purified by flash column chromatography (toluene) to collect a fraction at R_f 0.95. The solvent was evaporated to dryness to afford compound **26** as a black solid (3 mg, 33%).

(*b*) A solution of compound **28** (15 mg, 0.135 mmol) in distilled toluene (1.5 ml) was placed inside a 5 ml Schlenk tube fitted with a J.Young tap. Triisopropyl phosphite (0.15 ml) was added under argon and the mixture was refluxed for 24 hours. The reaction mixture was purified by flash column chromatography (toluene) to collect a fraction at R_f 0.95. The solvent was evaporated to dryness to afford compound **26** as a black solid (7 mg, 50%).

4.3.4.6 Synthesis of 36b

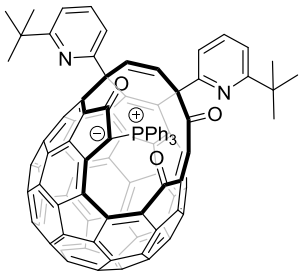

36b

Compound **29** (54 mg, 0.0482 mmol) and triphenylphosphine (200 mg, 0.762 mmol) were placed inside Schlenk tube under nitrogen atmosphere. Distilled toluene (5ml) was added and the solution was heated to 60 ˚C for 24 hours. The solution was concentrated under reduced pressure and then purified by flash column chromatography over silica gel (eluent gradient: toluene to 5% ethyl acetate in toluene). The fractions containing the spot running at R_f 0.16 (eluent: toluene) were collected and evaporated to afford compound **36b** as a dark green solid (56 mg, 86%).

^{1}H NMR (400 MHz, $CDCl_3$, δ): 8.60 - 8.35 (m, 1.5 H, phenyl), 8.25 – 8.10 (m, 1.4 H, phenyl), 8.05 – 7.95 (m, 1.5 H, phenyl), 7.95 – 7.85 (m, 1 H, phenyl), 7.85 – 7.70 (m, 1.7 H, phenyl), 7.70 – 7.48 (m, 3.8 H, phenyl), 7.55 (t, J = 7.8 Hz, 1H, H-4 of pyridyl), 7.53 (t, J = 7.7 Hz, 1H, H-4 of pyridyl), 7.48 – 7.38 (m, 1.8 H, phenyl), 7.44 (d, J = 7.8 Hz, 1H, H-3 or H-5 of pyridyl), 7.35 (d, J = 7.7 Hz, 1H, H-3 or H-5 of pyridyl), 7.26 (d, J = 10.2 Hz, 1H alkenyl), 7.17 (d, J = 7.7 Hz, 1H, H-3 or H-5 of pyridyl), 7.12 (d, J = 7.8 Hz, 1H, H-3 or H-5 of pyridyl), 6.93 (d, J = 10.2 Hz, 1H, alkenyl), 1.21(s, 9H, t-butyl), 1.15 (s, 9H, t-butyl).

^{13}C NMR: (125 MHz, $CDCl_3$, δ): 194.25, 191.81 (d, J = 9.6 Hz), 189.91, 168.46, 167.99, 164.41, 154.83, 154.74, 151.69, 151.22, 151.05, 149.78, 149.41, 149.17, 148.99, 148.94, 148.47, 148.23, 147.68, 147.59, 147.49, 147.35, 147.21, 147.18, 147.11, 146.62, 146.09, 146.02, 145.85, 145.42, 145.18, 145, 144.88, 144.53, 144.48, 143.98, 143.88, 143.66, 142.94, 142.74, 142.12, 142, 141.68, 141.34, 139.92, 139.72, 139.46, 137.9, 137.51, 136.88,

136.85, 136.66, 136.49, 136.35, 136.07, 134.7, 134.43, 134.34, 133.62, 133.37, 132.96, 132.5, 132.08, 130.86, 129.47, 129.38, 129.06, 128.88, 128.83, 128.77, 128.62, 128.57, 128.54, 128.25, 127.09, 125.33, 125.22, 123.28, 120.32, 120.1, 119.72, 117.06, 116.52, 84.73, 83.79, 59.03, 55.03, 37.75, 37.56, 30.02, 29.88.

{^{1}H}^{31}P NMR: (163 MHz, $CDCl_3$, δ): 18.42.

IR: (ν_{max}, cm^{-1}): 2960, 1734, 1630, 1570, 1514, 1440, 1409, 1355.

UV: (CH_2Cl_2, λ_{max}, nm): 257.11, 317.62.

MS: *m/z* (relative intensity, ion): 1350 (18%, $[M+H]^+$, **36b**), 579 (100%).

Note: compound **36b** was also synthesised from **29** and triphenylphosphine in toluene at room temperature in the presence of 3 Å molecular sieves. The same procedure described for the synthesis of **HF@36b** was used (cf. 4.3.8.2).

Ylide **36b** was also formed when **28** and triphenylphosphine in toluene-d_8 were reacted at room temperature, as detected by ^{31}P NMR.

4.3.5 Synthesis of 50

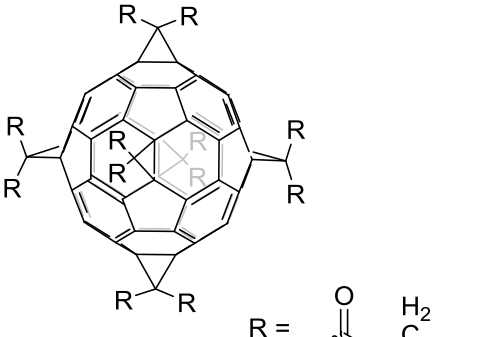

50

C_{60} (52 mg, 0.0722 mmol) and 9,10-dimethylanthracene (149 mg, 0.7216mmol) were placed inside a Schlenk flask under argon atmosphere. Distilled toluene (31 mL) was added under argon and the solution was stirred away from light for 4.5 hours. CBr_4 (239 mg, 0.7216 mmol) and diethyl malonate (116 mg, 0.7216 mmol) were added in one portion. Finally 1,8-diazabicyclo[5.4.0]undec-7-ene (220 mg, 1.4431 mmol) was added drop by drop. The solution was stirred at room temperature, away from light and under argon atmosphere for 17 hours. The reaction crude was dispersed over a small amount of silica gel and purified by flash column chromatography over silica gel (5% ethyl acetate in toluene). The fractions containing the spot located at Rf 0.12 were collected and evaporated to afford a bright yellow solid (40 mg, 33%).

^{1}H NMR (400 MHz, $CDCl_3$, δ):4.34 (q, J = 7.0 Hz, 24H, -CH_2-), 1.33 (t, J = 7.1 Hz, 36H, –CH_3).

^{13}C NMR: (100 MHz, $CDCl_3$, δ): 163.78 (CO), 145.74 (C_{60}-sp^2), 141.08 (C_{60}-sp^2), 69.04 (C_{60}-sp^3), 62.82 (-CH_2-) 45.33 (methano bridge), 14.03 (–CH_3).

MS-APPI: *m/z* (relative intensity, ion): 1668 (100%, $[M]^+$, **50**).

4.3.6 Synthesis of H_2O@50-d_{60}

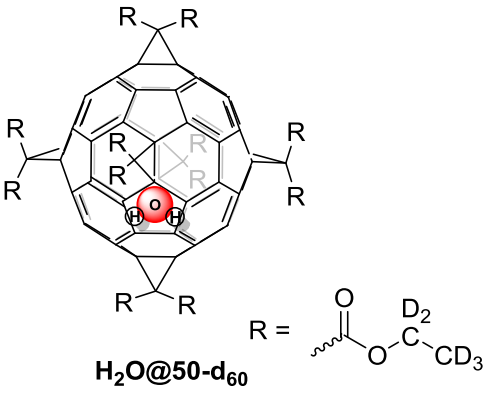

78% filled $H_2O@C_{60}$ (50 mg, 0.0677 mmol) and 9,10-dimethylanthracene (144 mg, 0.6981 mmol) were placed inside a Schlenk flask under argon atmosphere. Distilled toluene (30 mL) was added under argon and the solution was stirred in darkness for 4.5 hours. Tetrabromomethane (224 mg, 0.6769 mmol) and di(ethyl-d5) malonate (115 mg, 0.6769 mmol) were added in one portion. Finally 1,8-diazabicyclo[5.4.0]undec-7-ene (206 mg, 1.354 mmol) was added drop by drop. The solution was stirred at room temperature, in darkness and under argon atmosphere for 18 hours. The reaction mixture was evaporated over a small amount of silica gel and purified by flash column chromatography over silica gel (eluent: 5% ethyl acetate in toluene). The fractions containing the spot running at R_f 0.12 (eluent: 5% ethyl acetate in toluene) were collected and evaporated to afford 78% filled **H_2O@50-d_{60}** as a bright yellow solid (36 mg, 30%).

^{1}H NMR (400 MHz, $CDCl_3$, δ):4.34 (q, J = 6.9 Hz 0.32H, residual -CH_2-), 1.34 (t, J = 6.9 Hz 0.50H, residual –CH_3), -11.57 (s, 1.56H, endohedral H_2O).

^{13}C NMR: (100 MHz, $CDCl_3$, δ): 163.81(CO), 145.98 (C_{60}-sp^2), 141.22 (C_{60}-sp^2), 69.08 (C_{60}-sp^3), 45.34 (methano bridge).

Peaks due to **50** are visible at δ145.75, 141.09 and 69.05 ppm.

IR: (ν_{max}, cm^{-1}): 1738, 1262, 1229, 1188, 1173, 1081, 1044, 951, 708.

UV: (CH_2Cl_2, λ_{max}, nm): 245.13, 282.08, 316.88, 335.28.

MS-APPI: *m/z* (relative intensity, ion): 1746 (100%, $[M]^+$, **H_2O@50-d_{60}**), 1728 (10.5%, $[M]^+$, **50-d_{60}**).

4.3.7 Preparation and partial closure of hydrogen endofullerenes

4.3.7.1 Synthesis of H_2@29

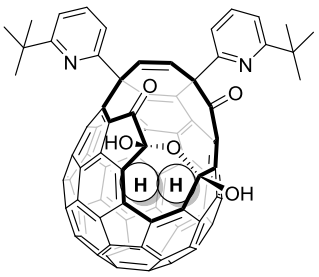

H_2@29

Compound **29** (50 mg) was placed inside a glass tube; Activated 3Á molecular sieves (1.4 g) and o-dichlorobenzene were added (12 ml). The tube was placed inside a Parr steel reactor. The reactor was sealed and then flushed by pressurising to 10 atm of hydrogen gas and then releasing the pressure (3 times). The reactor was then charged with hydrogen (120 atm) and the bottom part was immersed inside an oil bath preheated to 120 °C for 24 hours. After 20 hours the bomb was allowed to cool down to room temperature and the pressure was released. The reaction mixture was poured over a short silica column packed with toluene and eluted first with toluene to remove the o-dichlorobenzene and then with a 15% AcOEt in toluene solution to collect 60% filled **H_2@29** as a black solid (46 mg, 91%).

^{1}H-NMR: (400 MHz, $CDCl_3$, δ): 7.64 (t, J = 7.8 Hz, 1H, H-4 or H-4' of pyridyl), 7.57 (t, J = 7.8 Hz, 1H, H-4 or H-4' of pyridyl), 7.50 (d, J = 7.8 Hz, 1H, H-3 or H-3' of pyridyl), 7.21 (d, J = 7.8 Hz, 2H, H-5 and H-5' of pyridyl), 7.16 (d, J = 7.8 Hz, 1H, H-3 or H-3' of pyridyl), 7.11 (d, J = 10.0 Hz, 1H, vinylene), 7.01 (d, J = 10.0 Hz, 1H, vinylene), 6.20 (br s, 1H, OH), 5.96 (br s, 1H, OH), 1.24 (s, 9H, t-butyl group), 1.18 (s, 9H, t-butyl group), -7.17 (s, 1.22H, endohedral H_2).

^{13}C NMR: (125 MHz, odcb-d_4, δ): 198.88, 194.28, 168.7, 168.3, 164.54, 162.9, 153.68, 149.86, 149.33, 149.03, 148.86, 148.25, 147.72, 147.43, 147.01, 146.6, 146.42, 146.01, 145.18, 144.98, 144.75, 144.39, 144.3, 144.25, 144.16, 143.46, 143.39, 142.64, 142.51, 142.19, 142.11, 141.93, 141.07, 141.02, 140.61, 140.37, 140.19, 140.06, 139.82, 137.91, 137.18, 137.08, 137.02, 136.24, 136.14, 135.82, 135.62, 134.85, 134.54, 133.89, 133.83, 135.82, 135.62, 134.85, 134.54, 133.89, 133.83, 131.77, 131.62, 131.24, 130.94, 130.6, 129.01, 128.75, 119.88, 110.28, 96.69, 59.75, 54.88, 37.67, 37.46, 29.95, 29.81.

IR: (ν_{max}, cm^{-1}): 2958, 1760, 1693, 1572, 1515, 1444.

UV: (CH_2Cl_2, λ_{max}, nm): 256.73, 321.31.

MS-APPI: *m/z* (relative intensity, ion): 1123 (90%, $[M+H]^+$ **H_2@29**), 1121 (100%, $[M+H]^+$ empty **29**).

4.3.7.2 Synthesis of H_2@27

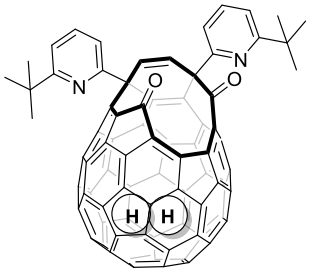

H_2@27

Compound **29** (200 mg 0.178 mmol) was placed inside a glass tube. Activated 3Å molecular sieves were added (~1 g) followed by o-dichlorobenzene (10 ml). The tube was placed inside a Parr reactor. The reactor was sealed and purged by pressurising it with 10 atm of hydrogen and then releasing the pressure (3 times). The reactor was then charged with hydrogen (120 atm) and the bottom part was immersed inside an oil bath preheated to 120 ˚C for 24 hours. The reactor was allowed to cool down to room temperature and depressurised then triphenylphosphine (730 mg) was added. The reactor was pressurised again and heated to 120 ˚C for 17 hours. The reaction mixture was cooled to room temperature and the pressure released. The reaction mixture was then concentrated and purified by flash column chromatography (eluent 1:1 toluene/hexane to remove excess phosphine then toluene to collect the product) to afford 60% filled **H_2@27** as a black solid (161 mg, 84%).

^{1}H NMR: (300 MHz, $CDCl_3$, δ): 7.69 (t, J = 7.8 Hz, 1H, H-4 of pyridyl), 7.66 (t, J = 7.8 Hz, 1H, H-4 of pyridyl) 7.52 (d, 1H, J = 7.8 Hz, H-2 or H-3 of pyridyl) 7.40 (d, 1H, J = 7.8 Hz, H-2 or H-3 of pyridyl), 7.25-7.21 (m, 2H, H-2 or H-3 of pyridyl), 7.21-7.17 (m, 2H, H alkene) 1.27 (s, 9H, t-butyl), 1.19 (s, 9H, t-butyl), -5.69 (s, 1.22H, endohedral H_2).

^{13}C NMR: (125 MHz, odcb-d_4, δ): 199.21, 191.46, 168.83, 168.51, 165.45, 162.43, 154.61, 149.69, 148.41, 148.33, 147.54, 147.51, 147.34, 147.04, 146.52, 146.42, 146.33, 146.15, 145.96, 145.72, 145.68, 145.65, 145.57, 145.49, 145.43, 145.39, 145.24, 145.05, 144.78, 144.64, 144.36, 144.28, 143.93, 143.63, 142.55, 142.34, 142.19, 141.93, 141.69, 141.64, 141.37, 140.7, 140.66, 140.31, 140.16, 139.9, 139.73, 139.53, 139.37, 139.31, 138.43, 137.5, 137.32, 137.12, 137.06, 136.23, 136.09, 134.8, 134.77,

133.86, 120.09, 119.71, 117.45, 116.73, 61.04, 54.85, 37.62, 37.53, 29.86, 29.83.

IR: (ν_{max}, cm^{-1}): 2958, 1745, 1697, 1571, 1444.

UV: (CH_2Cl_2, λ_{max}, nm): 257.11, 323.88.

MS: *m/z* (relative intensity, ion): 1073.4 (99%, $[M+H]^+$ **H_2@27**), 1071.7 (50% $[M+H]^+$ empty **27**)

4.3.7.3 Synthesis of H_2@26

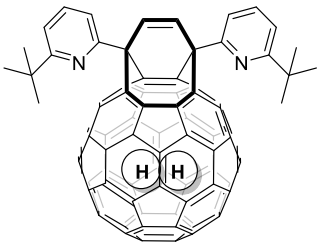

H_2@26

Compound 60% filled **H_2@27** (161 mg, 0.15 mmol) was placed inside a round-bottom flask connected to a straight condenser under argon atmosphere. Distilled toluene was added (16 ml) followed by triisopropyl phosphite (0.6 ml). The reaction mixture was refluxed for 26 hours and then allowed to cool down to room temperature. The mixture was concentrated and purified by flash column chromatography (eluent: toluene). The fractions containing the spot at R_f 0.95 were collected and evaporated to dryness to afford 60% filled **H_2@26** as a black solid (133 mg, 84%).

^{1}H-NMR: (400 MHz, $CDCl_3$, δ): 7.78 (t, 2H, J = 7.7 Hz, H-4 of pyridyl), 7.72 (d, 2H, J = 7.7 Hz, H-3 of pyridyl), 7.33 (d, 2H, J = 7.7 Hz, H-5 of pyridyl), 6.47 (s, 2H, alkene), 1.36 (s, 18H, t-butyl), –2.86 (s, 1.22H, H_2).

^{13}CNMR: (125 MHz, odcb-d_4, δ): 168.71, 165.01, 152.5, 149.69, 145.58, 145.18, 144.51, 144.43, 144.34, 144.11, 143.99, 143.92, 143.7, 143.67, 143.57, 143.46, 143.4, 143.19, 142.42, 141.41, 140.55, 140.44, 140.38, 140.32, 140.02, 138.11, 137.05, 136.96, 135.29, 134.98, 130.77, 129.01, 128.21, 127.75, 120.85, 117.06, 57.6, 37.58, 29.95,

IR: (ν_{max}, cm^{-1}): 2957, 1572, 1446.

UV: (CH_2Cl_2, λ_{max}, nm): 262.33, 328.67.

MS-ESI: *m/z* (relative intensity, ion): 1041 (23%, $[M+H]^+$ **H_2@26**), 1039 (21%, $[M+H]^+$ empty **26**), 521 (100%, $[M+2H]^{2+}$ **H_2@26**), 520 (18%, $[M+2H]^{2+}$ **26**).

Note: 60% filled **H_2@26** was also synthesised from **29** using the procedure below.

Compound **29** (50 mg, 0.045mmol) was placed inside a glass tube. Activated 3Å molecular sieves were added (~1 g) followed by o-dichlorobenzene (12 ml). The tube was placed inside a Parr reactor. The reactor was sealed and purged by pressurising it with 10 atm of hydrogen and then releasing the pressure (3 times). The reactor was then charged with hydrogen (120 atm) and the bottom part was immersed inside an oil bath preheated to 120 °C for 24 hours. The reactor was let cool down to room temperature and depressurised then triisopropyl phosphite (0.7 ml) was added. The reactor was pressurised with H_2 again and heated to 120 °C for 17 hours. The reaction mixture was cooled to room temperature and the pressure released. The reaction mixture was evaporated to dryness by vacuum distillation to afford a black solid that was purified by flash column chromatography (toluene) to afford 60% filled **H_2@26** as a black solid (24 mg, 50%).

4.3.8 Preparation and partial closure of hydrogen fluoride endofullerenes

4.3.8.1 Synthesis of HF@29

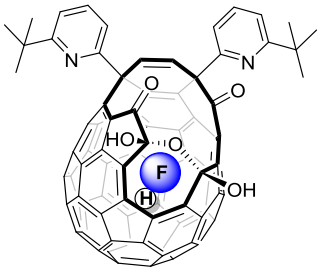

HF@29

Compound **29** (316 mg, 0.282 mmol) was placed inside an oven dried polytetrafluoroethylene (PTFE) tube equipped with a screw cap. The tube was flushed with nitrogen gas and distilled dichloromethane (16 mL) was added under nitrogen gas. 70% w/w hydrogen fluoride in pyridine (1.5 mL, 205 eq of HF) was added and the tube was closed. The mixture was stirred at room temperature for 23 hours. The reaction was quenched by dropping it, via PTFE tubing, inside a round-bottom flask containing Na2CO3 saturated solution (50 mL) and toluene (50 mL) under stirring. After the evolution of gas had stopped the organic layer was collected, washed with brine, dried over MgSO4, filtered and evaporated to dryness to afford a black solid. This material was purified by flash column chromatography over silica gel (eluent gradient 5% to 15% ethyl acetate in toluene). The fractions containing the spot located at Rf = 0.31 (eluent 15%

ethyl acetate in toluene) were collected and evaporated to yield 50% filled **HF@29** as a black solid (283 mg, 89%).

^{1}H NMR (400 MHz, $CDCl_3$, δ): 7.64 (t, J = 7.8 Hz, 1H, H-4 or H-4' of pyridyl), 7.57 (t, J = 7.8 Hz, 1H, H-4 or H-4' of pyridyl), 7.49 (dd, J = 7.5, 2.2 Hz, 1H, H-3 or H-5 of pyridyl), 7.23 (d, J = 7.8 Hz, 1H, H-3 or H-5 of pyridyl), 7.22 (d, J = 7.8 Hz, 1H, H-3 or H-5 of pyridyl), 7.17 (d, J = 7.7 Hz, 1H, H-3 or H-5 of pyridyl), 7.12 (d, J = 10.2 Hz, 1H, alkenyl), 7.02 (d, J = 10.1 Hz, 1H, alkenyl), 6.28 (s broad, 1H, hydroxyl), 6.00 (s broad, 1H, hydroxyl), 1.24 (s, 9H, t-butyl), 1.18 (s, 9H, t-butyl), -6.55 (d, J = 508 Hz, 0.5 H, endohedral HF).

^{13}C NMR: (125 MHz, odcb-d_4, δ): 198.77, 193.96, 168.71, 168.29, 164.42, 162.84, 153.56, 164.42, 162.84, 153.56, 149.94, 149.56, 149.5, 148.47, 148.39, 147.78, 147.63, 147.13, 147.04, 146.69, 146.15, 145.21, 145.16, 144.96, 144.42, 143.61, 143.48, 142.96, 142.57, 142.19, 141.19, 141.04, 140.64, 140.43, 140.17, 140, 139.82, 138.93, 138.2, 137.5, 137.32, 137.23, 137.11, 136.44, 135.77, 135.24, 134.73, 134.53, 134.3, 133.59, 133.54, 131.98, 131.45, 131.3, 129.02, 119.99, 119.86, 117.45, 117.42, 116.86, 116.83, 110.52, 96.97, 59.75, 59.72, 54.87, 37.65, 37.46, 29.94, 29.8.

^{19}F NMR: (376 MHz, $CDCl_3$, δ): -223.91 (d, J = 508 Hz).

{^{1}H}^{19}F NMR: (376 MHz, $CDCl_3$, δ): -223.91 (s).

IR: (ν_{max}, cm^{-1}): 3445, 2958, 1761, 1694, 1571, 1515, 1444, 1145, 1080.

UV: (CH_2Cl_2, λ_{max}, nm): 258.60 (92550), 327.93 (36421).

MS: *m/z* (relative intensity, ion): 1141 (100%, $[M+H]^+$, **HF@29**), 1121 (53%, $[M+H]^+$, **29**)

4.3.8.2 Synthesis of HF@36b

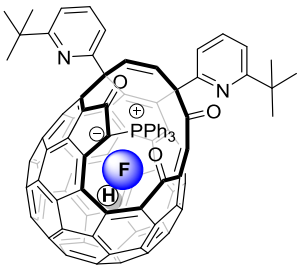

HF@36b

50% filled **HF@29** (40 mg, 0.0351 mmol), triphenylphosphine (147 mg, 0.5608 mmol) and 3Å activated molecular sieves (~250 mg) were placed inside a Schlenk tube fitted with a J. Young tap under nitrogen atmosphere. Distilled toluene (4 ml) was added and the solution was stirred at room temperature for 41 hours. The reaction mixture was concentrated under vacuum and purified by flash

column chromatography over silica gel (eluent gradient: toluene to 15% ethyl acetate in toluene). The fractions containing the spot running at R_f 0.16 (eluent: toluene) were collected and evaporated to afford **HF@36b** as a green solid (50% filling factor, 14 mg, 30%). The fractions containing the spot running at R_f 0.31 (eluent: 15% ethyl acetate in toluene) were collected and evaporated to recover the unmodified substrate 50% filled **HF@29** (19 mg, 47%).

^{1}H NMR (400 MHz, $CDCl_3$, δ): 8.60 - 8.35 (m, 2H, phenyl), 8.25 – 8.10 (m, 2H, phenyl), 8.05 – 7.95 (m, 2H, phenyl), 7.95 – 7.85 (m, 1.5H, phenyl), 7.85 – 7.70 (m, 2.5H, phenyl), 7.70 – 7.48 (m, 4H, phenyl), 7.55 (t, J = 7.8 Hz, 1H, H-4 of pyridyl), 7.54 (t, J = 7.8 Hz, 1H, H-4 of pyridyl), 7.48 – 7.38 (m, 1.6 H, phenyl), 7.44 (d, J = 7.4 Hz, 1H, H-3 or H-5 of pyridyl), 7.38 (d, J = 7.4 Hz, 1H, H-3 or H-5 of pyridyl), 7.28 (d, J = 10.4 Hz, 1H alkenyl), 7.18 (d, J = 7.7 Hz, 1H, H-3 or H-5 of pyridyl), 7.12 (d, J = 7.8 Hz, 1H, H-3 or H-5 of pyridyl), 6.94 (d, J = 10.1 Hz, 1H alkenyl), 1.21(s, 9H, t-butyl), 1.15 (s, 9H, t-butyl). -7.15 (d, J = 507 Hz, 0.5 H, endohedral HF).

^{13}C NMR: (125 MHz, $CDCl_3$, δ): 194.11, 191.41 (d, J = 9.5 Hz), 190.06, 168.42, 167.93, 164.33, 164.29, 164.22, 151.59, 151.36, 151.31, 151.08, 149.92, 149.68, 149.37, 149.23, 149.13, 148.5, 148.39, 148, 147.62, 147.52, 147.44, 147.3, 147.25, 147.15, 147.06, 146.99, 146.78, 146.02, 145.95, 145.79, 145.04, 144.92, 144.84, 144.74, 144.7, 144.65, 143.39, 143.77, 143.12, 142.81, 142.69, 141.85, 141.74, 141.64, 141.3, 139.92, 139.7, 139.37, 139.26, 137.86, 137.69, 137.64, 137.45, 136.89, 136.66, 136.48, 136.4, 136.17, 136.01, 134.81, 134.74, 134.59, 134.38, 134.06, 133.47, 133.01, 132.63, 132.46, 132.13, 131.9, 130.88, 130.77, 130.4, 129.44, 129.35, 128.83, 128.74, 128.6, 128.54, 128.44, 127.04, 126.95, 125.11, 123.37, 120.25, 119.91, 117.04, 116.53, 85.13, 84.18, 59, 54.99, 37.72, 37.5, 29.99, 29.84.

^{19}F NMR: (376 MHz, $CDCl_3$, δ): -225.52 (d, J = 506 Hz).

{^{1}H}^{19}F NMR: (376 MHz, $CDCl_3$, δ): -225.53 (s).

{^{1}H}^{31}P NMR: (162 MHz, $CDCl_3$, δ): 18.55 (**HF@36b**), 18.48 (empty **36b**).

IR: (ν_{max}, cm^{-1}): 2959, 1732, 1624, 1572, 1440, 1409, 1357, 906, 730.

UV: (CH_2Cl_2, λ_{max}, nm): 257.11, 321.49.

MS: *m/z* (relative intensity, ion): 1370 (100%, [M+H]+ **HF@36b**), 1350 (67%, [M+H]+ empty **36b**).

4.3.8.3 Synthesis of 51

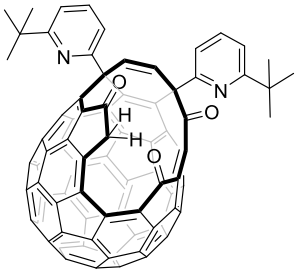

51

Compound **36b** (30 mg, 0.0222 mmol) was placed inside an oven dried PTFE tube equipped with a screw cap under nitrogen atmosphere. Distilled dichloromethane (2 ml) was added followed by 70% hydrogen fluoride pyridine (120 µl). The mixture was stirred at room temperature in the dark for 22 hours. The mixture was dropped via a cannula inside a round-bottom flask containing Na_2CO_3 saturated solution (20 mL) and toluene (20 ml). After the evolution of gas had stopped the organic layer was collected, washed with brine, dried over $MgSO_4$, filtered and evaporated to dryness to afford a black solid. This crude was purified by flash column chromatography over silica gel (eluent: toluene). The fractions containing the spot running at R_f 0.3 (eluent: toluene) were collected and evaporated to afford **51** as a black solid (10.5 mg, 44%). The fractions containing the spot running at R_f 0.16 (eluent: toluene) were collected and evaporated to afford unreacted **36b** as a green solid (8.2 mg, 27%).

^{1}H NMR (400 MHz, $CDCl_3$, δ): 7.61 (t, J = 7.8 Hz, 1H, H-4 of pyridyl), 7.59 (t, J = 7.8 Hz, 1H, H-4 of pyridyl), 7.33 (d, J = 7.8 Hz, 1H, H-3 or H-5 of pyridyl), 7.21(d, J = 8.4 Hz, 1H, H-3 or H-5 of pyridyl), 7.18 (d, J = 7.9 Hz, 1H, H-3 or H-5 of pyridyl), 7.02 (d, J = 10.2 Hz, 1H, alkenyl), 6.80 (d, J = 10.2 Hz, 1H, alkenyl), 4.75 (d, J = 22.9 Hz, 1H, methylene), 4.15(d, J = 22.7 Hz, 1H, methylene), 1.22 (s, 9H, t-butyl), 1.18 (s, 9H, t-butyl).

Note: the residual chloroform signal partially overlapped with the signal arising from one of the H-3 or H-5 protons of the pyridyl ring.

^{13}C NMR: (125 MHz, $CDCl_3$, δ): 197.78, 194.28, 193.92, 168.57, 168.33, 163.8, 162.95, 152.33, 150.84, 150.18, 149.49, 149.3, 149.08, 149.02, 148.69, 148.58, 148.17, 147.7, 147.54, 147.4, 147.07, 146.64, 146.42, 145.61, 145.13, 145.03, 144.84, 144.81, 144.7, 144.29, 143.82, 143.73, 143.31, 142.77, 142.55, 141.87, 141.4, 141.34, 141.25, 140.04, 139.44, 139.17, 139.14, 139.12, 138.43, 137.41, 136.96, 136.65, 136.41, 136.13, 136.12,

136.01, 135.94, 134.08, 134.06, 133.41, 133.29, 132.32, 132.3, 130.44, 129.99, 127.32, 125.77, 119.95, 119.84, 117.44, 116.93, 59.23, 54.76, 45.84, 37.73, 37.59, 29.94, 29.84.

IR: (ν_{max}, cm^{-1}): 2960, 1734, 1571, 1445, 907, 731.

UV: (CH_2Cl_2, λ_{max}, nm): 259.35, 325.36.

MS: *m/z* (relative intensity, ion): 1089 (77%, $[M+H]^+$, **51**), 183 (100%).

4.3.8.4 Synthesis of HF@27

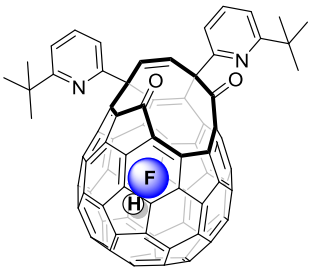

HF@27

Activated 3Å molecular sieves (~4 g) were placed inside a Schlenk tube fitted with a J. Young tap. The tube was heated at 220 ˚C under vacuum (1 mmHg) for 1 hour. The tube was allowed to cool down to room temperature under nitrogen gas. 50% filled **HF@29** (520 mg, 0.4557 mmol) and di(2-furyl)phenylphosphine (1.930 g, 7.97 mmol) were added under nitrogen flow followed by distilled toluene (53 ml). The tube was sealed under nitrogen atmosphere and the mixture was stirred at room temperature in the dark. After 138 hours the reaction mixture was filtered and concentrated under reduced pressure. The crude was purified by flash column chromatography over silica gel (eluent gradient: 1:1 toluene/hexanes to toluene). The fractions containing the spot running at R_f 0.5 (eluent: toluene) were collected and evaporated to dryness to afford 30% filled **HF@27** as a black solid (324 mg, 64%).

^{1}H NMR (400 MHz, $CDCl_3$, δ): 7.70 (t, J = 7.8 Hz, 1H, H-4 of pyridyl), 7.67 (t, J = 7.8 Hz, 1H, H-4 of pyridyl), 7.52 (d, J = 7.7 Hz, 1H, H-3 or H-5 of pyridyl), 7.40 (d, J = 7.7 Hz, 1H, H-3 or H-5 of pyridyl), 7.25 - 7.23 (m, 2H, H-3 or H-5 of pyridyl), 7.21 - 7.19 (m, 2H, alkenyl), 1.27 (s, 9H, t-butyl), 1.19 (s, 9H, t-butyl), -6.52 (d, J = 506 Hz, 0.3H, endohedral HF).

^{13}C NMR: (125 MHz, odcb-d_4, δ): 199.2, 199.13, 168.84, 168.52, 165.35, 162.35, 154.32, 149.88, 149.59, 148.54, 148.33, 147.71, 147.6, 147.5, 147.19, 146.39, 146.31, 146.16, 146.12, 146.09, 145.51, 145.31, 145.18, 144.9, 144.69, 144.49, 144.46, 144.02, 143.68, 142.63, 142.42, 142.36, 141.81, 141.67, 141.54, 141.38, 140.76, 140.37, 140.05, 139.91, 139.5, 139.38, 139.29, 139.22, 138.5, 138.44, 138.35, 138.23, 137.24, 137.15,

136.12, 135.58, 135.52, 134.88, 133.57, 132.06, 131.88, 131.15, 129.42, 129.22, 117.45, 116.77, 61.06, 54.81, 37.61, 37.51, 29.86.

^{19}F NMR: (376 MHz, $CDCl_3$, δ): -223.98 (d, J = 506 Hz).

{^{1}H}^{19}F NMR: (376 MHz, $CDCl_3$, δ): - 223.98 (s).

IR: (ν_{max}, cm^{-1}): 2558, 1746, 1697, 1576, 1415, 1447, 1444.

UV: (CH_2Cl_2, λ_{max}, nm): 257.85, 323.88.

MS: *m/z* (relative intensity, ion): 1091 (46%, $[M+H]^+$, **HF@27**), 1071 (71%, $[M+H]^+$, empty **27**), 536 (23%, $[M+2H]^{2+}$, empty **27**).

4.3.8.5 Synthesis of HF@26

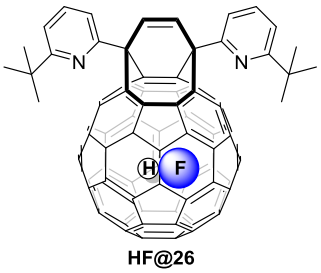

HF@26

30% filled **HF@27** (324 mg, 0.2969 mmol) was placed inside a Schlenk flask fitted with a straight condenser under nitrogen atmosphere. Distilled toluene (32 ml) was added followed by triisopropyl phosphite (1.2 ml). The solution was then refluxed for 24 hours. After this time the mixture was allowed to cool down to room temperature, concentrated under reduced pressure and finally purified by flash column chromatography (eluent: toluene). The fractions containing the spot running with the solvent front were collected and evaporated to afford 30% filled **HF @26** as a black solid (264 mg , 84%).

^{1}H NMR (400 MHz, $CDCl_3$, δ): 7.78 (t, J = 7.8 Hz, 2H, H-4 of pyridyl), 7.72 (d, J = 7.8 Hz, 2H, H-3 or H-5 of pyridyl), 7.33 (d, J = 7.8 Hz, 2H, H-3 or H-5 of pyridyl), 6.47 (s, 2H, alkenyl), 1.37 (s, 18H, t-butyl), -3.88 (d J = 506 Hz, 0.3H, endohedral HF).

^{13}C NMR: (125 MHz, $CDCl_3$, δ): 168.89, 164.81, 152.37, 149.73, 145.61, 145.56, 145.33, 144.73, 144.53, 144.42, 144.36, 144.29, 144.2, 144.01, 143.97, 143.82, 143.74, 143.59, 143.33, 142.13, 141.25, 140.65, 140.6, 140.51, 140.15, 138.25, 137.11, 137.02, 136.78, 135.28, 135.02, 130.79, 127.5, 120.79, 117.18, 57.52, 37.77, 30.05.

^{19}F NMR: (376 MHz, $CDCl_3$, δ): -220.42 (d, J = 506 Hz).

{^{1}H}^{19}F NMR: (376 MHz, $CDCl_3$, δ): -220.43 (s).

IR: (ν_{max}, cm^{-1}): 2960, 1573, 1447, 906, 811, 732.

UV: (CH_2Cl_2, λ_{max}, nm): 263.45, 328.67.

MS: *m/z* (relative intensity, ion): 1059 (15%, $[M+H]^+$, **HF@26**), 1039 (59%, $[M+H]^+$, **26**), 530 (32%, $[M+2H]^{2+}$, **HF@26**), 520 (100%, $[M+2H]^{2+}$, **26**).

4.3.9 Synthesis and purification of C_{60} endofullerenes

4.3.9.1 General procedure

Endofullerene **A@26** (0.1 mmol) and N-phenyl maleimide (0.4 mmol) were placed inside a round-bottom flask fitted with a straight condenser under argon atmosphere. Distilled 1-chloronaphthalene (5 ml) was added. The solution was degassed and the system was put under argon atmosphere. The reaction mixture was refluxed for 22 hours. The reaction mixture was allowed to cool down to room temperature and poured over a silica column packed with toluene. The column was eluted with toluene to collect a purple band. This solution was concentrated under reduced pressure and then evaporated to dryness by vacuum distillation to afford **A@C$_{60}$** containing minor impurities as a black solid (*circa* 80-90% yield).

The solid was washed with diethyl ether (3 times), then collected and placed inside a straight glass tube (12 mm OD, 30 cm long). The tube was connected to the sublimation apparatus via a Swagelok vacuum connection (Figure 27).

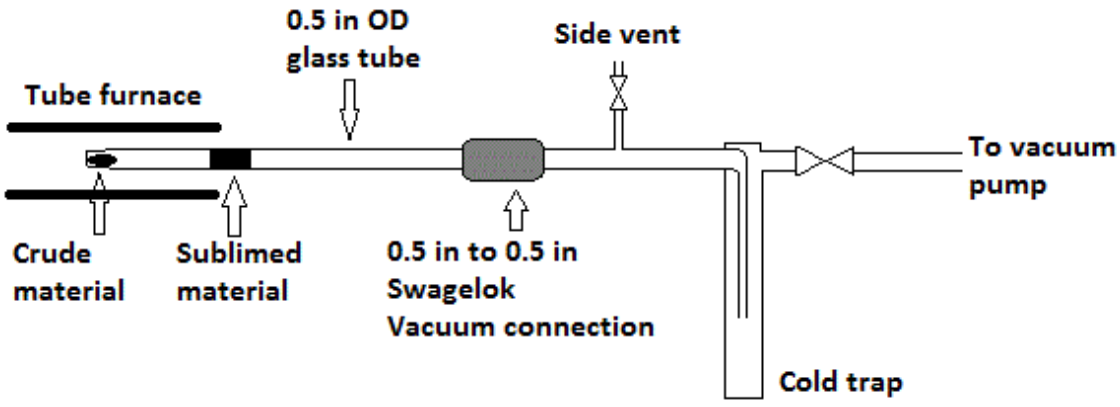

Figure 30: Apparatus for the sublimation of C_{60} endofullerenes.

The system was evacuated to 10^{-5} Torr, then the furnace was heated from room temperature to 550 ˚C with a ramp rate of 10 ˚C/min. The furnace temperature

was kept at 550 °C until the deposition on the cold part of the tube stopped. The system was allowed to cool down to room temperature and the apparatus was then isolated from the vacuum pump. The apparatus was then brought back to ambient pressure carefully opening the side vent. The sublimation tube was removed, the section containing the sublimate was cut and the material was collected to afford **$H_2O@C_{60}$** as a black solid (sublimation yield ~80% and overall yield *circa* 60-70%).

4.3.9.2 $H_2O@C_{60}$

H_2O@26 (106 mg 0.100 mmol) afforded **$H_2O@C_{60}$** (54 mg, 71%) after flash chromatography and sublimation.

^{1}H NMR: (400 MHz, odcb-d_4, δ): 4.85 (endohedral H_2O).

^{13}C NMR: (100 MHz, odcb-d_4, δ): 142.83 ($H_2O@C_{60}$), 142.72 (C_{60}).

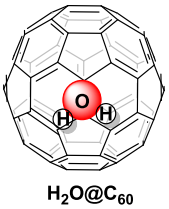

$H_2O@C_{60}$

HRMS-APCI (*m/z*): $[M]^+$ calcd for $C_{60}H_2O$, 738.010; found, 738.009.

Known compound; values consistent with reported data.[72]

4.3.9.3 $D_2O@C_{60}$

D_2O@26 (155 mg 0.149 mmol) afforded **$D_2O@C_{60}$** (79 mg, 72%) after flash chromatography and sublimation.

^{2}H NMR: (77 MHz, toluene, δ):- 4.80 (s, $D_2O@C_{60}$).

^{13}C NMR: (100 MHz, odcb-d_4, δ): 142.83 ($D_2O@C_{60}$), 142.72 (C_{60}).

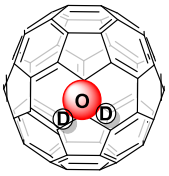

$D_2O@C_{60}$

HRMS-APCI (*m/z*): $[M]^+$ calcd for $C_{60}D_2O$, 740.022; found, 740.022.

Known compound; values consistent with reported data.[72]

4.3.9.4 $H_2@C_{60}$

H_2@26 (138 mg 0.130 mmol) afforded **$H_2@C_{60}$** (68 mg, 72%) after flash chromatography and sublimation.

^{1}H NMR: (400 MHz, odcb-d_4, δ): -1.48 (endohedral H_2).

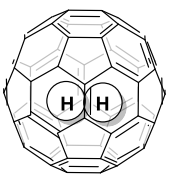

$H_2@C_{60}$

^{13}C NMR: (400 MHz, odcb-d_4, δ): 142.79 ($H_2@C_{60}$), 142.72 (C_{60}).

HRMS-APCI (*m/z*): $[M]^+$ calcd for $C_{60}H_2$, 722.015; found, 722.015.

Known compound; values consistent with reported data.[70]

4.3.9.5 HF@C_{60}

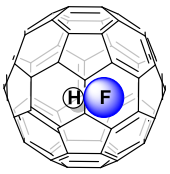

HF@C_{60}

HF@26 (257 mg 0.243 mmol) afforded **HF@C_{60}** (153 mg, 86%) after flash chromatography. Sublimation of part of this material (20 mg) afforded sublimed **HF@C_{60}** (15 mg 65%).

^{1}H NMR: (400 MHz, odcb-d_4, δ): -2.51 (d, J = 506 Hz, endohedral HF)

^{19}F NMR: (376 MHz, odcb-d_4, δ): -219.94 (d, J = 506 Hz).

{^{1}H}^{19}F NMR: (376 MHz, odcb-d_4, δ): -219.94 (s).

^{13}C NMR: (400 MHz, odcb-d_4, δ): 142.76 (HF@C_{60}), 142.72 (C_{60}).

UV: toluene λ_{max} (nm): 335.65.

HRMS-APCI (*m/z*): $[M]^+$ calcd for $C_{60}HF$, 740.006; found, 740.007.

4.3.9.6 Enrichment of HF@C_{60} by preparative HPLC

Sublimed 30% filled HF@C_{60} (15.00 mg) was dissolved in toluene (8 ml). The solution was injected (injection volume: 2ml) in a recycling HPLC fitted with two 20×250 mm Buckyprep columns (Figure 31) and subjected to a single run (eluent: toluene, eluent flow: 10 ml/min, detection: 326 nm).

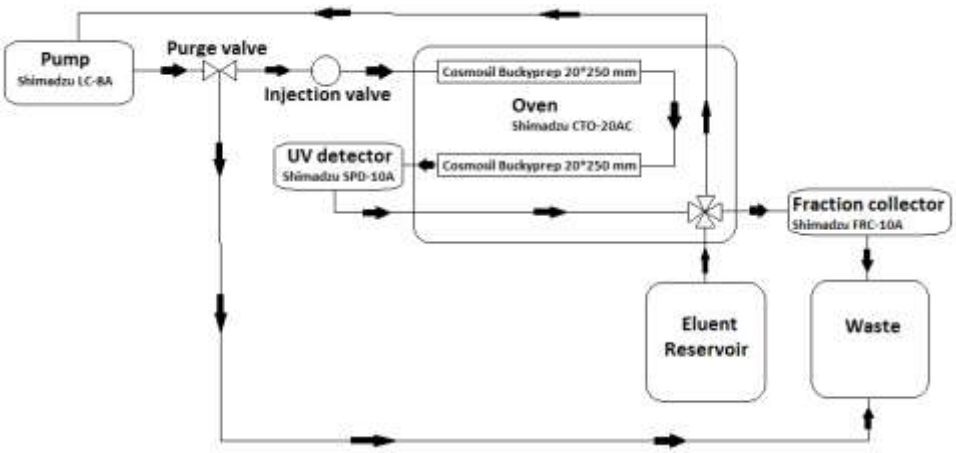

Figure 31: Recycling HPLC, black arrows indicate the direction of the flow.

All the fractions containing HF@C_{60} were collected and concentrated to afford a solution of 77% filled HF@C_{60}. This solution was again subjected to a single run. All the fractions containing HF@C_{60} were collected and evaporated to afford 100% filled HF@C_{60} (5.05 mg).

^{1}H NMR: (400 MHz, toluene-d_8, δ): -2.68 (d, J = 506 Hz, endohedral HF)

^{19}F NMR: (376 MHz, toluene-d_8, δ): -220.11 (d, J = 505 Hz).

{^{1}H}^{19}F NMR: (376 MHz, toluene-d_8, δ): -220.11 (s).

^{13}C NMR: (400 MHz, toluene-d_8, δ): 143.61 (HF@C_{60}).

HRMS-APCI (*m/z*): $[M]^+$ calcd for $C_{60}HF$, 740.006; found, 740.006.

Empty C_{60} was not detected by ^{13}C NMR and HRMS.

4.4 Computational

4.4.1 General

Computational experiments were carried out using the Gaussian 09 software package.[127] Structures were optimised using DFT at the B3LYP/6-31G(d) level of theory. Transition states were found by scanning the energy profile via forming or breaking of bonds. This assured that the transition states were connected to the reactant and product. Frequency calculations were carried out for each stationary point to check that the optimised geometry corresponded to a minimum or a transition state. No imaginary vibrational mode was found for minima, and a single imaginary vibrational mode was found for transition states. Frequency calculations were also used to compute free energies values at 298 K. NMR spectra were calculated using the GIAO approach at the B3LYP/6-311G(2d,p) level of theory, starting from geometries optimised at the B3LYP/6-31G(d) level of theory.

Table 1: DFT B3LYP/6-31G(d) calculated free energies (Hartree).

STRUCTURE	G (Ha) Ph3P	G (Ha) FuPh2P	G (Ha) Fu2PhP	G (Ha) Fu3P
R3P	-1036.07098	-1033.87609	-1031.68079	-1029.48401
R3PO	-1111.31788	-1109.12199	-1106.92411	-1104.72290
28	-3549.82066	-3549.82066	-3549.82066	-3549.82066
TS44a	-4585.83611	not calculated	not calculated	-4579.24414
44a	-4585.85231	not calculated	not calculated	-4579.25800
TS44b	-4585.84346	-4583.64643	-4581.449289	-4579.24974
44b	-4585.86711	-4583.66918	-4581.47140	-4579.27359
TS46	-4585.827901	-4583.6304	-4581.429008	-4579.230944
46	-4585.852453	-4583.653625	-4581.452598	-4579.255635
TS47	-4585.846407	-4583.647427	-4581.448843	-4579.252308
47	-3474.557628	-3474.557628	-3474.557628	-3474.557628
TS48	-3474.556121	-3474.556121	-3474.556121	-3474.556121
48	-3474.565209	-3474.565209	-3474.565209	-3474.565209
TS48o	-4510.574235	-4508.380836	-4506.182811	-4503.981871
TS49a	-4510.598165	-4508.403402	-4506.205665	-4504.00997
49a	-4510.602569	-4508.407191	-4506.20913	-4504.013203
TS36a	-4510.574957	-4508.380426	-4506.182288	-4503.987046
36a	-4510.615009	-4508.425092	-4506.231754	-4504.038962
TS27a	-4510.589289	-4508.400946	-4506.209475	-4504.016489
TS49b	-4510.604056	-4508.408178	-4506.211463	-4504.015673
49b	-4510.618001	-4508.42044	-4506.223804	-4504.026868
TS36b	-4510.602865	-4508.407056	-4506.2083	-4504.01108
36b	-4510.652493	-4508.457141	-4506.261756	-4504.064553
TS27b	-4510.591024	-4508.403507	-4506.210525	-4504.014177
27	-3399.374011	-3399.374011	-3399.374011	-3399.374011

Table 2: DFT B3LYP/6-31G(d) calculated free energies (KJ/mol).

STRUCTURE	G (KJ/mol) Ph3P	G (KJ/mol) FuPh2P	G (KJ/mol) Fu2PhP	G (KJ/mol) Fu3P
R3P	-2720203.32980	-2714440.63254	-2708676.88509	-2702909.24665
R3PO	-2917763.97737	-2911998.67562	-2906228.13338	-2900448.87185
28	-9320050.58513	-9320050.58513	-9320050.58513	-9320050.58513
TS44a	-12040108.12885	not calculated	not calculated	-12022800.90770
44a	-12040150.65143	not calculated	not calculated	-12022837.30237
TS44b	-12040127.41576	-12034359.12620	-12028590.52682	-12022815.61049
44b	-12040189.50094	-12034418.84842	-12028648.57923	-12022878.23652
TS46	-12040086.56825	-12034317.03157	-12028537.27908	-12022766.26424
46	-12040151.02950	-12034378.00878	-12028599.21460	-12022831.09044
TS47	-12040135.15573	-12034361.73594	-12028589.35585	-12022822.35540
47	-9122447.57776	-9122447.57776	-9122447.57776	-9122447.57776
TS48	-9122443.62113	-9122443.62113	-9122443.62113	-9122443.62113
48	-9122467.48166	-9122467.48166	-9122467.48166	-9122467.48166
TS48o	-11842508.14342	-11836749.37654	-11830978.46410	-11825199.89833
TS49a	-11842570.97161	-11836808.62355	-11831038.46725	-11825273.67223
49a	-11842582.53431	-11836818.57156	-11831047.56461	-11825282.16046
TS36a	-11842510.03903	-11836748.30008	-11830977.09096	-11825213.48529
36a	-11842615.19551	-11836865.57062	-11831106.96390	-11825349.79069
TS27a	-11842547.66768	-11836802.17532	-11831048.47040	-11825290.78785
TS49b	-11842586.43842	-11836821.16293	-11831053.68990	-11825288.64545
49b	-11842623.05101	-11836853.35680	-11831086.09118	-11825318.03791
TS36b	-11842583.31145	-11836818.21712	-11831045.38544	-11825276.58653
36b	-11842713.60972	-11836949.71524	-11831185.73412	-11825416.97984
TS27b	-11842552.22292	-11836808.89923	-11831051.22718	-11825284.71770
27	-8925053.06651	-8925053.06651	-8925053.06651	-8925053.06651

Table 3: Free energy profile (KJ/mol) for the reduction of **28** to **27** via oxepin **47** and ylide **36b**.

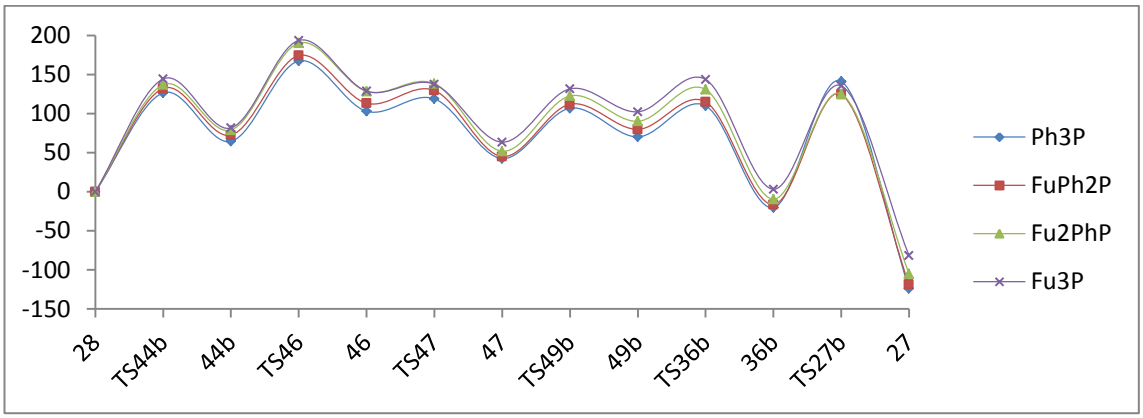

STRUCTURE	ΔG (KJ/mol) Ph3P	ΔG (KJ/mol) FuPh2P	ΔG (KJ/mol) Fu2PhP	ΔG (KJ/mol) Fu3P
28	0	0	0	0
TS44b	126.5	132.1	136.9	144.2
44b	64.4	72.4	78.9	81.6
TS46	167.3	174.2	190.2	193.6
46	102.9	113.2	128.3	128.7
TS47	118.8	129.5	138.1	137.5
47	42.4	45	51.8	63.4
TS49b	106.8	112	122.5	131.6
49b	70.2	79.8	90.1	102.2
TS36b	109.9	115	130.8	143.6
36b	-20.4	-16.5	-9.5	3.2
TS27b	141	124.3	125	135.5
27	-123.9	-118.6	-105	-81.7

Table 4: Free energy profile (KJ/mol) for the reduction of **28** to **27** via oxepin **47** and ylide **36a**.

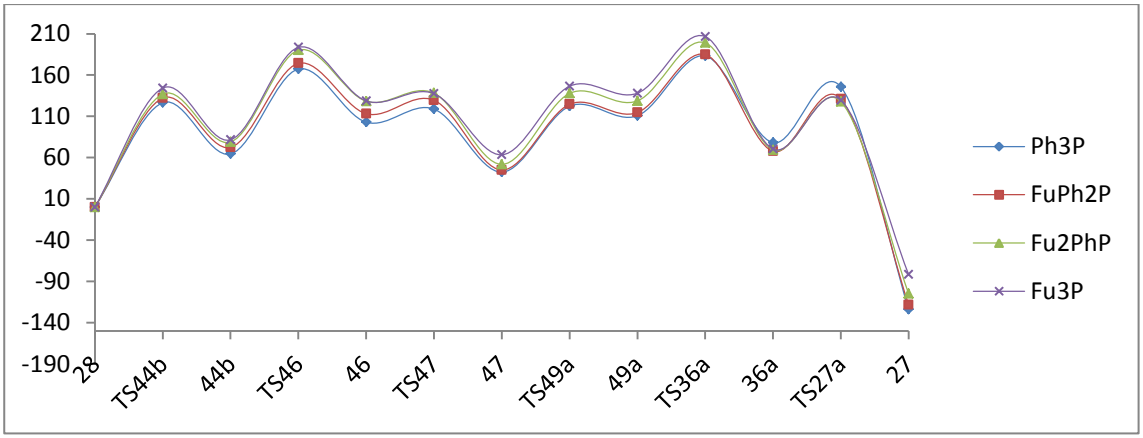

STRUCTURE	ΔG (KJ/mol) Ph3P	ΔG (KJ/mol) FuPh2P	ΔG (KJ/mol) Fu2PhP	ΔG (KJ/mol) Fu3P
28	0	0	0	0
TS44b	126.5	132.1	136.9	144.2
44b	64.4	72.4	78.9	81.6
TS46	167.3	174.2	190.2	193.6
46	102.9	113.2	128.3	128.7
TS47	118.8	129.5	138.1	137.5
47	42.4	45	51.8	63.4
TS49a	122.3	124.6	137.8	146.5
49a	110.7	114.6	128.7	138
TS36a	183.2	184.9	199.1	206.7
36a	78.1	67.6	69.3	70.4
TS27a	145.6	131	127.8	129.4
27	-123.9	-118.5	-105	-81.7

Table 5: Free energy profile (KJ/mol) for the reduction of **28** to **27** via epoxide **48**.

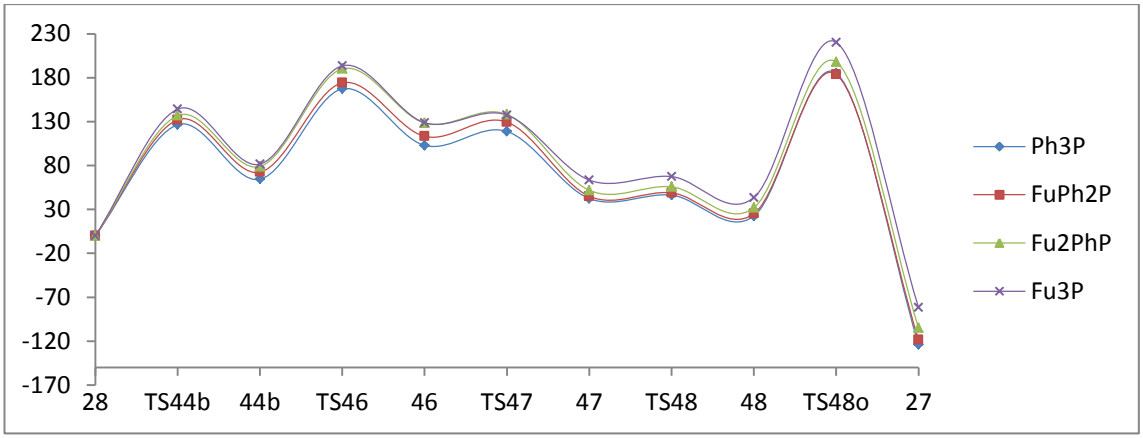

STRUCTURE	ΔG (KJ/mol) Ph3P	ΔG (KJ/mol) FuPh2P	ΔG (KJ/mol) Fu2PhP	ΔG (KJ/mol) Fu3P
28	0	0	0	0
TS44b	126.5	132.1	136.9	144.2
44b	64.4	72.4	78.9	81.6
TS46	167.3	174.2	190.2	193.6
46	102.9	113.2	128.3	128.7
TS47	118.8	129.5	138.1	137.5
47	42.4	45	51.8	63.4
TS48	46.3	48.9	55.7	67.4
48	22.4	25.1	31.9	43.5
TS48o	185.1	183.8	197.8	220.3
27	-123.9	-118.6	-105	-81.7

List of References

(1) Tisza, L. *Zeitschrift für Phys.* **1933**, *82*, 48.

(2) Haymet, A. D. J. *Chem. Phys. Lett.* **1985**, *122*, 421.

(3) Haymet, A. D. J. *J. Am. Chem. Soc.* **1986**, *108*, 319.

(4) Kroto, H. W.; Heath, J. R.; O'Brien, S. C.; Curl, R. F.; Smalley, R. E. *Nature* **1985**, *318*, 162.

(5) Krätschmer, W.; Fostiropoulos, K.; Huffman, D. R. *Chem. Phys. Lett.* **1990**, *170*, 167.

(6) Krätschmer, W.; Lamb, L. D.; Fostiropoulos, K.; Huffman, D. R. *Nature* **1990**, *347*, 354.

(7) Haufler, R. E.; Conceicao, J.; Chibante, L. P. F.; Chai, Y.; Byrne, N. E.; Flanagan, S.; Haley, M. M.; O'Brien, S. C.; Pan, C.; et al., . *J. Phys. Chem.* **1990**, *94*, 8634.

(8) Ozaki, M.; Taahashi, A. *Chem. Phys. Lett.* **1986**, *127*, 242.

(9) Yannoni, C. S.; Bernier, P. P.; Bethune, D. S.; Meijer, G.; Salem, J. R. *J. Am. Chem. Soc.* **1991**, *113*, 3190.

(10) Hedberg, K.; Hedberg, L.; Bethune, D. S.; Brown, C. A.; Dorn, H. C.; Johnson, R. D.; De Vries, M. *Science* **1991**, *254*, 410.

(11) Taylor, R.; Walton, D. R. M. *Nature* **1993**, *363*, 685.

(12) Anctil, A.; Babbitt, C. W.; Raffaelle, R. P.; Landi, B. J. *Environ. Sci. Technol.* **2011**, *45*, 2353.

(13) Goroff, N. S. *Acc. Chem. Res.* **1996**, *29*, 77.

(14) Smalley, R. E. *Acc. Chem. Res.* **1992**, *25*, 98.

(15) Hunter, J. M.; Fye, J. L.; Roskamp, E. J.; Jarrold, M. F. *J. Phys. Chem.* **1994**, *98*, 1810.

(16) Irle, S.; Zheng, G.; Wang, Z.; Morokuma, K. *J. Phys. Chem. B* **2006**, *110*, 14531.

(16a) Chuvilin, A.; Kaiser, U.; Bichoutskaia, E.; Besley, N. A.; Khlobystov, A. N. *Nature Chemistry* **2010**, *2*, 450-453.

(17) Boorum, M. M.; Vasil'ev, Y. V; Drewello, T.; Scott, L. T. *Science* **2001**, *294*, 828.

(18) Amsharov, K.; Abdurakhmanova, N.; Stepanow, S.; Rauschenbach, S.; Jansen, M.; Kern, K. *Angew. Chem. Int. Ed.* **2010**, *49*, 9392.

(19) Kabdulov, M.; Jansen, M.; Amsharov, K. Y. *Chemistry* **2013**, *19*, 17262.

(20) Thilgen, C. *Angew. Chem. Int. Ed.* **2012**, *51*, 7082.

(21) Scott, L. T.; Boorum, M. M.; McMahon, B. J.; Hagen, S.; Mack, J.; Blank, J.; Wegner, H.; de Meijere, A. *Science* **2002**, *295*, 1500.

(22) Otero, G.; Biddau, G.; Sánchez-Sánchez, C.; Caillard, R.; López, M. F.; Rogero, C.; Palomares, F. J.; Cabello, N.; Basanta, M. a; Ortega, J.; Méndez, J.; Echavarren, A. M.; Pérez, R.; Gómez-Lor, B.; Martín-Gago, J. a. *Nature* **2008**, *454*, 865.

(23) Gómez-Lor, B.; de Frutos, Ó.; Echavarren, A. M. *Chem. Commun.* **1999**, 2431.

(24) Faust, R. *Angew. Chem. Int. Ed.* **1998**, *37*, 2825.

(25) Adams, G. B.; O'Keeffe, M.; Ruoff, R. S. *J. Phys. Chem.* **1994**, *98*, 9465.

(26) Heath, J. R.; O'Brien, S. C.; Zhang, Q.; Liu, Y.; Curl, R. F.; Tittel, F. K.; Smalley, R. E. *J. Am. Chem. Soc.* **1985**, *107*, 7779.

(27) Cioslowski, J. *J. Am. Chem. Soc.* **1991**, *113*, 4139.

(28) Chai, Y.; Guo, T.; Jin, C.; Haufler, R. E.; Chibante, L. P. F.; Fure, J.; Wang, L.; Alford, J. M.; Smalley, R. E. *J. Phys. Chem.* **1991**, *95*, 7564.

(29) Stevenson, S.; Rice, G.; Glass, T.; Harich, K.; Cromer, F.; Jordan, M. R.; Craft, J.; Dorn, H. C. *Nature* **1999**, *80*, 80.

(30) Dunsch, L.; Krause, M.; Noack, J.; Georgi, P. *J. Phys. Chem. Solids* **2004**, *65*, 309.

(31) Chen, N.; Chaur, M. N.; Moore, C.; Pinzón, J. R.; Valencia, R.; Rodríguez-Fortea, A.; Poblet, J. M.; Echegoyen, L. *Chem. Commun.* **2010**, *46*, 4818.

(32) Krause, M.; Ziegs, F.; Popov, A. a; Dunsch, L. *Chemphyschem* **2007**, *8*, 537.

(33) Almeida Murphy, T.; Pawlik, T.; Weidinger, A.; Höhne, M.; Alcala, R.; Spaeth, J.-M. *Phys. Rev. Lett.* **1996**, *77*, 1075.

(34) Knapp, C.; Weiden, N.; Kass, H.; Dinse, K.-P.; Pietzak, B.; Waiblinger, M.; Weidinger, A. *Mol. Phys.* **1998**, *95*, 999.

(35) Kanai, M.; Porfyrakis, K.; Briggs, G. A. D.; Dennis, T. J. S. *Chem. Commun.* **2004**, 210.

(36) Suetsuna, T.; Dragoe, N.; Harneit, W.; Weidinger, A.; Shimotani, H.; Ito, S.; Takagi, H.; Kitazawa, K. *Chemistry* **2002**, *8*, 5079.

(37) Weiske, T.; Böhme, D. K.; Hrušák, J.; Krätschmer, W.; Schwarz, H. *Angew. Chem. Int. Ed.* **1991**, *30*, 884.

(38) Saunders, M.; Jiménez-Vázquez, H. A.; Cross, R. J.; Poreda, R. J. *Science* **1993**, *259*, 1428.

(39) Saunders, M.; Jimenez-Vazquez, H. A.; Cross, R. J.; Mroczkowski, S.; Gross, M. L.; Giblin, D. E.; Poreda, R. J. *J. Am. Chem. Soc.* **1994**, *116*, 2193.

(40) Vougioukalakis, G. C.; Roubelakis, M. M.; Orfanopoulos, M. *Chem. Soc. Rev.* **2010**, *39*, 817.

(41) Taliani, C.; Ruani, G.; Zamboni, R.; Danieli, R.; Rossini, S.; Denisov, V. N.; Burlakov, V. M.; Negri, F.; Orlandi, G.; Zerbetto, F. *J. Chem. Soc. Chem. Commun.* **1993**, 220.

(42) Hummelen, J. C.; Prato, M.; Wudl, F. *J. Am. Chem. Soc.* **1995**, *117*, 7003.

(43) Prato, M.; Li, Q. C.; Wudl, F.; Lucchini, V. *J. Am. Chem. Soc.* **1993**, *115*, 1148.

(44) Cases, M.; Duran, M.; Mestres, J.; Martín, N.; Solà, M. *J. Org. Chem.* **2001**, *66*, 433.

(45) Arbogast, J. W.; Darmanyan, A. P.; Foote, C. S.; Diederich, F. N.; Whetten, R. L.; Rubin, Y.; Alvarez, M. M.; Anz, S. J. *J. Phys. Chem.* **1991**, *95*, 11.

(46) Arce, M.-J.; Viado, A. L.; An, Y.-Z.; Khan, S. I.; Rubin, Y. *J. Am. Chem. Soc.* **1996**, *118*, 3775.

(47) Rubin, Y. *Chem. Eur. J.* **1997**, *3*, 1009.

(48) Schick, G.; Jarrosson, T.; Rubin, Y. *Angew. Chem. Int. Ed.* **1999**, *38*, 2360.

(49) Rubin, Y.; Jarrosson, T.; Wang, G.-W.; Bartberger, M. D.; Houk, K. N.; Schick, G.; Saunders, M.; Cross, R. J. *Angew. Chem. Int. Ed.* **2001**, *40*, 1543.

(50) Iwamatsu, S.; Vijayalakshmi, P. S.; Hamajima, M.; Suresh, C. H.; Koga, N.; Suzuki, T.; Murata, S. *Org. Lett.* **2002**, *4*, 1217.

(51) Inoue, H.; Yamaguchi, H.; Iwamatsu, S.; Uozaki, T.; Suzuki, T.; Akasaka, T.; Nagase, S.; Murata, S. *Tetrahedron Lett.* **2001**, *42*, 895.

(52) Iwamatsu, S.; Ono, F.; Murata, S. *Chem. Commun.* **2003**, 1268.

(53) Iwamatsu, S.; Kuwayama, T.; Kobayashi, K.; Nagase, S.; Murata, S. *Synthesis* **2004**, 2962.

(54) Iwamatsu, S.; Murata, S.; Andoh, Y.; Minoura, M.; Kobayashi, K.; Mizorogi, N.; Nagase, S. *J. Org. Chem.* **2005**, *70*, 4820.

(55) Stanisky, C. M.; Cross, R. J.; Saunders, M. *J. Am. Chem. Soc.* **2009**, *131*, 3392.

(56) Iwamatsu, S.; Uozaki, T.; Kobayashi, K.; Re, S.; Nagase, S.; Murata, S. *J. Am. Chem. Soc.* **2004**, *126*, 2668.

(57) Whitener Jr., K. E.; Frunzi, M.; Iwamatsu, S.; Murata, S.; Cross, R. J.; Saunders, M. *J. Am. Chem. Soc.* **2008**, *130*, 13996.

(58) Iwamatsu, S.; Stanisky, C. M.; Cross, R. J.; Saunders, M.; Mizorogi, N.; Nagase, S.; Murata, S. *Angew. Chem. Int. Ed.* **2006**, *45*, 5337.

(59) Whitener Jr., K. E.; Cross, R. J.; Saunders, M.; Iwamatsu, S.; Murata, S.; Mizorogi, N.; Nagase, S. *J. Am. Chem. Soc.* **2009**, *131*, 6338.

(60) Iwamatsu, S.; Murata, S. *Synlett* **2005**, 2117.

(61) Iwamatsu, S.; Ono, F.; Murata, S. *Chem. Lett.* **2003**, *32*, 614.

(62) Vougioukalakis, G. C.; Prassides, K.; Campanera, J. M.; Heggie, M. I.; Orfanopoulos, M. *J. Org. Chem.* **2004**, *69*, 4524.

(63) Iwamatsu, S.; Murata, S. *Tetrahedron Lett.* **2004**, *45*, 6391.

(64) Gan, L.; Huang, S.; Zhang, X.; Zhang, A.; Cheng, B.; Cheng, H.; Li, X.; Shang, G. *J. Am. Chem. Soc.* **2002**, *124*, 13384.

(65) Huang, S.; Xiao, Z.; Wang, F.; Zhou, J.; Yuan, G.; Zhang, S.; Chen, Z.; Thiel, W.; von Ragué Schleyer, P.; Zhang, X.; Hu, X.; Chen, B.; Gan, L. *Chemistry* **2005**, *11*, 5449.

(66) Zhang, Q.; Jia, Z.; Liu, S.; Zhang, G.; Xiao, Z.; Yang, D.; Gan, L.; Wang, Z.; Li, Y. *Org. Lett.* **2009**, *11*, 2772.

(67) Murata, Y.; Murata, M.; Komatsu, K. *J. Am. Chem. Soc.* **2003**, *125*, 7152.

(68) Murata, Y.; Murata, M.; Komatsu, K. *Chemistry* **2003**, *9*, 1600.

(69) An, Y.-Z.; Ellis, G. a.; Viado, A. L.; Rubin, Y. *J. Org. Chem.* **1996**, *61*, 1900.

(70) Komatsu, K.; Murata, M.; Murata, Y. *Science* **2005**, *307*, 238.

(71) Morinaka, Y.; Tanabe, F.; Murata, M.; Murata, Y.; Komatsu, K. *Chem. Commun.* **2010**, *46*, 4532.

(72) Kurotobi, K.; Murata, Y. *Science* **2011**, *333*, 613.

(73) Futagoishi, T.; Murata, M.; Wakamiya, A.; Sasamori, T.; Murata, Y. *Org. Lett.* **2013**, *15*, 2750.

(74) Ge, M.; Nagel, U.; Hüvonen, D.; Rõõm, T.; Mamone, S.; Levitt, M. H.; Carravetta, M.; Murata, Y.; Komatsu, K.; Chen, J. Y.-C.; Turro, N. J. *J. Chem. Phys.* **2011**, *134*, 054507.

(75) Mamone, S.; Ge, M.; Huvonen, D.; Nagel, U.; Danquigny, A.; Cuda, F.; Grossel, M. C.; Murata, Y.; Komatsu, K.; Levitt, M. H.; Room, T.; Carravetta, M. *J. Chem. Phys.* **2009**, *130*, 81103.

(76) Room, T.; Peedu, L.; Ge, M.; Huvonen, D.; Nagel, U.; Ye, S.; Xu, M.; Bacic, Z.; Mamone, S.; Levitt, M. H.; Carravetta, M.; Chen, J. Y. C.; Lei, X.; Turro, N. J.; Murata, Y.; Komatsu, K. *Phil. Trans. R. Soc. A* **2013**, *371*, 20110631.

(77) Beduz, C.; Carravetta, M.; Chen, J. Y. C.; Concistre, M.; Denning, M.; Frunzi, M.; Horsewill, A. J.; Johannessen, O. G.; Lawler, R.; Lei, X.; Levitt, M. H.; Li, Y.; Mamone, S.; Murata, Y.; Nagel, U.; Nishida, T.; Ollivier, J.; Rols, S.; Room, T.; Sarkar, R.; Turro, N. J.; Yang, Y. *Proc. Natl. Acad. Sci. USA* **2012**, *109*, 12894.

(78) Horsewill, A. J.; Goh, K.; Rols, S.; Ollivier, J.; Johnson, M. R.; Levitt, M. H.; Carravetta, M.; Mamone, S.; Murata, Y.; Chen, J. Y. C.; Johnson, J. A.; Lei, X.; Turro, N. J. *Phil. Trans. R. Soc. A* **2013**, *371*, 20110627.

(79) Horsewill, A. J.; Panesar, K. S.; Rols, S.; Johnson, M. R.; Murata, Y.; Komatsu, K.; Mamone, S.; Danquigny, A.; Cuda, F.; Maltsev, S.; Grossel, M. C.; Carravetta, M.; Levitt, M. H. *Phys. Rev. Lett.* **2009**, *102*.

(80) Levitt, M. H. *Phil. Trans. R. Soc. A* **2013**, *371*, 20120429.

(81) Rieke, R. D.; Li, P. T.-J.; Burns, T. P.; Uhm, S. T. *J. Org. Chem.* **1981**, *46*, 4323.

(82) Hintermann, L.; Xiao, L.; Labonne, A. *Angew. Chem. Int. Ed.* **2008**, *47*, 8246.

(83) King, A. O.; Okukado, N.; Negishi, E. *Chem. Commun.* **1977**, 683.

(84) Chekmarev, D. S.; Stepanov, A. E.; Kasatkin, A. N. *Tetrahedron Lett.* **2005**, *46*, 1303.

(85) Schuster, D. I.; Baran, P. S.; Hatch, R. K.; Khan, A. U.; Wilson, S. R. *Chem. Commun.* **1998**, 2493.

(86) Frank, H. S.; Evans, M. W. *J. Chem. Phys.* **1945**, *13*, 507.

(87) Pohorille, A.; Pratt, L. R. *J. Am. Chem. Soc.* **1990**, *112*, 5066.

(88) Pratt, L. R.; Pohorille, A. *Proc. Natl. Acad. Sci. USA* **1992**, *89*, 2995.

(89) Christian, S. D.; Taha, A. A.; Gash, B. W. *Q. Rev. Chem. Soc.* **1970**, *24*, 20.

(90) Wolfenden, R.; Radzicka, A. *Science* **1994**, *265*, 936.

(91) Vaitheeswaran, S.; Yin, H.; Rasaiah, J. C.; Hummer, G. *Proc. Natl. Acad. Sci. USA* **2004**, *101*, 17002.

(92) Frunzi, M.; Baldwin, A. M.; Shibata, N.; Iwamatsu, S.-I.; Lawler, R. G.; Turro, N. J. *J. Phys. Chem. A* **2011**, *115*, 735.

(93) Hashikawa, Y.; Murata, M.; Wakamiya, A.; Murata, Y. *Org. Lett.* **2014**, *16*, 2970.

(94) Wolinski, K.; Hinton, J. F.; Pulay, P. *J. Am. Chem. Soc.* **1990**, *112*, 8251.

(95) Zhang, Q.; Pankewitz, T.; Liu, S.; Klopper, W.; Gan, L. *Angew. Chem. Int. Ed.* **2010**, *49*, 9935.

(96) Guo, Y.; Yan, J.; Khashab, N. M. *Chemphyschem* **2012**, *13*, 751.

(97) Albright, T. A.; Gordon, M. D.; Freeman, W. J.; Schweizer, E. E. *J. Am. Chem. Soc.* **1976**, *98*, 6249.

(98) Borowitz, I. J.; Anschel, M.; Readio, P. D. *J. Org. Chem.* **1971**, *36*, 553.

(99) Vogel, E.; Günther, H. *Angew. Chem. Int. Ed.* **1967**, *6*, 385.

(100) Ensing, B.; Costanzo, F.; Silvestrelli, P. L. *J. Phys. Chem. A* **2012**, *116*, 12184.

(101) Eisenberg, R. *Acc. Chem. Res.* **1991**, *24*, 110.

(102) Dechent, J. F.; Buljubasich, L.; Schreiber, L. M.; Spiess, H. W.; Münnemann, K. *Phys. Chem. Chem. Phys.* **2012**, *14*, 2346.

(103) Mamone, S.; Concistrè, M.; Carignani, E.; Meier, B.; Krachmalnicoff, A.; Johannessen, O. G.; Lei, X.; Li, Y.; Denning, M.; Carravetta, M.; Goh, K.; Horsewill, A. J.; Whitby, R. J.; Levitt, M. H. *J. Chem. Phys.* **2014**, *140*, 194306.

(104) Camps, X.; Hirsch, A. *J. Chem. Soc. Perkin Trans. 1* **1997**, 1595.

(105) Bingel, C. *Chem. Ber.* **1993**, *126*, 1957.

(106) Hirsch, A.; Lamparth, I. *J. Am. Chem. Soc.* **1994**, *116*, 9385.

(107) Lamparth, I.; Maichle-Mössmer, C.; Hirsch, A. *Angew. Chem. Int. Ed.* **1995**, *34*, 1607.

(108) Olah, G. A.; Welch, J. T.; Vankar, Y. D.; Nojima, M.; Kerekes, I.; Olah, J. A. *J. Org. Chem.* **1979**, *44*, 3872.

(109) Olah, G. A.; Mathew, T.; Goeppert, A.; Torok, B.; Bucsi, I.; Li, X. Y.; Wang, Q.; Marinez, E. R.; Batamack, P.; Aniszfeld, R.; Prakash, G. K. *J. Am. Chem. Soc.* **2005**, *127*, 5964.

(110) MacLean, C.; Mackor, E. L. *J. Chem. Phys.* **1961**, *34*, 2207.

(111) Martin, J. S.; Fujiwara, F. Y. *J. Am. Chem. Soc.* **1974**, *96*, 7632.

(112) Muenter, J. S. *J. Chem. Phys.* **1970**, *52*, 6033.

(113) Rothenberg, G.; Royz, M.; Arrad, O.; Sasson, Y. *J. Chem. Soc. Perkin Trans. 1* **1999**, 1491.

(114) Mitsunobu, O. *Synthesis*, **1981**, *1*, 1–28.

(115) Hendrickson, J.; Hussoin, M. *J. Org. Chem.* **1987**, 4137.

(116) Appel, M.; Blaurock, S.; Berger, S. *Eur. J. Org. Chem.* **2002**, 1143.

(117) Schröder, U.; Berger, S. *Eur. J. Org. Chem.* **2000**, 2601.

(118) Ackermann, M.; Berger, S. *Tetrahedron* **2005**, *61*, 6764.

(119) Allen, D. W.; Hutley, B. G.; Mellor, M. T. J. *J. Chem. Soc., Perkin Trans. 2* **1972**, 63.

(120) Allen, D. W.; Hutley, B. G.; Rich, T. C. *J. Chem. Soc., Perkin Trans. 2* **1973**, 820.

(121) Ackermann, M.; Pascariu, a; Hocher, T.; Siehl, H. U.; Berger, S. *J. Am. Chem. Soc.* **2006**, *128*, 8434.

(122) Krachmalnicoff, A.; Levitt, M. H.; Whitby, R. J. *Chem. Commun.* **2014**, *50*, 13037.

(123) Batsanov, S. *Struct. Chem.* **1999**, *10*, 395.

(124) Dolgonos, G. A.; Peslherbe, G. H. *Phys. Chem. Chem. Phys.* **2014**, *16*, 26294.

(125) Cioslowski, J.; Nanayakkara, A. *Phys. Rev. Lett.* **1992**, *69*, 2871.

(126) Märkl, G.; Amrhein, J.; Stoiber, T.; Striebl, U.; Kreitmeier, P. *Tetrahedron* **2002**, *58*, 2551.

(127) Gaussian 09, Revision D.01, Frisch, M. J.; Trucks, G. W.; Schlegel, H. B.; Scuseria, G. E.; Robb, M. A.; Cheeseman, J. R.; Scalmani, G.; Barone, V.; Mennucci, B.; Petersson, G. A.; Nakatsuji, H.; Caricato, M.; Li, X.; Hratchian, H. P.; Izmaylov, A. F.; Bloino, J.; Zheng, G.; Sonnenberg, J. L.; Hada, M.; Ehara, M.; Toyota, K.; Fukuda, R.; Hasegawa, J.; Ishida, M.; Nakajima, T.; Honda, Y.; Kitao, O.; Nakai, H.; Vreven, T.; Montgomery, J. A., Jr.; Peralta, J. E.; Ogliaro, F.; Bearpark, M.; Heyd, J. J.; Brothers, E.; Kudin, K. N.; Staroverov, V. N.; Kobayashi,

R.; Normand, J.; Raghavachari, K.; Rendell, A.; Burant, J. C.; Iyengar, S. S.; Tomasi, J.; Cossi, M.; Rega, N.; Millam, M. J.; Klene, M.; Knox, J. E.; Cross, J. B.; Bakken, V.; Adamo, C.; Jaramillo, J.; Gomperts, R.; Stratmann, R. E.; Yazyev, O.; Austin, A. J.; Cammi, R.; Pomelli, C.; Ochterski, J. W.; Martin, R. L.; Morokuma, K.; Zakrzewski, V. G.; Voth, G. A.; Salvador, P.; Dannenberg, J. J.; Dapprich, S.; Daniels, A. D.; Farkas, Ö.; Foresman, J. B.; Ortiz, J. V.; Cioslowski, J.; Fox, D. J. Gaussian, Inc., Wallingford CT, 2009.